ONE- AND TWO- DIMENSIONAL COSINE MODULATED FILTER BANKS

Thesis by

Yuan-Pei Lin

In Partial Fulfillment of the Requirements

for the Degree of

Doctor of Philosophy

California Institute of Technology

Pasadena, California

1997

(Submitted Dec. 10, 1996)

Acknowledgements

It is a great fortune of mine to be working with Prof. Vaidyanathan in my graduate study at Caltech. P.P., as we all call him, is the best advisor one can ever find. I admire his brilliance and the persistent attitude he has towards research, which will always be an inspiration for me. He struck me, if not even more, as an educator. No matter how busy he is, he makes time for his students. He is always there for them with encouragement every step of the way. The amount of patience he has for his students never ceases to amaze me. For the past four years, he has been guiding me like a parent and like a friend. The discussions we had and the conferences we attended together are some of the most enjoyable experiences I had at Caltech; I will cherish dearly those moments. His friendship is the most unexpected gift I get out of my graduate study. I respect him from my heart as a scholar, as my advisor and as a friend.

My working and life experience at Caltech has been a most pleasant one. It is a great pleasure to acknowledge the colleagues who have made it possible: See-May Phoong, Jamal Tuqan and Ahmet Kirac, especially See-May Phoong for his constant feedback and inputs. I would like to thank Tsuhan Chen at AT&T, Igor Djokovic at Pairgain and Troung Nguyen at the University of Wisconsin at Madison for their various comments. Also the help provided by system manger Robert Freeman and, administrative assistants Lilian Porter and Lavonne Martin are greatly appreciated.

I would like to thank Prof. McEliece, Prof. Abu-Mostafa, Dr. Martin (at JPL) and Dr. Elachi (at JPL). Their lectures have been the most enjoyable. I appreciate their suggestions and support during my graduate study and also their time serving on my examination committees. I would also like to thank Dr. Pollara (at JPL) and Dr. Luthra (at General Instruments) for their interest in my work and for giving constructive comments to my thesis.

Finally, I would like to thank my family for their support and for providing me the opportunity to higher educations.

Abstract

Subband coding as a lossy data compression technique was first introduced for speech coding. It has been demonstrated to be a very competitive coding method for general audio signals as well as images. Subband coding has been incorporated in various popular coding standards. Essential to the implementation of subband coding is an M-channel filter bank that partitions the input signal into M subbands. In the context of 1D (one-dimensional) filter bank design, the CMFB (cosine modulated filter bank) is well-known for design and implementation efficiency. All the filters in the filter bank are cosine modulated versions of a prototype filter. As a result the cost of design as well as complexity is reduced dramatically by a factor of M. In this thesis we study the design of CMFB in 1D case and 2D (two-dimensional) case.

In previous works on 1D CMFB, the filters in the filter bank do not have linear phase, which is considered an important feature in image coding applications. The design of cosine modulated filter banks with linear-phase filters is the first topic to be presented in this thesis. Design examples will be given to show that filter banks with filters having good frequency selectivity can be obtained in spite of the linear phase constraint.

For the design of 2D cosine modulated filter banks, the simplest approach is to cascade 1D filter banks in the form of a tree. This type of 2D filter banks are referred to as separable. The frequency support of the filters in a separable filter bank are restricted to rectangular shapes. Nonseparable filter banks allow more flexible partitions of the frequency plane and achieve better performance. Almost all the existing design techniques for 2D nonseparable filter banks are developed exclusively for the two-channel case. We will consider two types of 2D M-channel nonseparable filter banks, the two-parallelogram type and the four-parallelogram type. These are respectively the classes of filter banks in which the passbands of the filters consist of two and four parallelograms. In these designs additional cosine modulated constraints will be incorporated for design and implementation economy.

Contents

List of Figures

List of Tables

Chapter 1

Introduction

Filter banks for the application of subband coding of speech were introduced in the 1970s. Since then, studies on filter banks, subband coding and in general the potential applications have been booming. Today it is one of the most effective lossy data compression techniques. It has been used in various popular standards, e.g., MPEG (motion picture expert group) and NTSC (National Television Standard Committee).

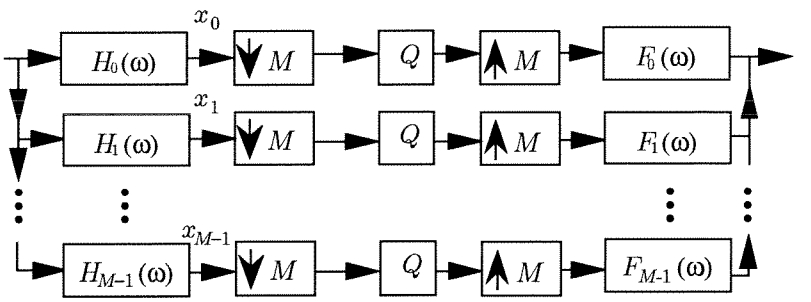

Fig. 1.1. The M-channel uniform filter bank.

The essential instrument in the implementation of subband coding is the M-channel filter bank as shown in Fig. 1.1. The input signal $x(n)$ is first split into subbands using a set of M analysis filters $H_k(z)$, with typical frequency stacking as shown in Fig. 1.2. The subband signals $x_k(n)$ are then processed for storage, or transmission, depending on the underlying application. Typically, quantizers are inserted in the subbands and bits are allocated among $x_k(n)$ to meet a target bit rate. Bit allocation is conducted judiciously such that the recombined signal $\widehat{x}(n)$ bears a closer resemblance (perceptually and quantitatively) to the input $x(n)$ than direct quantization of $x(n)$ for the same bit rate. Equivalently, subband coders are able to achieve the same perceptual or quantitative quality with a lower bit rate.

There are several reasons why subband coding has been enjoying so much popularity recently. A

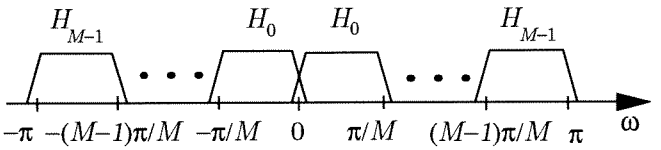

Fig. 1.2. The typical stacking of an M-channel uniform filter bank.

distinctive property of subband coding is that it is in good accordance with the human visual system and the auditory system. For example, by repeatedly spitting the lower subband of a two-channel filter bank (Fig. 1.1 with $M = 2$) we obtain the so-called octave-band filter bank as shown in 1.3(a). This yields an overall frequency partition as shown 1.3(b) and these octave bands better capture the logarithmic feature of the human hearing system. A subband coder allows direct control over information in different frequency bands and allows natural incorporation of perception models, e.g., the masking pattern of hearing. It is understood that the ability of ears to detect noise is affected by the presence of another sound in the same spectral and temporal localities; this phenomenon is called masking [3]. Subband bit allocation can be adjusted accordingly to take advantage of masking. Perceptual subband coding has been widely used in *psychoacoustic* audio coders such as MUSICAM (Masking-pattern Universal Subband Integrated Coding and Multiplexing), and AC-2 system developed by Dolby. MUSICAM is later adopted in the the audio layers of MPEG-1 as well as MPEG-2; AC-2 is proposed to be used in a new system of NTSC for HDTV (High Definition Television) services [78]. Similar masking patterns exist in human visual system. Based on the framework of subband coding, visual perception criteria have also been integrated into image or video coder designs [68, 80].

While VQ (Vector Quantization) requires data training, code book design, and code book storage and table lookup at the decoder, signal independent filter bank design works very well in general. The whole subband coder operates like an open loop system. As a initial step, the filter bank can be obtained through one of the standard design techniques. (Today even the design step is not necessary; filter coefficients of the filters in the filter banks have been widely tabulated for various numbers of channels.) The only signal dependent element is bit allocation, which can be done easily by computing the subband variances. The implementation of a subband coder, the encoder as well as the decoder requires little storage memory. Moreover the subband coding scheme lends itself well to the incorporation of other compression techniques. For example DPCM (Differential Pulse Coded Modulation) quantizers are often inserted in the subbands instead of simple uniform quantizers to improve the performance [109]. The use of VQ in the subbands (subband VQ) has also been studied [14].

Subband coders also offer the well-known *multiresolution* feature [58, 98, 106], which provides a natural framework for progressive transmission. A quick display of the compressed image at low

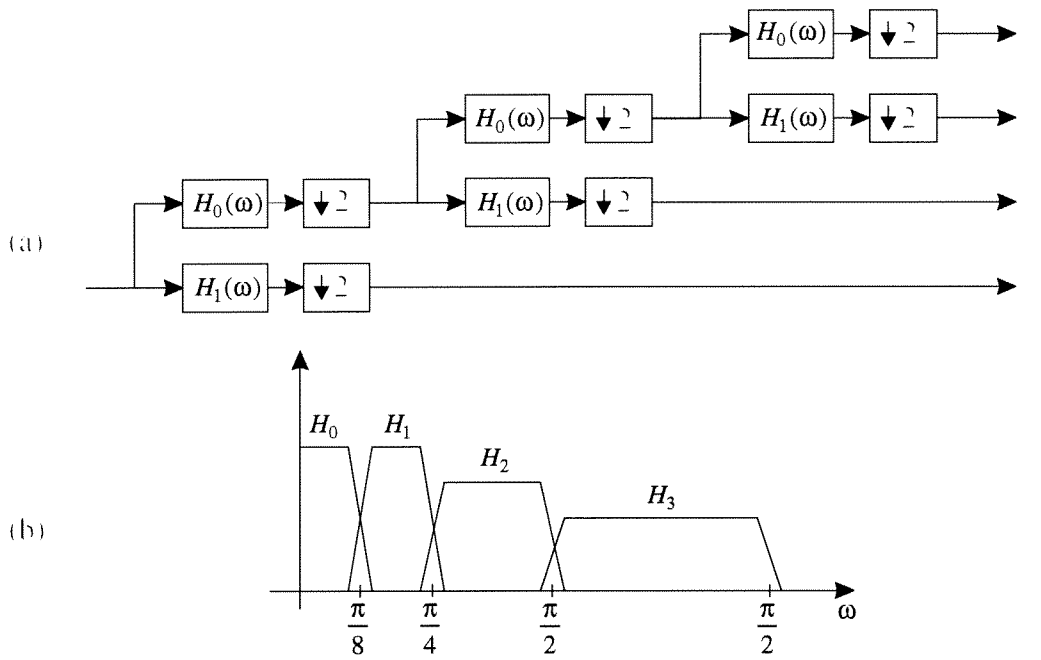

Fig. 1.3. The octave-band filter bank: (a) tree structure; (b) frequency stacking.

resolution is possible without decoding the whole image. Renditions of progressively better quality can be then displayed with more added resolution at the viewers' choice. This property is very useful in the application of *telebrowsing* and also in applications where displays of varying resolutions are desired, e.g., printers and monitors [32]. Fig. 1.4 shows an example of displaying a subband coded test image at three resolutions. The original test image (Fig. 1.4(a)) is of size 512 by 512, with each pixel represented by 8 bits. The subband coded test image (using the algorithm by Said and Pearlman [82]) has a bit rate of 0.5 bit/pixel and the reconstructed image is shown in Fig. 1.4(d). Fig. 1.4(b) and (c) are obtained by reconstructing from part of the compressed image; the bit rates for these two cases are respectively .05 bit/pixel and .2 bit/pixel.

Subband coders are also useful for images coding in *facsimile transmission* [63]. Facsimile are black and white documents. When gray-level images are transmitted, they are usually first processed using halftoning technique to give gray-level renditions. Neuhoff and Pappas proposed that, instead of pre-transmission halftoning, gray-level images be subband coded, transmitted and decoded at the receiver end followed by halftoning process. It has been demonstrated that such halftone renditions are indistinguishable or almost indistinguishable from those without the subband coding stage while a significantly lower transmission rate can be achieved, especially when the output device has a high resolution (e.g. a 600 dpi printer).

Besides data compression, filter banks also find applications in telecommunications such as *trans-multiplexing* and *message encryption*. An important problem in digital telephone network is the

(a)

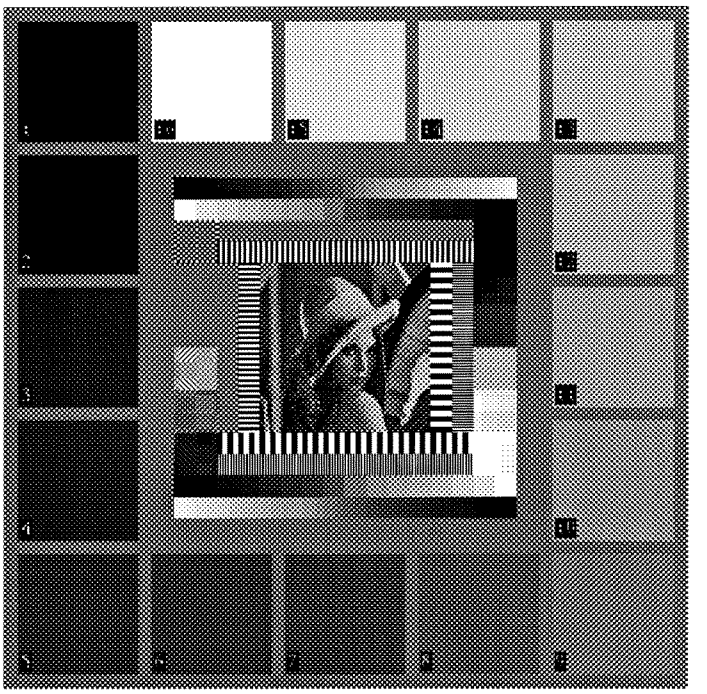

(b)

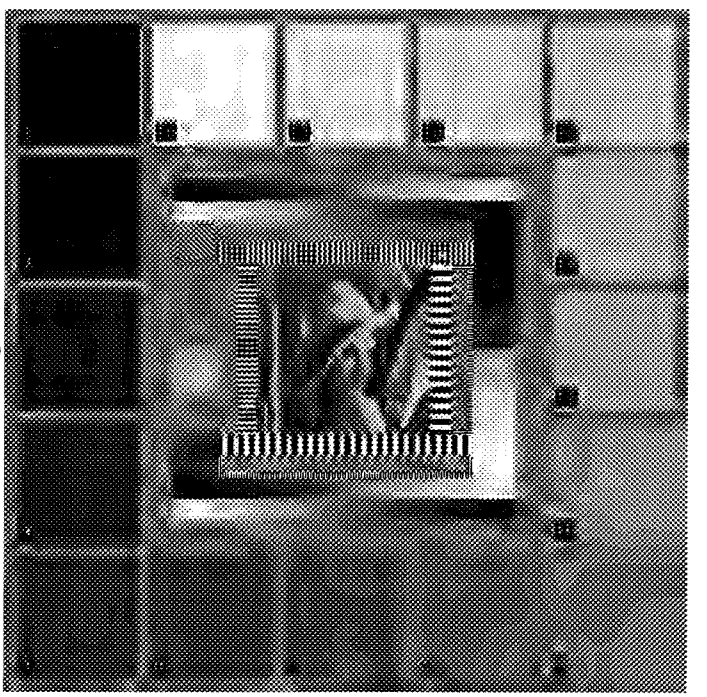

(c)

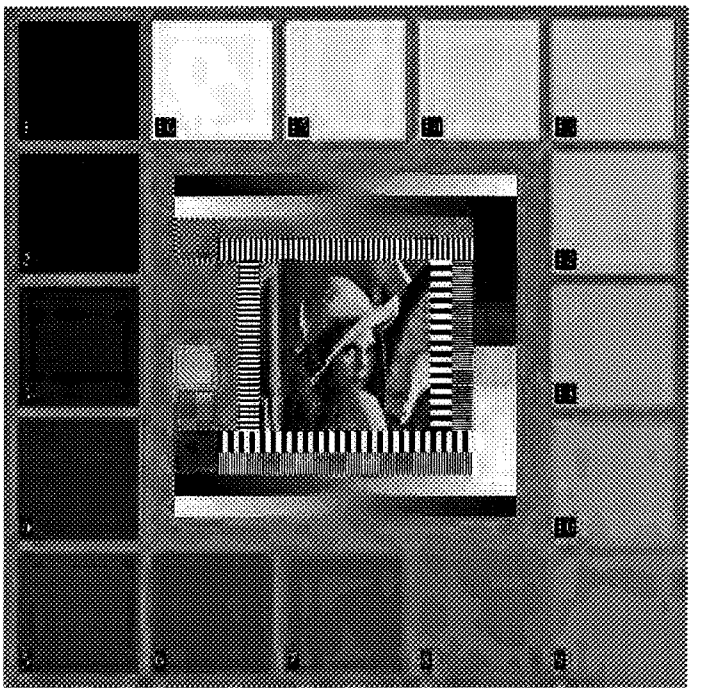

(d)

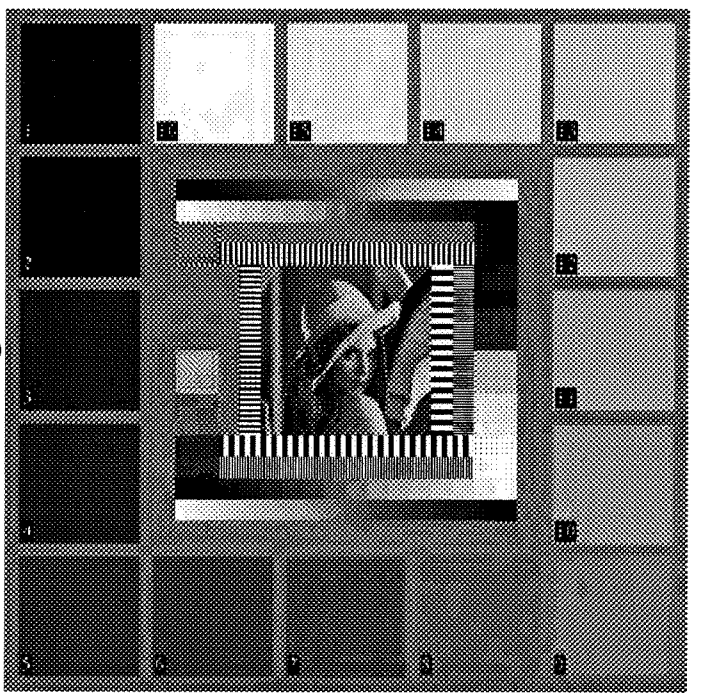

Fig. 1.4. Multiresolution displays: Test image (a) and reconstructed images at (b) 0.05 bit/pixel (c) 0.2 bit/pixel and (d) 0.5 bit/pixel.

conversion of signal formats from TDM (Time-Division Multiplexed) to FDM (Frequency-Division Multiplexed). This is called transmultiplexing [5]. A connection between this and filter bank theory was established by Vetterli [103, 104]. This observation prompts the realization of cross-talk free channels with full bandwidth utilization [37]. In the transmission of voice signals, the messages are sometimes encrypted to ensure privacy. By using a filter bank, a signal is first split into subbands followed by permutation and re-combination for transmission. This can prevent eavesdropping during transmission [16]. In addition, applications of filter banks as *convolvers* [100, 69] and *equalizers* [44, 45] have also been studied.

1.1 Developments of Filter Bank Design Techniques

1.1.1 Design of One-Dimensional Filter Banks

The introduction of subband coding has stirred up widespread interest in different approaches to the design of filter banks. In the absence of quantizers in the subbands a filter bank in general introduces two types of error: aliasing error and distortion error. When a filter bank is alias-free, it is an LTI system. If, in addition, the filter bank is also distortion-free, in this case the output is a replica of the input and the filter bank has *perfect reconstruction*. If these two conditions are only approximately satisfied, we say the system has *approximate reconstruction*.

The design techniques of filter banks have gradually evolved over time; some techniques are in the general context while some are driven by specific applications. Generally speaking, these advances have taken the course of proceeding to perfect reconstruction from approximation reconstruction case and to M-channel from two-channel case. Two-channel filter banks with approximate reconstruction were proposed in [17] for speech coding. Perfect reconstruction for two-channel case is achieved in [86]. Filter banks with more than two channels can be obtained by cascading two-channel filter banks in the form of a tree. However for large number of channels (e.g., 32, which is now a popular number used for audio coding) such cascades often introduce undesired huge amount of delay. The development of M-channel filter banks is driven by theoretical as well as practical interests. An M-channel filter bank with approximate reconstruction is designed in [79]. The advance to perfect reconstruction case is made independently by Vetterli [104] and Vaidyanathan [94, 95]. In particular in [94], the paraunitary systems, a subclass of perfect reconstruction filter banks, are parameterized. The introduction of the paraunitary (also called orthogonal or orthonormal) class turns out to be a very important step in filter bank theory and design. It leads to a series of further developments and also helps to simplify the filter bank design problem. Nevertheless the problem of designing M-channel filter banks is still not a simple one; the design problem becomes much simplified in cosine modulated setup, which will be elaborated in the subsequent discussion.

In the developments of filter bank theory and design, various systems and deign techniques have

been proposed: For removing blocking effects that often appear in transform image coding, the LOT (Lapped Orthogonal Transform) and its efficient implementation are developed. The LOT systems are paraunitary; the biorthogonal (non-paraunitary) extension of LOT, which is called the BOLT (BiOrthogonal Lapped Transform), is given in [101]. For removing ringing effect that occurs around edges, time varying (spatially varying) filter banks are proposed [29, 26, 71, 88]. Also for the application of image coding, it is important for the filters to have linear phase. Two-channel filter banks with linear-phase filters are designed in [28] and a factorization approach to the design of linear phase M-channel paraunitary filter bank is given in [89]. For efficient filter bank implementation, the cosine modulated filter banks (CMFB) are developed [79]. To improve the stopband attenuation of the filters for audio coding, NPR (Near Perfect Reconstruction) CMFB are designed [65, 90]. Also for a given input statistics and a given orthogonal filter bank, optimum pre- and post filters can be inserted to improve the SNR (signal to noise ratio) [19]. Signal dependent optimum orthogonal subband coder designs are considered in [93, 92, 99].

Recently, some techniques are developed to improve the perceptual and quantitative quality of subband coded signals: For better time-frequency analysis, signal dependent tree structured filter banks are considered in [76]. For a given input the tree is grown on a rate distortion sense to achieve a higher SNR. By exploiting subband correlations and taking into consideration that the quantized bit stream will be entropy coded, Shapiro introduced the *embedded zero-tree wavelet* (EZW) algorithm [84]. EZW enables the signal to be efficiently coded and leads to better results subjectively compared to the conventional SNR based bit allocation followed by separate entropy coding of each subband. The coding efficiency and coding performance are further improved by Said and Perlman [81, 82]. These new subband coding schemes have brought subband coding to a even more competitive level with other coding methods.

Cosine Modulated Filter Banks

In the contexts of filter bank design as well as implementation, the most notable is the class of the cosine modulated filter banks (CMFB). The CMFB is well-known for its low design cost and implementation efficiency. All the analysis filters are cosine modulated versions of a prototype filter, hence the name CMFB. The design of the filter bank involves only the prototype. Of even greater importance is that the complexity of the analysis (or synthesis) bank is comparable to that of the prototype plus a low-complexity DCT matrix. The CMFB technique dramatically reduces the implementation cost approximately by a factor of M.

An M-channel CMFB is typically obtained by starting from a $2M$ channel uniform DFT filter bank (Fig. 1.5), [98]. Each filter in the DFT filter bank is a shifted version of a lowpass prototype $P(\omega)$ (Fig. 1.5) with bandwidth π/M, which is half the total bandwidth of each filter in the desired M-channel system. The filters in the DFT filter bank are then shifted by $\pi/2M$ and paired to obtain

real-coefficient analysis filters (Fig. 1.2) of the M channel CMFB. Each analysis filter has total bandwidth $2\pi/M$, which is two times that of the prototype. In almost all the designs the synthesis filters are the time reversed version of the analysis filters and hence have the same magnitude responses. Two types of cosine modulated filter banks have been developed, pseudo QMF systems (approximate reconstruction) [66, 79, 12] and later paraunitary systems (perfect reconstruction implied) [74, 60, 37].

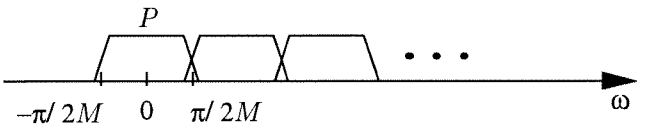

Fig. 1.5. A $2M$-channel DFT filter bank with P denoting the prototype filter.

Design examples have demonstrated that perfect reconstruction (or approximate reconstruction) and very good filter responses can be achieved simultaneously. Due to the efficiency of CMFB, virtually all the subband audio coders now in use are cosine modulated based, including the aforementioned MUSICAM (for MPEG-1 and MPEG-2), and the AC-2 systems. For example, the MUSICAM system uses a 32-channel CMFB with perceptually-tuned quantization in the subbands. The prototype is a lowpass filter with length 512 and stopband attenuation about 100 dB. For CD quality that is indistinguishable from the original recording, a typical compression ratio of this system is between 4 and 6.

However in these CMFB designs (approximate or perfect reconstruction) the individual filters do not have linear phase, which is an important property in image processing [42]. It is a necessary feature, in some cases, e.g., when symmetric extension technique is used in subband coding. (Symmetric extension technique is a method that can effectively remove boundary effect in image coding [87].) In this thesis we will design CMFB with linear phase analysis and synthesis filters. This is especially important because there has been an general (false) impression that this is theoretically impossible. The linear phase CMFB continues to enjoy all the advantages of traditional CMFB such as design and implementation efficiency. Examples will be given to show that very good CMFB designs can be obtained in spite of linear phase constraints. A brief overview of linear phase CMFB is given in Sec. 1.2.1 and a more complete treatment is given in Sec. 3.

1.1.2 Design of Two-Dimensional Filter Banks

Basic Building Blocks. Two of the basic building blocks in a multirate system of any dimension are the decimator $\downarrow \mathbf{M}$ and the expander $\uparrow \mathbf{M}$. In 1D systems, the M-fold decimator keeps only the samples that are multiples of M. In 2D systems, the decimator $\mathbf{M}$ is a 2×2 nonsingular integer

matrix. The decimation matrix $\downarrow \mathbf{M}$ keeps those samples that are on the lattice generated by $\mathbf{M}$. The lattice generated by an integer matrix $\mathbf{M}$ is the set of integer vectors of the form

$$\mathbf{Md}, \quad \text{for some } 2 \times 1 \text{ integer vector } \mathbf{d} .$$

For example, let $\mathbf{M}$ be a diagonal matrix

$$\mathbf{M} = \begin{pmatrix} M_1 & 0 \\ 0 & M_2 \end{pmatrix}. \tag{1.1}$$

Then the lattice is a rectangular lattice; an example with $M_1 = 2$ and $M_2 = 1$ is shown in Fig. 1.6(a), where dots denote integer vectors and black dots denote the vectors on the lattice. When M is a diagonal matrix, the decimation or expansion operation can be performed in each dimension separately. For a non diagonal example, consider the so-called quincunx matrix

$$\mathbf{M} = \begin{pmatrix} 1 & 1 \\ -1 & 1 \end{pmatrix}.$$

The corresponding lattice is shown in Fig. 1.6(b); this is called the quincunx lattice. The output of the decimator $\mathbf{M}$ contains only the samples on the lattice of $\mathbf{M}$.

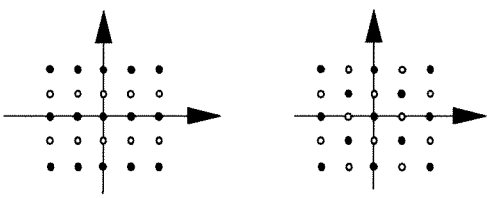

Fig. 1.6. (a) A rectangular lattice and (b) the quincunx lattice.

In a 2D multirate system the filters are two-dimensional. The simplest way to obtain a 2D filter is by cascading two 1D filters. For example suppose we are given two 1D lowpass filters with bandwidths $2\pi/M_1$ and $2\pi/M_2$. By cascading these two filters (Fig. 1.7(a)), we obtain a 2D filter $F(\omega_0, \omega_1)$ with rectangular support (Fig. 1.7(b)). This type of filters are called separable. Let the 1D filters be FIR with filter lengths N_1 and N_2, then the 2D filter $F(\omega_0, \omega_1)$ has $N_1 N_2$ coefficients and a rectangular time-domain support. In this case $F(\omega_0, \omega_1)$, as implemented in Fig. 1.7(a), allows filtering process to be done in each dimension separately; the computational complexity per output sample is proportional to $N_1 + N_2$. Furthermore if $G(\omega)$ and $H(\omega)$ are decimation filters for $\downarrow M_1$

and $\downarrow M_2$, the 2D filter is a decimation filter for the diagonal $\mathbf{M}$ in (1.1). We can see that when $\mathbf{M}$ is not diagonal, we will need to use a nonseparable decimation filter. For a nonseparable filter with N^2 coefficients, the complexity per output sample is in general proportional to N^2.

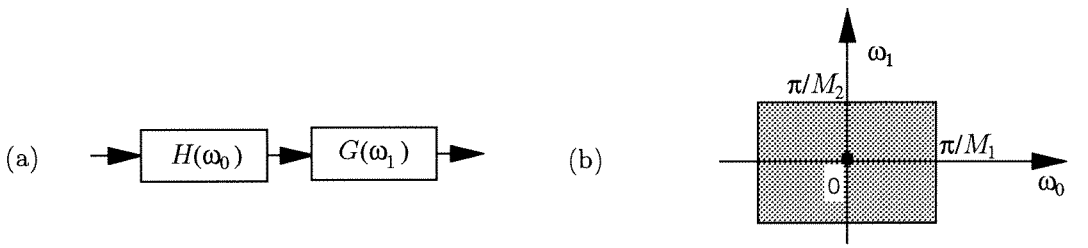

Fig. 1.7. (a) Separable 2D filters as a cascade of two 1D filters; (b) a separable filter.

Clearly separable decimation and filtering is much easier in concept and implementation. However in some applications it is necessary to use nonseparable operations. Such applications include the conversion between interlaced signals, used in television and video, and progressive signals, used in movies. For interlaced signals, the samples are located on the quincunx lattice whereas for the progressive signals the samples are on rectangular lattices. The conversion between these two requires nonseparable decimation, expansion and nonseparable filters.

Separable Filter Banks

In a 1D M-channel filter bank, the analysis filters typically have bandwidth $2\pi/M$ and the outputs allow M-fold decimation without creating too much aliasing (aliasing due to the non-ideal roll off in the transition bands are canceled in the synthesis bank). That is to say, each analysis filter is close to a decimation filter for $\downarrow M$. It is argued that such a setup is necessary for good filter bank designs [52] and the same principle applies to the 2D case. In a manner similar to cascading two 1D lowpass filters in two directions to obtain separable filters, we can cascade two 1D filter banks in the form of a tree structure to obtain a 2D filter bank, e.g, the four-channel tree structured filter bank shown in Fig. 1.8. In these tree-structured filter banks, the decimation matrix $\mathbf{M}$ is diagonal and data is processed in each dimension separately. This type of systems is referred to as *separable*. This is the most popular and simplest way to design 2D filter banks; almost all the 2D subband coders used in practice are based on separable filter banks [110, 59].

For a D-dimensional separable filter bank, design cost is equivalent to D times that of 1D filter banks; complexity of design and implementation grows linearly with the number of dimensions. In this case, the supports of the analysis and synthesis filter are D-dimensional rectangles. For 2D separable two-channel systems, the support configuration will be as in Fig. 1.9(a) or Fig. 1.9(b) when the analysis and synthesis filters have real coefficients. (The analysis and the synthesis filters typically have the same supports; only the supports of the analysis filters are shown.) The tree

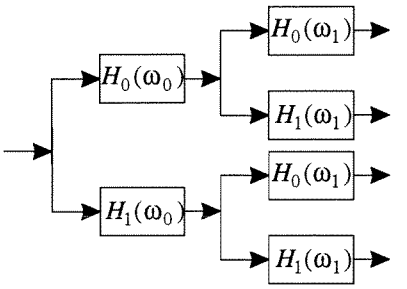

Fig. 1.8. Tree structured filter bank. Splitting of the kth subband.

structure cascade of these two systems yields the four-channel filter bank shown in Fig. 1.9(c).

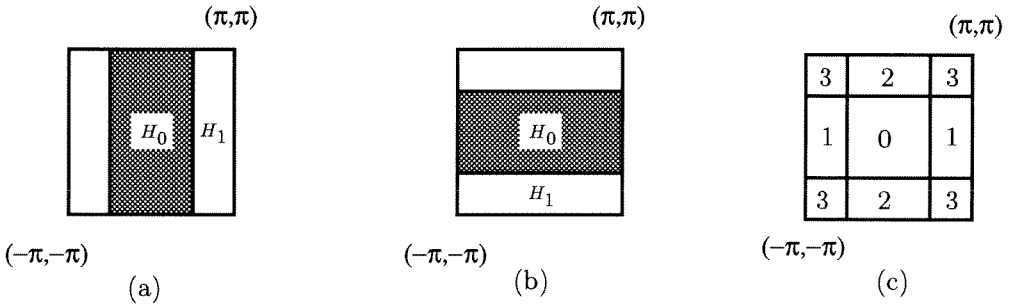

Fig. 1.9. (a) and (b): Two types of two-channel separable filter banks. (c) A four-channel separable filter bank obtained as a tree structure of the systems in (a) and (b).

Nonseparable Filter Banks

For the more general case of nonseparable filter banks, the supports of the analysis and synthesis filters could have a variety of shapes, e.g., parallelepipeds that are not rectangles. The support configuration can be tailored according to the underlying application and gives better coding performance. For example, it is known that the human eyes are less sensitive to high frequency error, especially error at a 45 degree orientation [61]. The two-channel diamond filter bank (configuration as shown in Fig. 1.10) facilitates the incorporation of visual masking model much better than the two-channel separable systems in Fig. 1.9(a) or Fig. 1.9(b). This has been demonstrated by various researchers, e.g., [1, 10]. In directional subband coding applications [4, 41], where directional sensitivity of the filters is important, the use of quadrant filter banks (Fig. 1.10(b)), filter banks with fan filters (Fig. 1.10(c)), or parallelogram filter banks (Fig. 1.10(d)), are preferred to separable filter banks. None of these support configurations, diamond, quadrant, fan or parallelogram, can be achieved by separable filter banks. Although nonseparable filter banks offer more flexibility and usually provide better performance, in most cases their design is considerably more difficult than

separable filter banks. The implementation complexity of nonseparable filter banks is usually also higher.

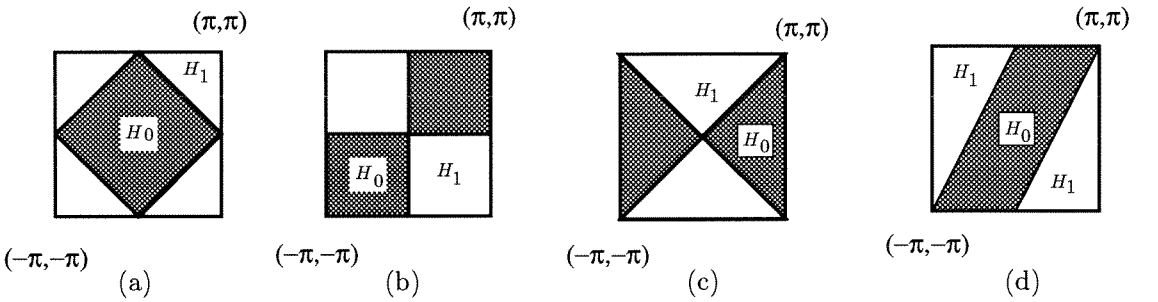

Fig. 1.10. Support configurations of (a) diamond filter bank, (b) quadrant filter bank, (c) fan filter bank and (d) parallelogram filter bank.

Research in the area of MD (multidimensional) filter banks started in 1980s. Some of the earliest contributions were due to Vetterli [102], and Woods and O'Neil [109]. The idea of lattice decimation and expansion is an indispensable aspect of MD multirate systems. An introduction to MD sampling and signal processing can be found in [21]. A more detailed treatment is given in [98]. The theoretical aspects of MD systems are studied in [7]. An excellent tutorial of MD filter banks is given in [108]. Reviews of fundamentals of MD filter banks can be found in [96, 10] and also Chapter 12 of [98]. Results on the commutativity of MD decimators and expanders have been reported in [38, 33, 9, 22, 25]. The Multidimensional Chinese Remainder Theorem for the application of MD FFT is explored in [46]. The relation between filter banks and discrete wavelet transform has been extended to the MD case [13, 39].

Previous Results on the Design of Nonseparable Filter Banks

In the past most of the design techniques for 2D filter banks were for two-channel case (Fig. 1.1 with $|\det \mathbf{M}| = 2$). In particular, the diamond filter bank (Fig. 1.10(a)), first introduced by Vetterli [102], is of special interest in some image coding applications. There is also some interest in the filter bank with quadrant filters as shown in Fig. 1.10(b), [4, 41, 91]. Recently, using 1D to 2D mapping, designs of the diamond filter bank with efficient structures have been reported [35, 70].

For more than two channels case, 2D nonseparable filter banks are considerably more difficult to design than 1D filter banks, various 1D to 2D transformations have been proposed for designing suboptimal 2D filter banks without actually optimizing 2D filters. Two types of transformation have been proposed: In [97], the so-called unimodular transformation is developed. By use of the unimodular transformation, we can convert a 2D separable filter bank to a nonseparable one. The supports of the resulting analysis filters consists of 4 parallelograms Fig. 1.11; the nonseparable filter banks thus obtained constitute a subclass of four-parallelogram filter banks. Another transformation

of 1D filter banks to 2D filter banks is studied by Kalker and Shah [33]. Although in this transformation perfect reconstruction is preserved, characteristics of 1D filters are not faithfully translated. Even if the 1D analysis filters have good stopband attenuation, the 2D analysis and synthesis filters resulting from the transformation may not look like filters at all and subband splitting holds the key to successful subband coding. In [85], a design of nonseparable filter banks is proposed. In this design good filters can be obtained, but the filter bank has perfect reconstruction only for the class of inputs whose frequency supports fall within a certain hexagon.

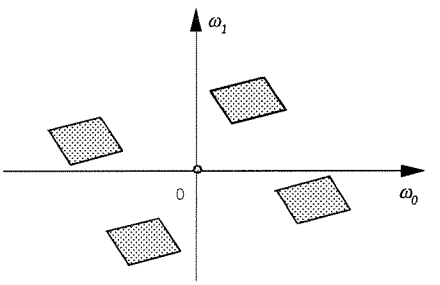

Fig. 1.11. Typical support of a four-parallelogram filter.

On the other hand it has been observed that filter banks with certain support configurations can not have filters with good frequency selectivity. A configuration of this nature is called *nonpermissible* and should be avoided if good filters are desired [11]. The 1D and 2D DFT filter banks are known to be such nonpermissible examples. The notion of permissibility is particularly crucial in designing 2D filter banks. We will discuss this detail in Chapter 4.

2D CMFB and 2D Parallelogram Filter Banks

The success with 1D CMFB motivates us to approach the design of 2D filter bank using cosine modulated concept. The reasons are twofold. First, for a given a support configuration the usual direct design approaches do not work as well as 1D case because of the huge number of parameters to be optimized. The cosine modulation constraint greatly simplifies the problem. Secondly, since 2D processing usually involves massive amount of data, implementation efficiency becomes an important factor in filter bank designs, especially in the nonseparable case. The low complexity advantage of CMFB clearly stands out among all the other possible constructions.

In Chapter 4 and 5 of this thesis we will construct and design 2D CMFB. As parallelograms can form a tiling of the 2D plane, we will use a prototype filter of parallelogram support. Two types of 2D CMFB will be considered: two-parallelogram (*Two-P*) type and four-parallelogram (*Four-P*) type. In *Two-P* CMFB, each analysis filter consists of two copies of the prototype and the support is the

union of two parallelograms (Fig. 1.12(a)). Similarly in *Four-P* each analysis filter consists of four copies of the prototype and the support is the union of four parallelograms (Fig. 1.11). Clearly the *Two-P* and *Four-P* CMFB are subclasses of *Two-P* and *Four-P* filter banks. As a first step towards the design of 2D filter banks, we will identify the necessary ingredients for successful filter bank design and then study in detail such requirements for the classes of *Two-P* and *Four-P* filter banks. We will take a pictorial approach to the general understanding of 2D filter banks based on the experiences with 1D filter bank designs. The *Two-P* and *Four-P* filter banks are then analyzed by exploiting the concept of permissibility. Finally using this analysis, we design the *Two-P* CMFB (Chapter 4) and *Four-P* CMFB (Chapter 5). A brief discussion of these two systems are given in the next section.

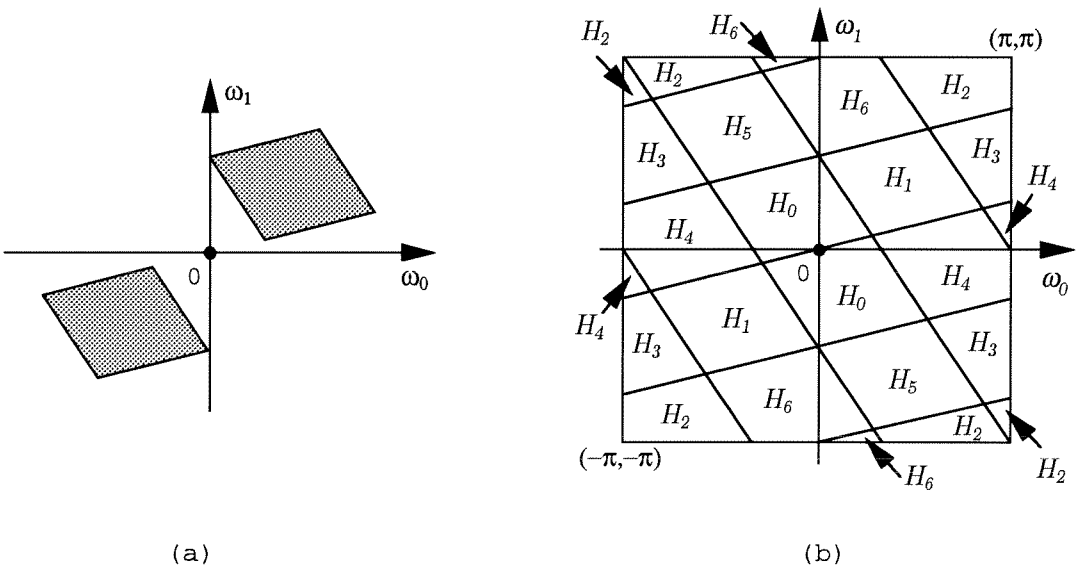

Fig. 1.12. (a) Typical support of a two-parallelogram filter; (b) support configuration of a typical two-parallelogram filter bank.

1.2 Outline and Overview

Outline. A brief review of multidimensional multirate systems and fundamentals of integer matrices pertaining to our discussion are provided in chapter 2. The linear phase cosine modulated filter banks is presented in chapter 3. Chapters 4 and 5 are devoted respectively to two-parallelogram filter banks and four-parallelogram filter banks.

1.2.1 Linear Phase Cosine Modulated Filter Banks (Chapter 3)

We propose a novel way to design maximally decimated FIR cosine modulated filter banks, in which each analysis and synthesis filter has linear phase. The system can be designed to have either the

approximate reconstruction property (pseudo-QMF system) or perfect reconstruction property (PR system). In the PR case, the system is a paraunitary filter bank.

As in earlier work on cosine modulated systems, all the analysis filters come from a FIR prototype filter. However, unlike in any of the previous designs, all but two of the analysis filters have a total bandwidth of $2\pi/M$ rather than π/M in the range $-\pi \leq \omega \leq \pi$ (where $2M$ is the number of channels in our notation). While this implies that these subbands undergo severe aliasing upon decimation by $2M$ (which is the decimation ratio in a maximally decimated system), perfect reconstruction is nevertheless possible. Moreover, in the context of subband coding where the subband signals are quantized (often heavily) we show that considerable coding gain is obtainable in spite of this aliasing. Furthermore a simple interpretation is possible in terms of the complex (hypothetical) analytic signal corresponding to each bandpass subband, and it is shown that this analytic signal *does not undergo severe aliasing* upon decimation by $2M$.

The coding gain of the new system is comparable to that of a traditional M-channel system (rather than a $2M$-channel system). This is primarily because there are typically two bandpass filters with the same passband support. Correspondingly, the cost of the system (in terms of complexity of implementation) is also comparable to that of an M-channel system. We also demonstrate that very good attenuation characteristics can be obtained with the new system. Prototype filter coefficients are tabulated for various number of channels and various levels of stopband attenuation.

1.2.2 Two-P Filter Banks (Chapter 4)

In the construction of 2D filter banks, we have more flexibility in terms of possible configurations. Even if we impose the condition that all the analysis filters have real coefficients and have only two passbands, it is possible to have more than one configuration for a filter bank with decimation matrix $\mathbf{M}$. Various shapes can be used for the passbands of the individual filters, e.g., triangles [31] and parallelograms [47, 48]. In Chapter 4, we study the two-parallelogram (*Two-P*) filter banks, the class of 2D filter banks in which the support of each analysis and synthesis filter is the union of two parallelograms (Fig. 1.12(a)). A typical two-parallelogram filter bank has support configuration as shown in Fig. 1.12(b). This is a natural 2D generalization of the 1D support configuration in Fig. 1.2. For a two-parallelogram filter bank with decimation matrix $\mathbf{M}$ as in Fig. 1.1, we will present the conditions such that the configuration allows good filter design. As the geometry of a *Two-P* filter is of a more intricate nature than 1D bandpass filters, a finer classification of permissibility will be considered.

Two-Parallelogram CMFB. For a filter bank decimation matrix $\mathbf{M}$, non-diagonal in general, we start from a uniform 2D DFT filter bank with twice the number of channels. All the filters in the DFT filter bank are shifted versions of a prototype filter, which has a parallelogram support,

nonseparable in general. The filters in the DFT filter bank are shifted and then paired to obtain real-coefficient analysis filters. Each analysis filter consists of two copies of a real-coefficient prototype (cosine modulated version of the prototype) and is a *Two-P* filter. The synthesis filters have the same spectral supports as the corresponding analysis filters. For a given decimation matrix, we will construct all the possible configurations and study their permissibility. For those satisfying the principle of permissibility, we further constrain the prototype to ensure perfect reconstruction of the two-parallelogram CMFB.

We can conceive that in the more general case of 2D filter banks the individual filters can have any even number of parallelograms. In Chapter 5, we will study the *four-parallelogram (Four-P) filter banks* [48], the 2D filter banks in which the supports of the analysis filters consist of four parallelograms.

1.2.3 Four-P Filter Banks (Chapter 5)

The most commonly used 2D filter banks are separable filter banks, which can be obtained by cascading two 1D filter banks in the form of a tree. The supports of the analysis and synthesis filters in the separable systems are unions of four rectangles, e.g., the four-channel filter bank shown in Fig. 1.9(c). The natural nonseparable generalization of such supports are those that are unions of four parallelograms (Fig. 1.11). In Chapter 5, we study four parallelogram filter banks, the class of two-dimensional filter banks in which the supports of the analysis and synthesis filters consist of four parallelograms. For a given a decimation matrix there could be more than one possible configuration (the collection of passbands of the analysis filters). Various types of configuration will be constructed for four-parallelogram filter banks. Based on the concept of permissibility, conditions on the configurations will be derived such that good design of analysis and synthesis filters are possible. We will see that there is only one category of these filter banks other than some special cases. The configurations of four-parallelogram filter banks in this category can always be achieved by designing filter banks of low design cost.

Note that two-parallelogram filter banks are fundamentally different from 2D separable filter banks obtained from 1D filter banks. But four-parallelogram filter banks will reduce to separable 2D filter bank in special cases.

Chapter 2

A Review of Multidimensional Multirate Systems

The idea of lattice decimation and expansion is crucial for the development of MD (multidimensional) multirate signal processing; integer matrices play an important role in the understanding of MD multirate systems. We will first provide a summary of fundamentals of integer matrices that are relevant to our discussion and then give reviews of MD multirate systems and filter banks. Review on integer matrices and multirate systems can be also found in [10, 96, 98, 108].

2.1 Fundamentals of Integer Matrices

1. *Unimodular matrix.* An integer matrix $\mathbf{U}$ is unimodular if $|\det \mathbf{U}| = 1$.

2. *Notations $FPD(\mathbf{M})$ and $SPD(\mathbf{M})$.* Let $\mathbf{M}$ be a $D \times D$ nonsingular integer matrix. The fundamental parallelepiped $FPD(\mathbf{M})$ generate by $\mathbf{M}$ is defined as

$$FPD(\mathbf{M}) = \left\{ \mathbf{Mx},\ \mathbf{x} \in [0,1)^D \right\}.$$

   The symmetric parallelepiped $SPD(\mathbf{M})$ of $\mathbf{M}$ is defined as

$$SPD(\mathbf{M}) = \left\{ \mathbf{Mx},\ \mathbf{x} \in [-1,1)^D \right\}.$$

3. *Notations $\mathcal{N}(\mathbf{M})$ and $|\mathbf{M}|$.* The notation $\mathcal{N}(\mathbf{M})$ is defined as the set of integer vectors in $FPD(\mathbf{M})$. The number of elements in $\mathcal{N}(\mathbf{M})$ can be shown to be equal to $|\det \mathbf{M}|$, which will be denoted by $|\mathbf{M}|$. In 1D case $D = 1$, and $\mathcal{N}(M) = \{ 0, 1, \ldots, M-1 \}$.

4. *Division theorem for integer vectors.* Let $\mathbf{M}$ be a $D \times D$ matrix and $\mathbf{n}$ be a $D \times 1$ integer vector $\mathbf{n}$. We can express $\mathbf{n}$ as

$$\mathbf{n} = \mathbf{n}_0 + \mathbf{Mk}, \quad \text{where } \mathbf{n}_0 \in \mathcal{N}(\mathbf{M}).$$

Moreover, $\mathbf{n}_0$ and $\mathbf{k}$ are unique. This relation is denoted by

$$\mathbf{n} = \mathbf{n}_0 \bmod \mathbf{M}.$$

5. *Lattices.* The lattice generated by an integer matrix $\mathbf{M}$, denoted by $LAT(\mathbf{M})$, is the set of integer vectors of the form

$$\mathbf{Mn}, \text{ where } \mathbf{n} \text{ is an integer vector .}$$

6. *Cosets.* Using division theorem for integer vectors, we can group all the integer vectors into $|\mathbf{M}|$ sets, called cosets. All the vectors in the same cosets have the same remainder when taking modulo $\mathbf{M}$. When two vectors $\mathbf{n}$ and $\mathbf{m}$ are in the same coset, we will use the notation

$$\mathbf{n} \overset{\mathbf{M}}{=} \mathbf{m}.$$

7. *The Smith form.* A $D \times D$ integer matrix $\mathbf{M}$ can always be factorized as

$$\mathbf{M} = \mathbf{U}\mathbf{\Lambda}\mathbf{V},$$

where $\mathbf{U}$ and $\mathbf{V}$ are unimodular integer matrices and $\mathbf{\Lambda}$ is a diagonal integer matrix,

$$\mathbf{\Lambda} = \begin{pmatrix} \lambda_0 & 0 & \dots & 0 \\ 0 & \lambda_1 & \dots & 0 \\ \vdots & & & \vdots \\ 0 & 0 & \dots & \lambda_{D-1} \end{pmatrix}.$$

Furthermore, we can always ensure that the diagonal elements λ_i are positive integers and λ_{ii} divides $\lambda_{i+1,i+1}$. In this case, $\mathbf{\Lambda}$ is unique and is called the Smith form of $\mathbf{M}$.

2.2 Basics of MD Multirate Systems

Fourier transform and Z-transform. Consider a D dimensional signal $x(\mathbf{n})$, where $\mathbf{n}$ is a $D \times 1$ integer column vector. The Fourier transformation and Z-transform of $x(\mathbf{n})$ will be denoted respectively by $X(\boldsymbol{\omega})$ and $X(\mathbf{z})$; they will be distinguished by the given argument, $\boldsymbol{\omega}$ for Fourier transform and $\mathbf{z}$ for Z-transform. The Fourier transform of $x(\mathbf{n})$ is defined as

$$X(\boldsymbol{\omega}) = \sum_{\mathbf{n} \in \mathcal{Z}^D} x(\mathbf{n}) e^{-j\boldsymbol{\omega}^T \mathbf{n}},$$

where $\boldsymbol{\omega}$ is a $D \times 1$ vector with $\boldsymbol{\omega} = \begin{pmatrix} \omega_0 & \omega_1 & \dots & \omega_{D-1} \end{pmatrix}^T$ and $\mathcal{Z}^D$ is the set of all $D \times 1$ integer vectors. The notations $X(\boldsymbol{\omega})$ and $X(\omega_0, \omega_1, \dots, \omega_{D-1})$ will be used interchangeably. The Z-transform of $x(\mathbf{n})$, where it converges, is given by

$$X(\mathbf{z}) = \sum_{\mathbf{n} \in \mathcal{Z}^D} x(\mathbf{n}) \mathbf{z}^{-\mathbf{n}},$$

where $\mathbf{z} = \begin{pmatrix} z_0 & z_1 & \dots z_{D-1} \end{pmatrix}.^T$ A vector raised to a vector power, as in $\mathbf{z}^{-\mathbf{n}}$ above, gives a scalar quantity defined as

$$\mathbf{z}^{\mathbf{n}} = z_0^{n_0} z_1^{n_1} \dots z_{D-1}^{n_{D-1}}, \quad \mathbf{n} = \begin{pmatrix} n_0 & n_1 & \dots & n_{D-1} \end{pmatrix}^T.$$

Basic Building Blocks: Decimators and Expanders

For a decimator $\downarrow \mathbf{M}$ (Fig. 2.1(a)), the input $x(\mathbf{n})$ and the output $y(\mathbf{n})$ are related by

$$y(\mathbf{n}) = x(\mathbf{M}\mathbf{n}).$$

In the frequency domain, the relation is

$$Y(\boldsymbol{\omega}) = \frac{1}{|\mathbf{M}|} \sum_{\mathbf{k} \in \mathcal{N}(\mathbf{M}^T)} X(\mathbf{M}^{-T}(\boldsymbol{\omega} - 2\pi\mathbf{k})).$$

When $\mathbf{M}$ is a unimodular matrix, i.e., $|\mathbf{M}| = 1$, the output data rate remains the same. The decimator simply rearranges the input data.

Given an expander $\uparrow \mathbf{M}$ (Fig. 2.1(b)), the input $x(\mathbf{n})$ and the output $y(\mathbf{n})$ are related by

$$y(\mathbf{n}) = \begin{cases} x(\mathbf{M}^{-1}\mathbf{n}), & \mathbf{n} \in LAT(\mathbf{M}) \\ \mathbf{0}, & \text{otherwise}. \end{cases}$$

In the frequency domain, the relation is

$$Y(\boldsymbol{\omega}) = X(\mathbf{M}^T \boldsymbol{\omega}).$$

Their Z-transforms are related by $Y(\mathbf{z}) = X(\mathbf{z}^{\mathbf{M}})$, where $\mathbf{z}^{\mathbf{M}}$ is defined as

$$\mathbf{z}^{\mathbf{M}} = \begin{pmatrix} \mathbf{z}^{\mathbf{m}_0} & \mathbf{z}^{\mathbf{m}_1} & \dots & \mathbf{z}^{\mathbf{m}_{D-1}} \end{pmatrix}^T,$$

with $\mathbf{m}_i$ denoting the ith column of $\mathbf{M}$.

Decimation followed by expansion. Consider the concatenation of the M-fold decimator and M-fold

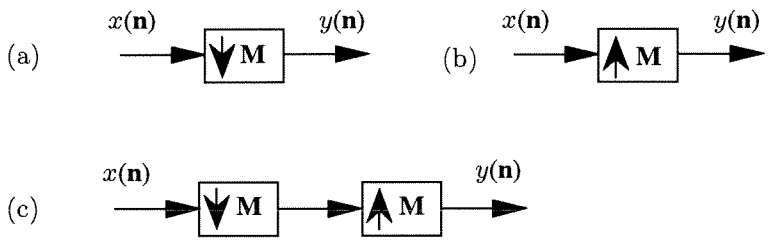

Fig. 2.1. (a) The decimator $\downarrow \mathbf{M}$, (b) the expander $\uparrow \mathbf{M}$ and (c) the decimator follow by expander.

expander in Fig. 2.1(c). The input $x(\mathbf{n})$ and the output $y(\mathbf{n})$ are related by

$$y(\mathbf{n}) = \begin{cases} x(\mathbf{n}), & \mathbf{n} \in LAT(\mathbf{M}) \\ 0, & \text{otherwise} . \end{cases}$$

In the frequency domain, the relation becomes

$$Y(\boldsymbol{\omega}) = \frac{1}{|\mathbf{M}|} \sum_{\mathbf{k} \in \mathcal{N}(\mathbf{M}^T)} X(\boldsymbol{\omega} - 2\pi \mathbf{M}^{-T}\mathbf{k}).$$

The output $Y(\boldsymbol{\omega})$ contains $X(\boldsymbol{\omega})$ and $|\mathbf{M}| - 1$ shifted versions $X(\boldsymbol{\omega} - 2\pi\mathbf{M}^{-T}\mathbf{k})$ (images of $X(\boldsymbol{\omega})$). If $\mathbf{M}$ is unimodular, we have $y(\mathbf{n}) = x(\mathbf{n})$.

Noble identities. Fig. 2.2 shows two useful multirate identities for multidimensional systems. These allow the movement of multirate building blocks across transfer functions under some conditions.

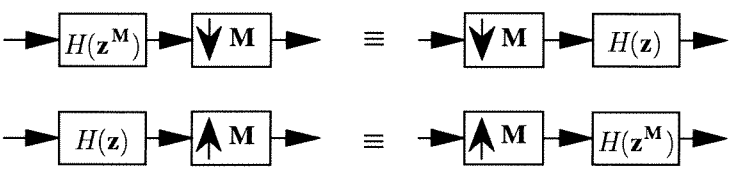

Fig. 2.2. Noble identities for multidimensional decimators and expanders.

Polyphase Decomposition

For a given integer matrix $\mathbf{M}$, we can divide all the integer vectors into $|\mathbf{M}|$ cosets. Thus given a sequence $x(\mathbf{n})$, we can identify $|\mathbf{M}|$ sequences.

$$e_i(\mathbf{n}) = x(\mathbf{M}\mathbf{n} + \mathbf{n}_i), \quad \mathbf{n}_i \in \mathcal{N}(\mathbf{M}).$$

The signals $e_i(\mathbf{n})$ are called the type I polyphase components of $x(\mathbf{n})$. Each polyphase component

contains the samples of $x(\mathbf{n})$ that are in the same coset. These $|\mathbf{M}|$ polyphase components can be obtained from $x(\mathbf{n})$ as shown in Fig. 2.3. Define $y_i(\mathbf{n})$ to be the expanded version of $e_i(\mathbf{n})$, i.e., $y_i(\mathbf{n}) = e_i(\mathbf{n})_{\uparrow \mathbf{M}}$. Then the signal $x(\mathbf{n})$ can be synthesized from the type I polyphase components by $x(\mathbf{n}) = \sum_{i=0}^{|\mathbf{M}|-1} y_i(\mathbf{n} + \mathbf{n}_i)$ as illustrated in Fig. 2.3.

The type II polyphase components of $x(\mathbf{n})$ are defined as

$$r_i(\mathbf{n}) = x(\mathbf{M}\mathbf{n} - \mathbf{n}_i), \quad \mathbf{n}_i \in \mathcal{N}(\mathbf{M}).$$

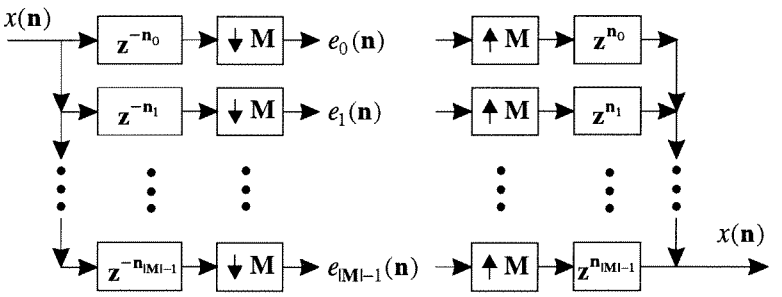

Fig. 2.3. Polyphase decomposition of a signal $x(\mathbf{n})$.

Special Filters

- *Nyquist*(M) *filters.* A filter $H(\boldsymbol{\omega})$ with impulse response $h(\mathbf{n})$ is called Nyquist(M) if $h(\mathbf{M}\mathbf{n})$ has only one nonzero coefficient. In 1D case, if $M = 2$, $H(z)$ is called a halfband filter.

- *Linear and zero-phase filters.* A filter $H(\boldsymbol{\omega})$ is said to have linear phase if

$$H(\boldsymbol{\omega}) = ce^{-j\mathbf{k}^T\boldsymbol{\omega}} H_R(\boldsymbol{\omega}),$$

where $\mathbf{k}$ is a constant vector, c is a scalar (possibly complex) constant and $H_R(\boldsymbol{\omega})$ is a real function. A linear phase filter $H(\boldsymbol{\omega})$ is called zero-phase if $H(\boldsymbol{\omega})$ is a real function. It can be shown that a filter has zero phase if and only if

$$h(\mathbf{n}) = h^*(-\mathbf{n}).$$

2.3 Multidimensional Filter Banks

Consider the MD filter bank in Fig. 2.4. Let $\mathcal{N}(\mathbf{M}^T) = \{ \mathbf{k}_i \}_{i=0}^{|\mathbf{M}|-1}$ and the vector $\mathbf{k}_0 = \mathbf{0}$. The output $\widehat{X}(\boldsymbol{\omega})$ is given by

$$\widehat{X}(\boldsymbol{\omega}) = T(\boldsymbol{\omega})X(\boldsymbol{\omega}) + \sum_{i=1}^{|\mathbf{M}|-1} A_i(\boldsymbol{\omega})X(\boldsymbol{\omega} - 2\pi\mathbf{M}^{-T}\mathbf{k}_i),$$

where $T(\boldsymbol{\omega})$ is the distortion function and $A_i(\boldsymbol{\omega})$ is the aliasing transfer function. The distortion function $T(\boldsymbol{\omega})$ is defined as

$$T(\boldsymbol{\omega}) = \frac{1}{|\mathbf{M}|} \sum_{m=0}^{|\mathbf{M}|-1} H_m(\boldsymbol{\omega})F_m(\boldsymbol{\omega}).$$

The aliasing transfer function $A_i(\boldsymbol{\omega})$ is defined as

$$A_i(\boldsymbol{\omega}) = \frac{1}{|\mathbf{M}|} \sum_{m=0}^{|\mathbf{M}|-1} H_m(\boldsymbol{\omega} - 2\pi\mathbf{M}^{-T}\mathbf{k}_i)F_m(\boldsymbol{\omega}).$$

The MD filter bank is free from aliasing if $A_i(\boldsymbol{\omega}) = 0$, for $i = 1, 2, \cdots, |\mathbf{M}| - 1$. In this case, the filter bank is an LTI (Linear Time Invariant) system. The filter bank has *perfect reconstruction* if it is free from aliasing and the distortion function $T(\boldsymbol{\omega})$ is a delay. In this case, $\widehat{X}(\boldsymbol{\omega})$ is a scaled and delayed version of $X(\boldsymbol{\omega})$. As in 1D filter banks, the perfect reconstruction condition can be interpreted in terms of the polyphase matrices.

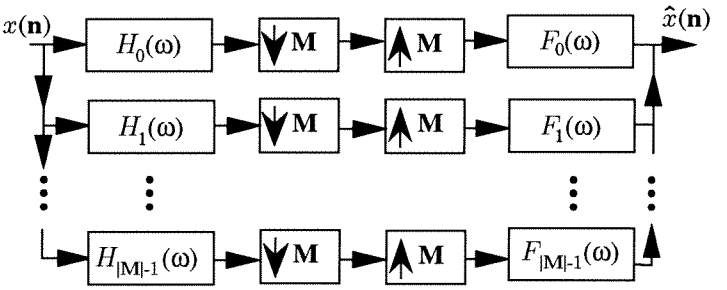

Fig. 2.4. A $|\mathbf{M}|$-channel multidimensional filter bank.

Polyphase Matrices and Paraunitary Filter Banks

Using type I polyphase decomposition for the analysis filters and type II decomposition for the

synthesis filters, we have

$$H_m(\boldsymbol{\omega}) = \sum_{\mathbf{n}_i \in \mathcal{N}(\mathbf{M})} E_{m,i}(\mathbf{M}^T\boldsymbol{\omega}) e^{-j\boldsymbol{\omega}^T \mathbf{n}_i}, \quad m = 0, 1, \ldots, |\mathbf{M}| - 1,$$
$$F_m(\boldsymbol{\omega}) = \sum_{\mathbf{n}_i \in \mathcal{N}(\mathbf{M})} R_{i,m}(\mathbf{M}^T\boldsymbol{\omega}) e^{j\boldsymbol{\omega}^T \mathbf{n}_i}, \quad m = 0, 1, \ldots, |\mathbf{M}| - 1.$$

The $|\mathbf{M}| \times |\mathbf{M}|$ matrices $\mathbf{E}(\boldsymbol{\omega})$ and $\mathbf{R}(\boldsymbol{\omega})$ with $[\mathbf{E}(\boldsymbol{\omega})]_{m,i} = E_{m,i}(\boldsymbol{\omega})$ and $[\mathbf{R}(\boldsymbol{\omega})]_{m,i} = R_{m,i}(\boldsymbol{\omega})$ are respectively called the polyphase matrices for the analysis bank and the synthesis bank. Polyphase implementation of the filter bank is shown in Fig. 2.5(a), which can be efficiently implemented as in Fig. 2.5(b) using noble identities. The MD filter bank has perfect reconstruction if

$$\mathbf{R}(\boldsymbol{\omega})\mathbf{E}(\boldsymbol{\omega}) = \mathbf{I}.$$

The filter bank is paraunitary (or orthonormal) if $\mathbf{E}(\boldsymbol{\omega})$ is a unitary matrix for all $\boldsymbol{\omega}$, i.e.,

$$\mathbf{E}^\dagger(\boldsymbol{\omega})\mathbf{E}(\boldsymbol{\omega}) = \mathbf{I}, \text{ for all } \boldsymbol{\omega}.$$

Perfect reconstruction is trivially satisfied by choosing $\mathbf{R}(\boldsymbol{\omega}) = \mathbf{E}^\dagger(\boldsymbol{\omega})$. In this case, the synthesis filters are given by $F_m(\boldsymbol{\omega}) = H_m^*(\boldsymbol{\omega})$ or $f_m(\mathbf{n}) = h_m^*(-\mathbf{n})$.

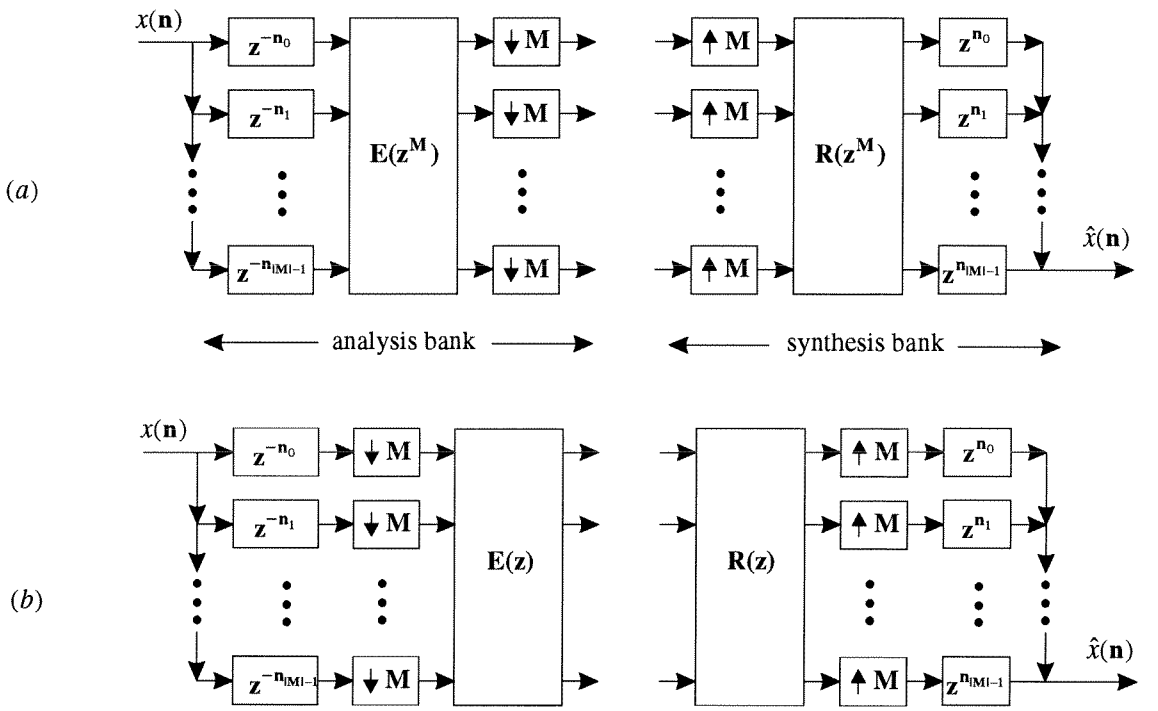

Fig. 2.5. Representation of the analysis and synthesis banks in terms of the polyphase matrices.

Chapter 3

Linear Phase Cosine Modulated Filter Banks

3.1 Introduction

The M-channel maximally decimated cosine modulated filter bank shown in Fig. 1.1 has been studied extensively in the past [18, 86, 104, 94, 98]. When the system in Fig. 1.1 is alias free, it is an LTI system with transfer function $T(z)$, as indicated in Fig. 1.1. $T(z)$ will be called the distortion function or the overall response in the following discussion.

The system in Fig. 1.1 is said to be a cosine modulated filter bank if all analysis and synthesis filters are generated by cosine or sine modulation of one or two prototype filters. Cosine modulated filter banks are well known for their design cost saving and implementation saving. Two types of cosine modulated filter banks have been developed: pseudo QMF systems [66, 79, 12, 62, 15] and perfect reconstruction systems [73, 37, 74, 60, 64, 24]. Unlike a PR system, a pseudo QMF filter bank is only approximately alias free and has approximate reconstruction property (and the approximation improves with filter order).

3.1.1 Previous Work

In [12], Chu mentioned three approaches for designing cosine modulated filter banks with approximate aliasing cancelation. The first one involves designing two prototype filters. The implementation cost for the analysis bank is that of two prototype filters plus cosine and sine modulation. The second method, similar to the one proposed earlier by Rothweiler [79], requires only one prototype filter. Its distortion $T(z)$ has linear phase and approximately flat magnitude response, but individual analysis and synthesis filters do not have linear phase, which is important for image coding applications. The third method, given in [12], needs also only one prototype filter. With this method all the analysis and synthesis filters have linear phase, but the resulting $|T(e^{j\omega})|$ has a peak or a null at zero frequency and at π.

Recently, some cosine modulated maximally decimated systems with perfect reconstruction property have been proposed [73, 37, 74, 60, 64, 24]. In [73], the individual filters in the filter bank have linear phase but the length of the prototype can not be larger than the number of channels. Although the length of the prototype in [37, 74, 60, 64, 24] is not as restricted, the individual analysis and synthesis filters do not have linear phase even if the prototypes have linear phase. In [89], some techniques for characterizing and designing paraunitary linear phase filter banks have been developed, but these are *not* cosine modulated.

In general, the following results are typically desired in a filter bank:

1. *Cancelation of aliasing errors*: Exact or approximate alias cancelation is desired.

2. *Distortion function*: $T(z)$ is exactly or nearly a delay. In particular the magnitude response $|T(e^{j\omega})|$ is required to be flat.

3. *Cosine modulation*: All filters must be cosine modulated versions of a prototype. In this case, only the design of the prototype filter is needed. Besides the implementation cost is only that of the prototype filter plus one DCT matrix working at a decimated rate. For instance, in an M-channel maximally decimated filter bank, the DCT matrix computation is performed after M fold decimators. Design cost and implementation cost are significantly reduced.

4. *Linear phase property of analysis and synthesis filters*: These are desired in image coding applications, when the subbands are heavily quantized. (The nonlinearity of phase of individual filters leads to some artifacts in the reconstructed image.)

5. *Filter length*: If the filters are restricted to be short, they can not have very good attenuation. So the length of the filters should be allowed to be large.

In this chapter, we will show how to achieve all of these properties. (While this work was under preparation, we learnt from Dr. Fliege of Hamburg University that he has developed similar results. See [23] for more details.)

3.1.2 The New System

We propose a novel way to design a cosine modulated filter bank with perfect reconstruction or approximate reconstruction. The set up of this new filter bank is shown in Fig. 3.1. It has $2M$ channels and is maximally decimated. Every analysis and synthesis filter in this system is some cosine modulated version of the same prototype filter. In the approximate reconstruction case, the new filter bank can be designed to be almost alias free. Its overall response, $T(z)$, has approximately flat magnitude response and linear phase. In the PR case aliasing is canceled exactly and $T(z)$ is merely a delay. In both systems, every analysis and synthesis filter has linear phase property.

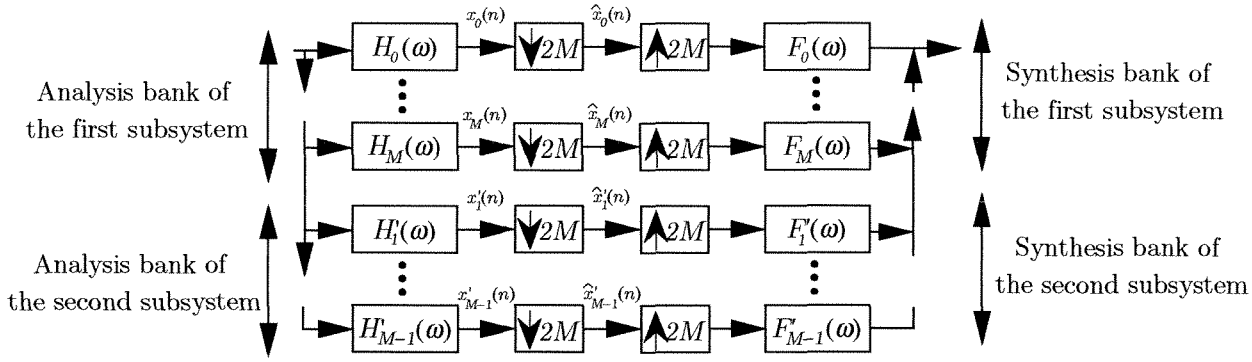

Fig. 3.1. The new set up for derivation of the cosine modulated maximally decimated filter bank.

We would like to regard this filter bank as a connection of two subsystems. The first subsystem has $M+1$ channels and the second subsystem has $M-1$ channels. Fig. 3.2(a) and (b) show, respectively, the magnitude response sketches of analysis filters in the two subsystems. Notice that the second subsystem does not have filters covering zero frequency or π while the first subsystem does. The synthesis filters are time-reversed versions of analysis filters, and therefore have identical magnitude responses.

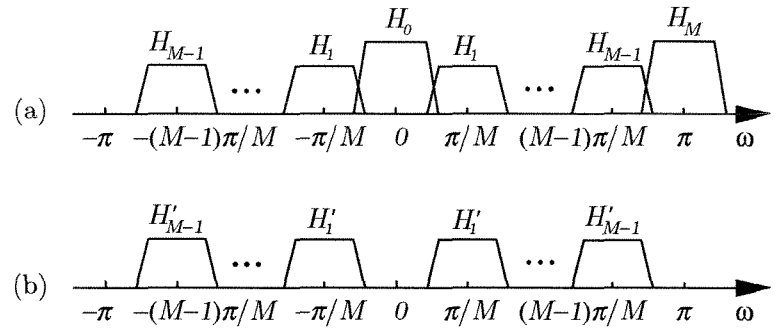

Fig. 3.2. Magnitude responses of the cosine modulated analysis bank filters: (a) the first subsystem; (b) the second subsystem.

In a conventional N-channel maximally decimated cosine modulated PR or approximately PR system, all filters have the same total bandwidth $2\pi/N$ (including positive and negative frequency) and the same height in passband. Their pass-bands do not overlap significantly. When the subband signals are decimated by N, there is no severe aliasing. Aliasing is caused only by the non-ideal nature of the bandpass filters, which have a finite stopband attenuation and nonzero transition bandwidth.

The new system, however, is unusual. As shown in Fig. 3.2(a), $H_k(z)$ and $H_k'(z)$ have the same spectral supports and total bandwidth $2\pi/M$, i.e., two times wider than they are in the traditional case while $H_0(z)$ and $H_M(z)$ have total bandwidth only π/M. Also $H_0(z)$ and $H_M(z)$ have $\sqrt{2}$ times

the height of other filters. In each channel serious aliasing occurs. However, since there is spectral overlapping of the filters in the first and second subsystems, we are able to cancel this aliasing. Cancelation of these aliasing components is possible by judiciously choosing the parameters. The supports of the analysis filters are similar to those given in [73]. In addition, perfect reconstruction is possible with this scheme by imposing certain conditions on polyphase components of the prototype filter.

Furthermore, in conventional N-channel filter banks, each subband signal represents the input signal in that particular subband. In the presence of quantizers in the subbands, bits are allocated based on subband energy. We will explain in Sec. 3.5 that the $2M$-channel cosine modulated filter bank can be interpreted as a modified DFT filter bank. As a result, the subband signals retain the usual meaning and can still be quantized in the usual manner although some filters in the new system have twice the bandwidth of a filter in a typical M-channel filter bank. Detailed discussion is given in Sec. 3.5. An image coding example is included to demonstrate the usefulness of the system.

Although this is a $2M$-channel system, we will show that design cost and implementation cost are equivalent to that of a conventional M-channel maximally decimated cosine modulated filter bank. The coding gain performance is also close to that of an M-channel system.

3.1.3 Chapter Outline and Chapter Specific Notations

This chapter is organized as follows: In Sec. 3.2, we introduce the new maximally decimated linear phase cosine modulated filter bank with approximate reconstruction property. The prototype filter is further constrained in Sec. 3.3 to achieve perfect reconstruction. Necessary and sufficient conditions for PR with this scheme will be given therein. Efficient implementation of this new filter bank is presented in Sec. 3.4. Coding gain and optimal bit allocation of the new system will be discussed in Sec. 3.5. Numerical examples and tables of prototype filter coefficients are given in Sec. 3.6.

Chapter Specific Notations

1. Boldfaced quantities are used to represent matrices. The notations $\mathbf{A}^T$, $\mathbf{A}^*$ and $\mathbf{A}^\dagger$ represent the transpose, conjugate and transpose-conjugate of $\mathbf{A}$. The 'tilde' notation is defined as follows: $\widetilde{\mathbf{A}}(z) = \mathbf{A}^\dagger(1/z^*)$.

2. Matrix $\mathbf{J}_k$ denotes a $k \times k$ reversal matrix with

$$\mathbf{J}_k = \begin{pmatrix} 0 & \dots & 0 & 1 \\ 0 & \dots & 1 & 0 \\ \vdots & & \vdots & \vdots \\ 1 & \dots & 0 & 0 \end{pmatrix}$$

3. The delay chain $\mathbf{e}(z)$ is the vector

$$\mathbf{e}(z) = [1\ z^{-1} \ldots z^{-(M-1)}]^T.$$

4. The unit-pulse, denoted as $\delta(n)$, is defined according to

$$\delta(n) = \begin{cases} 1 & n = 0, \\ 0 & \text{otherwise.} \end{cases}$$

5. The value of the function, $\lceil x \rceil$, is the smallest integer greater or equal to x and the value of the function, $\lfloor x \rfloor$, is the largest integer less or equal to x.

3.2 Linear Phase Cosine Modulated Filter Banks with Approximate Reconstruction

In this section we introduce a new maximally decimated linear phase cosine modulated filter bank with approximate reconstruction property. The system is nearly alias free. Aliasing errors decrease as the stopband attenuation of the prototype increases. The distortion function $T(z)$ has linear phase and approximately flat magnitude response. Every analysis and synthesis filter comes from modulation of the same prototype filter. Furthermore all of them have linear phase.

Consider the $2M$-channel maximally decimated filter bank shown in Fig. 3.1. Suppose prototype filter $P_0(z)$ is of order N and linear-phase. Let

$$U_k(z) = P_0(zW_{2M}^k), \tag{3.1}$$

where $W_{2M} = e^{-j\pi/M}$. In all equations to follow unsubscripted W stands for W_{2M} unless otherwise indicated. Magnitude responses of $P_0(z)$ and $U_k(z)$ are shown in Fig. 3.3. As we can observe from Fig. 3.3, $|U_k(e^{j\omega})|$ is a shift of $|P_0(e^{j\omega})|$ by $k\pi/M$. For $H_k(z)$ to be a cosine modulation of $P_0(z)$, we can choose

$$H_k(z) = a_k U_k(z) + a_k^* U_{-k}(z),$$

for some a_k. Taking a hint from paraunitary perfect reconstruction filter banks, let us constrain

$$F_k(z) = z^{-i_0}\widetilde{H_k}(z), \qquad F_k'(z) = z^{-i_0}\widetilde{H_k'}(z), \tag{3.2}$$

for some i_0. We will show that the choice

$$H'_k(z) = z^{-M}\big(a'_k U_k(z) + a'^*_k U_{-k}(z)\big), \qquad k = 1, 2, \ldots, M-1,$$

for the second set of filters will yield approximate reconstruction for appropriate choice of a'_k to be determined later. To keep $F'_k(z)$ causal, we will take $i_0 = M + N$ in (3.2).

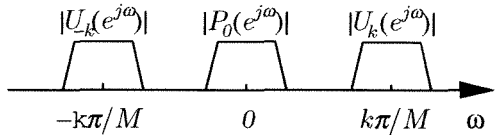

Fig. 3.3. Magnitude responses of $P_0(z)$ and $U_k(z)$.

Summarizing, the filters to be considered in our system will have the form:

$$\begin{aligned}
H_k(z) &= a_k U_k(z) + a^*_k U_{-k}(z), && k = 0, 1, \ldots, M,\\
H'_k(z) &= z^{-M}(a'_k U_k(z) + a'^*_k U_{-k}(z)), && k = 1, 2, \ldots, M-1,\\
F_k(z) &= z^{-(N+M)}\widetilde{H}_k(z), && k = 0, 1, \ldots, M,\\
F'_k(z) &= z^{-(N+M)}\widetilde{H}'_k(z), && k = 1, 2, \ldots, M-1.
\end{aligned} \tag{3.3}$$

We now show that with proper design of $P_0(z)$ and appropriate choices of a_k, a'_k, this filter bank has the following four properties. (1) $|T(e^{j\omega})|$ is approximately flat. (2) $T(z)$ has linear phase. (3) The system is nearly alias free. (4) Every analysis and synthesis filter has linear phase.

(1) Flatness of $|T(e^{j\omega})|$

From [98], we know that the distortion function $T(z)$ of the $2M$-channel system in Fig. 3.1 can be expressed as

$$T(z) = \frac{1}{2M}\left(\sum_{k=0}^{M} H_k(z)F_k(z) + \sum_{k=1}^{M-1} H'_k(z)F'_k(z)\right). \tag{3.4}$$

Assume that nonadjacent bands of $U_k(z)$ do not overlap, i.e.,

$$|U_k(e^{j\omega})U_k(e^{j\omega}W^i)| \approx 0, \; i = 2, \ldots, 2M-2. \tag{3.5}$$

This assumption is reasonable if $P_0(z)$ has stopband edge $\omega_s < \frac{\pi}{M}$ and large enough stopband attenuation. In this case the distortion function becomes

$$T(e^{j\omega}) \approx \frac{z^{-(N+M)}}{2M}\Big(\qquad 4|a_0|^2|U_0(e^{j\omega})|^2 + 4|a_M|^2|U_M(e^{j\omega})|^2$$

$$+\sum_{k=1}^{M-1}\left(|a_k|^2+|a'_k|^2\right)\left(|U_k(e^{j\omega})|^2+|U_{-k}(e^{j\omega})|^2\right)\Big).$$

If we choose $|a_k| = |a'_k| = 1$, for $k = 1, \ldots, M-1$ and

$$a_0 = a_M = \frac{1}{\sqrt{2}}, \tag{3.6}$$

then we have

$$T(e^{j\omega}) \approx \frac{z^{-(N+M)}}{M} \sum_{k=0}^{2M-1} |U_k(e^{j\omega})|^2, \tag{3.7}$$

which can be designed to be nearly flat by optimizing over the filter coefficients of $P_0(z)$ [98].

(2) Linear Phase Property of $T(z)$

Using our constraint that the synthesis filters are time-reversed versions of the corresponding analysis filters, the distortion function assumes the form

$$T(e^{j\omega}) = e^{-j\omega(N+M)}\frac{1}{2M}\left(\sum_{k=0}^{M}|H_k(e^{j\omega})|^2+\sum_{k=1}^{M-1}|H'_k(e^{j\omega})|^2\right),$$

which shows that $T(z)$ has linear phase.

(3) Approximate Alias Cancelation

A $2M$-channel maximally decimated filter bank as in Fig. 3.1 is alias free if all alias transfer functions are zero. The alias transfer function of the ith alias component as defined in [98] is

$$A_i(z) = \frac{1}{2M}\left(\sum_{k=0}^{M} H_k(zW^i)F_k(z) + \sum_{k=1}^{M-1} H'_k(zW^i)F'_k(z)\right). \tag{3.8}$$

We say that the system in Fig. 3.1 is alias free if $A_i(z) = 0$, for $i = 1, 2, \ldots, 2M-1$. With the choice of analysis and synthesis filters in (3.3), we have

$$A_i(z) = \frac{z^{-(N+M)}}{2M}\left(2U_0(zW^i)\widetilde{U}_0(z) + 2U_M(zW^i)\widetilde{U}_M(z) + A_i^{(1)}(z) + A_i^{(2)}(z) + A_i^{(3)}(z) + A_i^{(4)}(z)\right) \tag{3.9}$$

where

$$A_i^{(1)}(z) = \sum_{k=1}^{M-1}(1+W^{-Mi})U_k(zW^i)\widetilde{U}_k(z)$$
$$A_i^{(2)}(z) = \sum_{k=1}^{M-1}(a_k^{*2} + a_k'^{*2}W^{-Mi})U_{-k}(zW^i)\widetilde{U}_k(z)$$
$$A_i^{(3)}(z) = \sum_{k=1}^{M-1}(a_k{}^2 + a_k'{}^2W^{-Mi})U_k(zW^i)\widetilde{U}_{-k}(z)$$

$$A_i^{(4)}(z) = \sum_{k=1}^{M-1}(1 + W^{-Mi})U_{-k}(zW^i)\widetilde{U}_{-k}(z).$$

By appropriate choice of a_0 and a_M and some relation between N and M, we will ensure that $A_i(z) \approx 0$. More specifically, if we choose

$$a_k = 1,\ a'_k = -\sqrt{-1}, \qquad k = 1, 2, \ldots, M-1, \tag{3.10}$$

and

$$N = (2m_0 + 1)M \quad \text{for arbitrary integer } m_0\ , \tag{3.11}$$

and further constrain a_0 and a_M as in (3.6), then we can verify that $A_i(z) \approx 0$ (to be verified in Appendix A). The above values of a_k and a'_k are chosen for simplicity. A more generalized formula can be derived. However, the more generalized expressions for a_k and a'_k do not provide more flexibility in the design of the prototype. They will not be discussed.

(4) Linear Phase Property of Individual Analysis and Synthesis Filters

Having determined the parameters a_k and a'_k, we can write the impulse responses of the analysis and synthesis filters,

$$\begin{aligned}
h_k(n) &= \sqrt{2}p_0(n)\cos(\tfrac{\pi}{M}kn), && k = 0 \text{ or } M,\\
h_k(n) &= 2p_0(n)\cos(\tfrac{\pi}{M}kn), && k = 1, \ldots, M-1,\\
h'_k(n) &= 2p_0(n-M)\sin(\tfrac{\pi}{M}k(n-M)), && k = 1, \ldots, M-1,\\
f_k(n) &= h_k(N+M-n), && k = 0, \ldots, M,\\
f'_k(n) &= h'_k(N+M-n), && k = 1, \ldots, M-1.
\end{aligned} \tag{3.12}$$

By using the linear phase property of $P_0(z)$ and the constraint $N = (2m_0+1)M$ we can verify that every filter above has linear phase. The number of symmetric filters and antisymmetric filters agrees with the result from [89]; in a $2M$-channel linear-phase paraunitary filter bank, M analysis filters are required to be symmetric and the remaining M filters are antisymmetric.

Relation to a Paraunitary System

Having decided the values of a_k and a'_k in (3.3), we can obtain symbolic magnitude responses of $H_k(z)$ and $H'_k(z)$ as in Fig. 3.2. In our formulation, the synthesis filters are constrained to be the time-reversed versions of corresponding analysis filters. Consequently, if the system in Fig. 3.1 is PR, then it is a paraunitary system. In a paraunitary system, every filter has the same energy, i.e., $\sum_n |f_k(n)|^2$ is a constant for all k. But the total bandwidth of $H_0(z)$ and $H_M(z)$ are only half that of all other filters. In order to have about the same energy as the other filters, $|H_0(e^{j\omega})|$ and $|H_M(e^{j\omega})|$ have $\sqrt{2}$ times the heights of other filters. In the derivation of properties (1) and (3), we

need $H_0(z)$ and $H_M(z)$ to have $\sqrt{2}$ times the heights of other filters for aliasing cancelation and flat $|T(e^{j\omega})|$. This is consistent with the equal energy property of filters in paraunitary systems.

It can be verified that when the prototype filter is an ideal brick-wall filter, the system in Fig. 3.1 is indeed a PR system.

Design Cost

An objective function reflecting the non-flatness of $|T(e^{j\omega})|$ in (3.7) and the stop attenuation of $P_0(z)$ is [98]

$$\phi = \alpha \int_0^{\pi/M} \left(|P_0(e^{j\omega})|^2 + |P_0(e^{j(\omega-\frac{\pi}{M})})|^2 - 1\right)^2 d\omega + (1-\alpha) \int_{(\pi/2M)+\epsilon}^{\pi} |P_0(e^{j\omega})|^2 d\omega.$$

The objective function can be minimized by using nonlinear optimization packages (e.g., [72]). The optimization is the same as in the case of traditional M-channel cosine modulated filter banks [98].

Summarizing the results, we have shown that the system in Fig. 3.1 is a cosine modulated maximally decimated filter bank with approximate reconstruction property if the analysis and synthesis filters are chosen as in (3.12), $N = (2m_0 + 1)M$ and the linear-phase prototype $P_0(z)$ is properly designed.

3.3 Linear Phase Cosine Modulated Filter Banks with Perfect Reconstruction

Cosine modulated PR filter banks were reported in [37, 74, 60]. In [37], perfect reconstruction property is achieved by imposing some conditions on the polyphase components of the prototype filter so that the resulting filter bank is paraunitary. We will do something similar on the $2M$-channel system. We will show that the filter bank in Fig. 3.1 with analysis and synthesis filters as in (3.12) is paraunitary and hence PR if the polyphase components of $P_0(z)$ satisfy some conditions to be derived in this section.

Let

$$P_0(z) = \sum_{n=0}^{2M-1} G_n(z^{2M}) z^{-n},$$

where $G_n(z)$ is the nth type 1 polyphase component of $P_0(z)$. Then

$$U_k(z) = \sum_{n=0}^{2M-1} G_n(z^{2M}) z^{-n} W^{-kn}. \tag{3.13}$$

Rewriting analysis filters in (3.3) in terms of polyphase components of $P_0(z)$ with a_k, a'_k and N as

determined in Sec. 3.2, we obtain

$$\begin{aligned} H_k(z) &= 2\sum_{n=0}^{2M-1} G_n(z^{2M}) z^{-n} \cos(\tfrac{\pi}{M} kn), && k = 0, 1, \ldots, M, \\ H'_k(z) &= 2z^{-M} \sum_{n=0}^{2M-1} G_n(z^{2M}) z^{-n} \sin(\tfrac{\pi}{M} kn), && k = 1, 2, \ldots, M-1. \end{aligned} \tag{3.14}$$

Define the following $2M$-component vectors

$$\mathbf{h}(z) = \begin{pmatrix} H_0(z) \\ \vdots \\ H_M(z) \\ H'_1(z) \\ \vdots \\ H'_{M-1}(z) \end{pmatrix}, \quad \text{and} \quad \mathbf{f}(z) = \begin{pmatrix} F_0(z) \\ \vdots \\ F_M(z) \\ F'_1(z) \\ \vdots \\ F'_{M-1}(z) \end{pmatrix}.$$

Using (3.14) the vector $\mathbf{h}(z)$ can be written as

$$\mathbf{h}(z) = \begin{pmatrix} \mathbf{I}_{M+1} & \mathbf{0} \\ \mathbf{0} & z^{-M}\mathbf{I}_{M-1} \end{pmatrix} \begin{pmatrix} \mathbf{C} & \mathbf{\Lambda}_1\mathbf{C} \\ \mathbf{S} & \mathbf{\Lambda}_2\mathbf{S} \end{pmatrix} \begin{pmatrix} \mathbf{g}_0(z^{2M}) & \mathbf{0} \\ \mathbf{0} & \mathbf{g}_1(z^{2M}) \end{pmatrix} \begin{pmatrix} \mathbf{e}(z) \\ z^{-M}\mathbf{e}(z) \end{pmatrix}, \tag{3.15}$$

where $\mathbf{g}_i(z)$ and $\mathbf{\Lambda}_i$ are diagonal matrices with

$$[\mathbf{g}_0(z)]_{kk} = G_k(z), \qquad [\mathbf{g}_1(z)]_{kk} = G_{k+M}(z), \qquad k = 0, 1, \ldots, M-1, \tag{3.16}$$

$$\begin{aligned} [\mathbf{\Lambda}_1]_{kk} &= (-1)^k, && k = 0, 1, \ldots, M, \\ [\mathbf{\Lambda}_2]_{kk} &= (-1)^k, && k = 1, 2, \ldots, M-1. \end{aligned} \tag{3.17}$$

And $\mathbf{C}$ and $\mathbf{S}$ are $(M+1) \times M$ and $(M-1) \times M$ matrices with

$$\begin{aligned} [\mathbf{C}]_{mn} &= \kappa_m \cos(\tfrac{\pi}{M} mn), && m = 0, \ldots, M, \quad n = 0, \ldots, M-1, \\ [\mathbf{S}]_{mn} &= \sin(\tfrac{\pi}{M} mn), && m = 1, \ldots, M-1, \quad n = 0, \ldots, M-1, \end{aligned} \tag{3.18}$$

where

$$\kappa_m = \begin{cases} \frac{1}{\sqrt{2}}, & \text{if } m = 0, M, \\ 1, & \text{otherwise}. \end{cases}$$

We can rearrange (3.15) and obtain

$$\mathbf{h}(z) = \begin{pmatrix} \mathbf{C}\mathbf{g}_0(z^{2M}) & \mathbf{\Lambda}_1\mathbf{C}\mathbf{g}_1(z^{2M}) \\ z^{-2M}\mathbf{\Lambda}_2\mathbf{S}\mathbf{g}_1(z^{2M}) & \mathbf{S}\mathbf{g}_0(z^{2M}) \end{pmatrix} \begin{pmatrix} \mathbf{e}(z) \\ z^{-M}\mathbf{e}(z) \end{pmatrix}. \tag{3.19}$$

The analysis bank has type I polyphase matrix [98] given by,

$$\mathbf{E}(z) = \begin{pmatrix} \mathbf{C}\mathbf{g}_0(z) & \mathbf{\Lambda}_1\mathbf{C}\mathbf{g}_1(z) \\ z^{-1}\mathbf{\Lambda}_2\mathbf{S}\mathbf{g}_1(z) & \mathbf{S}\mathbf{g}_0(z) \end{pmatrix}. \tag{3.20}$$

Since the synthesis filters are time-reversed versions of corresponding analysis filters (3.3), we can write $\mathbf{f}^T(z) = z^{-(N+M)}\widetilde{\mathbf{h}}(z)$. The synthesis bank has type II polyphase matrix given by,

$$\mathbf{R}(z) = z^{-(N+M)}\widetilde{\mathbf{E}}(z). \tag{3.21}$$

From [98] we know if $\mathbf{R}(z)\mathbf{E}(z) = cz^{-n_0}\mathbf{I}$ for some constant c and nonnegative integer n_0, then the system in Fig. 3.1 is PR. By (3.20) and (3.21)

$$z^{N+M}\mathbf{R}(z)\mathbf{E}(z) = \begin{pmatrix} \widetilde{\mathbf{g}}_0(z)\mathbf{C}^T\mathbf{C}\mathbf{g}_0(z) + \widetilde{\mathbf{g}}_1(z)\mathbf{S}^T\mathbf{S}\mathbf{g}_1(z) & \widetilde{\mathbf{g}}_0(z)\mathbf{C}^T\mathbf{\Lambda}_1\mathbf{C}\mathbf{g}_1(z) + z\widetilde{\mathbf{g}}_1(z)\mathbf{S}^T\mathbf{\Lambda}_2\mathbf{S}\mathbf{g}_0(z) \\ \widetilde{\mathbf{g}}_1(z)\mathbf{C}^T\mathbf{\Lambda}_1\mathbf{C}\mathbf{g}_0(z) + z^{-1}\widetilde{\mathbf{g}}_0(z)\mathbf{S}^T\mathbf{\Lambda}_2\mathbf{S}\mathbf{g}_1(z) & \widetilde{\mathbf{g}}_1(z)\mathbf{C}^T\mathbf{C}\mathbf{g}_1(z) + \widetilde{\mathbf{g}}_0(z)\mathbf{S}^T\mathbf{S}\mathbf{g}_0(z) \end{pmatrix}$$

By exploiting the properties of $\mathbf{C}$ and $\mathbf{S}$ and using the same choice of N as in (3.11), we obtain the following equation (Appendix B):

$$\frac{2z^{N+M}}{M}\mathbf{R}(z)\mathbf{E}(z) = \begin{pmatrix} \widetilde{\mathbf{g}}_0 \begin{pmatrix} 2 & \mathbf{0} \\ \mathbf{0} & \mathbf{I}_{M-1} \end{pmatrix} \mathbf{g}_0 + \widetilde{\mathbf{g}}_1 \begin{pmatrix} 0 & \mathbf{0} \\ \mathbf{0} & \mathbf{I}_{M-1} \end{pmatrix} \mathbf{g}_1 & \mathbf{0} \\ \mathbf{0} & \widetilde{\mathbf{g}}_1 \begin{pmatrix} 2 & \mathbf{0} \\ \mathbf{0} & \mathbf{I}_{M-1} \end{pmatrix} \mathbf{g}_1 + \widetilde{\mathbf{g}}_0 \begin{pmatrix} 0 & \mathbf{0} \\ \mathbf{0} & \mathbf{I}_{M-1} \end{pmatrix} \mathbf{g}_0 \end{pmatrix} \tag{3.22}$$

In the above equation $\mathbf{g}_i(z)$ is abbreviated by $\mathbf{g}_i$ for convenience. The right hand side of (3.22) is equal to $2\mathbf{I}_{2M}$ if and only if the following two conditions are true:

$$\text{Condition 1:} \qquad \widetilde{G}_0(z)G_0(z) = 1, \quad \text{and} \quad \widetilde{G}_M(z)G_M(z) = 1. \tag{3.23}$$

$$\text{Condition 2:} \qquad \widetilde{G}_k(z)G_k(z) + \widetilde{G}_{k+M}(z)G_{k+M}(z) = 2, \quad \text{for } k = 1, 2, \ldots, M-1. \tag{3.24}$$

Summarizing, we have the following theorem.

Theorem 3.1 *If the above two conditions are imposed on $G_k(z)$, and furthermore the analysis and synthesis filters are as in (3.12) with the order of the prototype filter chosen as in (3.11), then the $2M$-channel maximally decimated system in Fig. 3.1 has the following properties.*

1. *It is a cosine modulated system.*

2. *It has perfect reconstruction, i.e.,* $\hat{x}(n) = cx(n - n_0)$.

3. *Each of the* $2M$ *analysis and synthesis filters has linear phase.*

4. *The prototype filter* $P_0(z)$ *is Nyquist*$(2M)$ *and* $P_0(z)\widetilde{P}_0(z)$ *is also Nyquist*$(2M)$.

Remark on Theorem 3.1. In the theorem, we have constrained the order of the prototype N to be an odd multiple of M. It can be shown that the theorem can be extended to the case when $N + M$ is even.

Nonzero Samples and Free Parameters of $P_0(z)$

Although $P_0(z)$ is of order N, the number of free parameters in $P_0(z)$ is only about $N/4$ for reasons to be explained below. Notice that with $N = (2m_0 + 1)M$ the first $M + 1$ polyphase components of $P_0(z)$ have order m_0 and the last $M - 1$ polyphase components of $P_0(z)$ have order $m_0 - 1$. Suppose that $G_k(z)$ has impulse response $g_k(n)$. To satisfy (3.24), it can be verified that $g_k(0)$ or $g_k(m_0)$ must be zero for $k = 1, 2, \ldots, M - 1$. From (3.23) we see that $G_0(z)$ and $G_M(z)$ are merely delays, i.e., of the form cz^{-n_0}. The nonzero samples and free parameters of $P_0(z)$ are discussed in two cases: odd M and even M.

Case 1. M **is odd:** Both $G_k(z)$ and $G_{k+M}(z)$, for $k = 1, 2, \ldots, M - 1$ have m_0 nonzero samples. As a result, $P_0(z)$ has $2m_0(M - 1) + 2$ nonzero samples. Since $P_0(z)$ is linear-phase, the polyphase components $G_k(z)$ and G_{M-k}, for $k = 1, 2, \ldots, M - 1$ are time-reversed versions of each other. So are $G_{k+M}(z)$ and G_{2M-k} for $k = 1, 2, \ldots, M - 1$. These constraints reduce the number of free parameters to about $N/2$. But $G_{k+M}(z)$ is also related to $G_k(z)$ by (3.24). The number of free parameters is again cut down by half. The number of free parameters for $P_0(z)$ is only $(M - 1)m_0/2 \approx N/4$.

Case 2. M **is even:** In this case, $G_k(z)$ are constrained as in odd M case with $G_{\frac{M}{2}}(z)$ and $G_{\frac{3M}{2}}(z)$ satisfying additional conditions. By (3.24), $G_{\frac{M}{2}}(z)$ and $G_{\frac{3M}{2}}(z)$ form a power complementary pair and they both have linear phase because $P_0(z)$ is linear-phase. As a result, $G_{\frac{M}{2}}(z)$ and $G_{\frac{3M}{2}}(z)$ are further constrained in the following.

$$\begin{aligned} \text{even } m_0\text{:} \quad & \widetilde{G}_{\frac{M}{2}}(z)G_{\frac{M}{2}}(z) = 2, \quad \text{and} \quad G_{\frac{3M}{2}}(z) = 0, \\ \text{odd } m_0\text{:} \quad & G_{\frac{M}{2}}(z) = 0 \quad \text{and} \quad \widetilde{G}_{\frac{3M}{2}}(z)G_{\frac{3M}{2}}(z) = 2. \end{aligned}$$

In the even M case $P_0(z)$ has $2m_0(M - 2) + 1$ nonzero samples and free parameters $\frac{M-2}{2}m_0$, which is equal to the total number of parameters for $M - 1$ case and is also close to $N/4$. So when

we increase the number of channels from $2(M-1)$ to $2M$ (where $M-1$ is odd), the number of free parameters for $P_0(z)$ does not increase.

Design Complexity

Since the system in this case is PR, it is sufficient to minimize the stopband energy of the prototype filter under the two conditions in (3.23) and (3.24). This is similar to the case of traditional M-channel cosine modulated filter banks [98].

3.4 Efficient Implementation of the Linear Phase Cosine Modulated Filter Bank

The implementation cost of a conventional M-channel maximally decimated cosine modulated filter bank is that of the prototype filter plus one DCT matrix working at M-fold decimated rate [98]. We will show that the proposed $2M$-channel linear phase cosine modulated system in Fig. 3.1 has nearly the same cost, i.e., number of computations per input sample is nearly the same. The implementation proposed here can be applied to both the approximate PR case (Sec. 3.2) and the PR case (Sec. 3.3).

Define two $M \times 2M$ matrices

$$\mathbf{T}_1 = \begin{pmatrix} \mathbf{C} & \mathbf{\Lambda}_1\mathbf{C} \end{pmatrix} \qquad \text{and} \qquad \mathbf{T}_2 = \begin{pmatrix} \mathbf{S} & \mathbf{\Lambda}_2\mathbf{S} \end{pmatrix},$$

where $\mathbf{C}$, $\mathbf{S}$, $\mathbf{\Lambda}_1$, and $\mathbf{\Lambda}_2$ are as defined in (3.17) and (3.18). From (3.15), we can draw Fig. 3.4, the implementation of the $2M$-channel cosine modulated system. The input to $\mathbf{T}_1$, $\mathbf{a}(n)$, is partitioned according to

$$\mathbf{a}(n) = \begin{pmatrix} \mathbf{a}_1(n) \\ \mathbf{a}_2(n) \end{pmatrix}.$$

Similarly, $\mathbf{b}(n)$, the input vector to $\mathbf{T}_2$, is partitioned as

$$\mathbf{b}(n) = \begin{pmatrix} \mathbf{b}_1(n) \\ \mathbf{b}_2(n) \end{pmatrix}.$$

The vectors $\mathbf{a}_1(n)$, $\mathbf{a}_2(n)$, $\mathbf{b}_1(n)$, and $\mathbf{b}_2(n)$ are all of dimension $M \times 1$. Their dependence on n will be dropped for convenience. As indicated in Fig. 3.4 outputs of $\mathbf{T}_1$ and $\mathbf{T}_2$ are $\mathbf{d}_1$ and $\mathbf{d}_2$, respectively.

$$\mathbf{d}_1 = \mathbf{T}_1\mathbf{a}, \qquad \text{and} \qquad \mathbf{d}_2 = \mathbf{T}_2\mathbf{b}.$$

They can also be expressed in terms of $\mathbf{a}_1$, $\mathbf{a}_2$, $\mathbf{b}_1$ and $\mathbf{b}_2$ as (Appendix C)

$$\mathbf{d}_1 = \mathbf{C}\left(\mathbf{a}_1 + \begin{pmatrix} 0 & \mathbf{0} \\ \mathbf{0} & \mathbf{J}_{M-1} \end{pmatrix}\mathbf{a}_2\right) + \sqrt{2}[\mathbf{a}_2]_0\,\mathbf{r}, \quad \mathbf{d}_1 = \mathbf{S}\left(\mathbf{b}_1 - \begin{pmatrix} 0 & \mathbf{0} \\ \mathbf{0} & \mathbf{J}_{M-1} \end{pmatrix}\mathbf{b}_2\right), \tag{3.25}$$

where $[\mathbf{a}_2]_0$ is the 0th element of $\mathbf{a}_2$, and $\mathbf{r}$ is $\sqrt{\frac{M}{2}}$ the last column of $\mathbf{C}$. From (3.25), we observe that the major computation in $\mathbf{T}_1$ is only the matrix $\mathbf{C}$ and the major computation in $\mathbf{T}_2$ is the matrix $\mathbf{S}$. Matrices $\mathbf{C}$ and $\mathbf{S}$ can be implemented by fast algorithms for DCT and DST matrices [77]. But both computations are done after $2M$-fold decimation, which is equivalent to computing *one* matrix after M-fold decimation. That is the same as the case in a conventional M-channel maximally decimated cosine modulated filter bank [98]. The implementation of synthesis bank is similar.

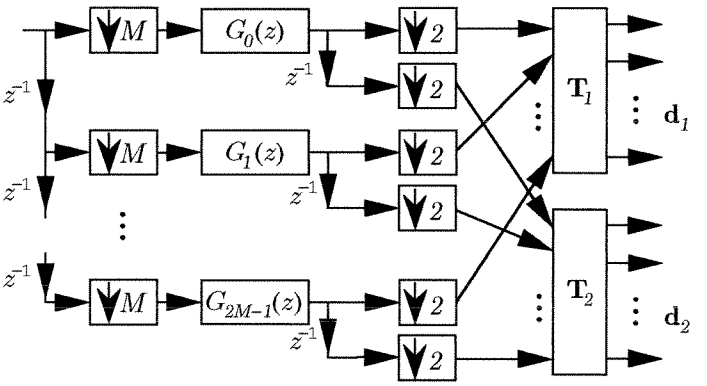

Fig. 3.4. Implementation of the $2M$-channel system. Both T_1 and T_2 in the figure are of dimension $2M$ by M.

Notice that quantization of filter coefficients will not affect the relation that $G_k(z)$ is the time-reversed version of $G_{M-k}(z)$, for $k = 1, 2, \ldots, M-1$. Similarly for $G_{2M-k}(z)$ and $G_{k+M}(z)$, for $k = 1, 2, \ldots, M-1$. We conclude that the linear phase property of the individual analysis and synthesis filters is preserved in spite of filter coefficient quantization.

3.5 Subband Signals, Coding Gain, and Optimal Bit Allocation

In a traditional N-channel subband coding system, the output $x_k(n)$ of the kth analysis filter has total bandwidth $2\pi/N$ in $[-\pi, \pi)$ and is decimated by N. This decimation does not cause aliasing except for the reason that the analysis filters are not ideal bandlimiting functions and cannot have

infinitely sharp roll-off. This aliasing created due to practical limitations of filters is canceled by the choice of synthesis filters.

In the $2M$-channel maximally decimated system of Fig. 3.1, however, the situation is very unusual. Each analysis filter has a total bandwidth of $2\pi/M$ in $[-\pi, \pi)$ [except $H_0(z)$ and $H_M(z)$] and yet its output is decimated by $2M$. This means there will be severe aliasing even if the filters were ideal bandpass filters. Even this aliasing is cancelled by appropriate choice of synthesis filters, as already proved in the preceding sections in this chapter.

In the context of subband quantization and coding, one wonders how this system would perform: with such severe aliasing in the subbands, would it still be possible to obtain the usual coding gain advantage? That is, would it still be possible to exploit the energy distribution of the original input signal $x(n)$ in the usual way? In short, does the proposed filter bank scheme make sense as a subband coder? We now look deeper into this important aspect.

3.5.1 An Interpretation of the Subband Signals

To explain this, consider the filter bank in Fig. 3.1. Suppose $x(n)$ is the input. Let $x_k(n)$ and $x'_k(n)$ denote the outputs of $H_k(z)$ and $H'_k(z)$ respectively, as in Fig. 3.5(a). With the filters constructed as in (3.12), we obtain

$$X_k(z) = X(z)\big(U_k(z) + U_{-k}(z)\big), \qquad k = 0, 1, \ldots, M \tag{3.26}$$

$$X'_k(z) = z^{-M}X(z)\big(-jU_k(z) + jU_{-k}(z)\big), \qquad k = 1, 2, \ldots, M-1, \tag{3.27}$$

where $j = \sqrt{-1}$. With (3.26) and (3.27), we get the following expression

$$2z^{-M}X(z)U_k(z) = z^{-M}X_k(z) + jX'_k(z), \quad k = 1, \ldots, M-1. \tag{3.28}$$

If we take a real signal $x(n)$ as the input of the complex coefficient filter $2z^{-M}U_k(z)$, then the output is the right hand side of (3.28). The output represents the energy of $x(n)$ in the $U_k(z)$ subband (Fig. 3.3). From (3.28), we observe that the output of $2U_k(z)$ has real part $x_k(n)$ and imaginary part $x'_k(n+M)$. Fig. 3.5(b) illustrates this relation.

Thus, except for delays and scale factors, the signals $x_k(n)$ and $x'_k(n)$ can be interpreted as the real and imaginary parts of the one-sided (hypothetical) complex subband signal $y_k(n)$ (which is analogous to the analytic signal of $x_k(n)$ [75]). So $x_k(n)$ and $x'_k(n+M)$ together retain the usual meaning of subband signals. From the fact that $H_k(z)$ and $H'_k(z)$ have the same spectral occupancy (Fig. 3.2) we see that the energies of $x_k(n)$ and $x'_k(n)$ are essentially the same. These in turn are proportional to the energy of the hypothetical complex subband signal $y_k(n)$. The decimation of $x_k(n)$ and $x'_k(n)$ by $2M$ is equivalent to decimating $y_k(n)$ by $2M$. Because $y_k(n)$ has bandwidth

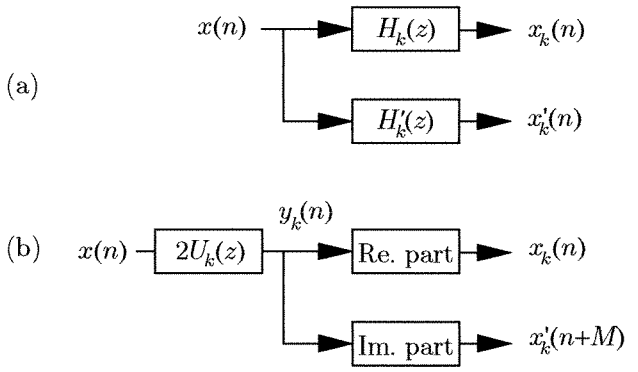

Fig. 3.5. An interpretation of $x_k(n)$ and $x'_k(n+M)$, for $k = 1, 2, \ldots, M-1$.

$2\pi/2M$, the decimation of $y_k(n)$ by $2M$ does not lead to severe aliasing other than due to usual filter non ideality. So even though the decimation of the subband signals in Fig. 3.1 creates severe aliasing, it still makes sense to quantize and encode the decimated signals based on the energy distributions of the undecimated signals. In Sec. 3.6, we provide an image coding example (Example 3.2), which shows that subband quantization and reconstruction work in the usual way. We now proceed to give the quantitative details.

3.5.2 Coding Gain

In Sec. 3.3 the type I polyphase matrix of the analysis bank is constrained to be paraunitary, i.e., $\widetilde{\mathbf{E}}(z)\mathbf{E}(z) = cz^{-n_0}\mathbf{I}$, so that the system in Fig. 3.1 is PR. The resulting new cosine modulated filter bank with perfect reconstruction falls into the category of paraunitary filter banks. The coding gain and optimal bit allocation for paraunitary systems can be found in [100].

Suppose that the real input signal $x(n)$ has power spectral density $S_{xx}(\omega)$ and variance σ_x^2. Let $\sigma_{x_k}^2$ be the variance of $x_k(n)$ and $\sigma_{x'_k}^2$ be the variance of $x'_k(n)$.

$$\sigma_{x_k}^2 = \frac{1}{2\pi}\int_0^{2\pi} S_{xx}(\omega)|H_k(e^{j\omega})|^2 d\omega \tag{3.29}$$

$$\sigma_{x'_k}^2 = \frac{1}{2\pi}\int_0^{2\pi} S_{xx}(\omega)|H'_k(e^{j\omega})|^2 d\omega \tag{3.30}$$

A $2M$-channel paraunitary filter bank in Fig. 3.1, has coding gain G_{2M} [100],

$$G_{2M} = \frac{\sigma_x^2}{\left(\prod_{k=0}^{M}\sigma_{x_k}^2 \prod_{k=1}^{M-1}\sigma_{x'_k}^2\right)^{1/2M}} \tag{3.31}$$

Assume that the prototype filter $P_0(z)$ has large enough stopband attenuation and $U_k(z)$ and $U_{-k}(z)$ do not overlap in passbands, i.e., $|U_k(e^{j\omega})U_{-k}(e^{j\omega})| \approx 0$ (see Fig. 3.3). From (3.29) and (3.30), we have

$$\sigma_{x_k}^2 \approx \sigma_{x_k'}^2, \qquad k = 1, 2, \ldots, M-1.$$

Eq. (3.31) then becomes

$$G_{2M} \approx \frac{\sigma_x^2}{\left(\sigma_{x_0}^2 \sigma_{x_M}^2\right)^{1/2M} \left(\prod_{k=1}^{M-1} \sigma_{x_k}^2\right)^{1/M}}$$

which is closer to the coding gain of M-channel rather than $2M$-channel paraunitary systems.

3.5.3 Optimal Bit Allocation

In a conventional M-channel filter bank with quantizers in the subbands, bits are allocated according to the energy of subband signals [98]. Let $\widehat{x}_k(n)$ and $\widehat{x}_k'(n)$ be decimated signals of $x_k(n)$ and $x_k'(n)$. Since decimators do not change signal variances, we have $\sigma_{\widehat{x}_k}^2 = \sigma_{x_k}^2$ and $\sigma_{\widehat{x}_k'}^2 = \sigma_{x_k'}^2$. Allocating bits according to $\sigma_{\widehat{x}_k}^2$ and $\sigma_{\widehat{x}_k'}^2$ is equivalent to allocating bits according to $\sigma_{x_k}^2$ and $\sigma_{x_k'}^2$, which represent the energy of the the subband signals. So the idea of optimal bit allocation in this $2M$-channel system is the same as the conventional case.

In the approximate PR case, if we ignore the residual aliasing and reconstruction errors, we can use the above formula for coding gain and optimal bit allocation.

3.6 Numerical Examples and Tables of Prototype Filter Coefficients

We now present two design examples. This will be followed by tables of prototype filter coefficients for the PR case.

All of them are obtained by using nonlinear optimization programs in [72].

Example 3.1. *Approximately PR system with $M = 7$, i.e., fourteen channels.* The prototype filter has order $N = 49$, stopband attenuation 39 dB and stopband edge $\omega_s = 0.133\pi$. Fig. 3.6(a) and (b) show, respectively, magnitude responses of the first set of analysis filters and the second set of analysis filters. (In Fig. 3.6(a) magnitude responses are all normalized with maximum value of 0 dB.) Fig. 3.6(c) is a plot of aliasing error $\sqrt{\sum_{i=1}^{i=2M-1} |A_i(e^{j\omega})|^2}$. Aliasing error is suppressed satisfactorily; worst peak aliasing error is very small, only about 0.0013. We can see from Fig. 3.6(d) that the amplitude distortion function is approximately flat with peak amplitude distortion 0.02.

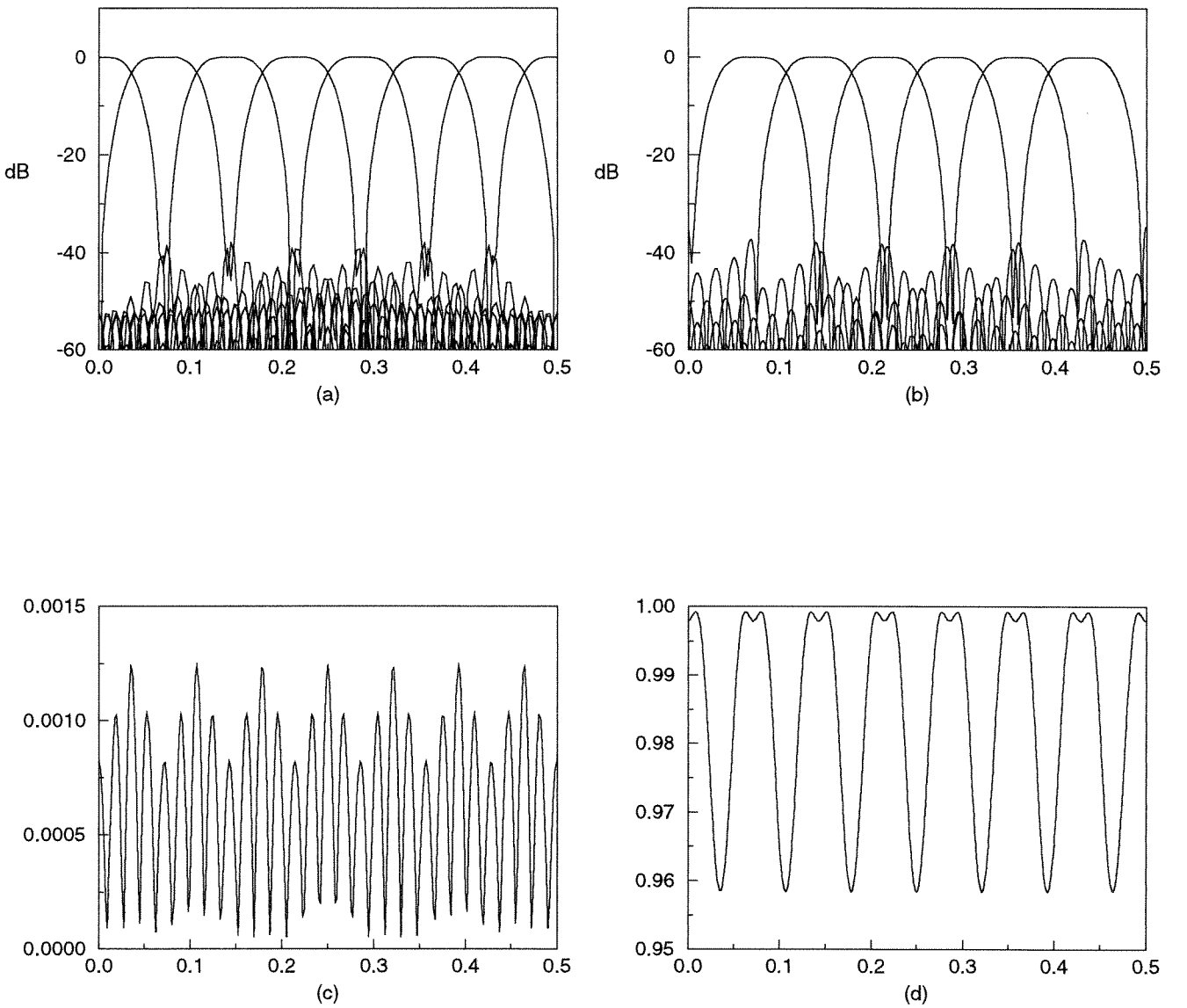

Fig. 3.6. Example 3.1. Approximate PR system: (a) Normalized magnitude responses of the first set of analysis filter; (b) magnitude responses of the second set of analysis filters; (c) plot of aliasing error $\left(\sum_{i=1}^{2M-1} |A_i(e^{j\omega})|^2\right)^{1/2}$; (d) plot of amplitude distortion function, $M|T(e^{j\omega})|$.

Example 3.2. *Image coding.* For this, a two-dimensional separable filter bank is used, which is based on the one-dimensional example above. We apply the separable filter bank on the 512×512 picture "Lenna." The original image with 8 bits/pixel is shown in Fig. 3.7(a). Bit allocation and entropy coding are performed in the subbands. The reconstructed image shown in Fig. 3.7(b) has a subband bit rate of 0.35 bit/pixel. The peak signal to noise ratio (PSNR) is 35.5 dB.

$$\text{PSNR} \triangleq 10\log_{10}\frac{(\text{peak-to-peak value of the original image})^2}{\text{MSE}},$$

where MSE is the mean square error of the reconstructed image. We notice that the reconstruction quality is very good and shows no artifacts due to the excess passband width discussed at the beginning of Sec. 3.5.

Example 3.3. *PR system with $M = 19$, i.e., thirty eight channels.* The prototype $P_0(z)$ in this example is of order 133. Following the discussion in Sec. 3.3, the number of nonzero samples of $P_0(z)$ is 110. It has stopband attenuation 40 dB and stopband edge ω_s 0.06π. Fig. 3.8 (a)-(b) show, respectively, normalized magnitude responses of the first set of analysis filters and the second set of analysis filters.

In both of these examples, the analysis filters have linear phase by construction, so we have not shown the phase responses. In the second example the system has PR property by construction so we have not shown any aliasing error or the magnitude response of the distortion function.

Tables of Prototype Filter Coefficients for Perfect Reconstruction

We list two groups of filter banks. Only the coefficients of the prototype filters $p_0(n)$ are listed. The filters in the first group are of order $N = 3M$ (where the meaning of M is the same as in Fig. 3.1) . The filters in the second group has order $N = 7M$. The prototype filters are linear-phase; only the first half of the coefficients are shown. From the coefficients of the prototype $P_0(z)$ we can find the coefficients of all analysis and synthesis filters using (3.12).

1. Filters with order $3M$. Prototype filter coefficients $p_0(n)$ are listed in Table 3.1. Filters in this group have stopband attenuation $A_s \approx 25$ dB.

2. Filters with order $7M$. Prototype filter coefficients $p_0(n)$ are listed in Table 3.2. Filters in this group have $A_s \approx 40$ dB.

Notice that in Tables 3.1 and 3.2 every prototype filter starts with $\lceil \frac{M+1}{2} \rceil$ zeros. The notation $\lceil\ \rceil$ and the notation $\lfloor\ \rfloor$ to be used later are defined in Sec. 3.1. Those zeros at the beginning of the prototype filters are the result of optimization. As indicated in Sec. 3.3, $g_k(0)$ or $g_k(m_0)$ must be zero for $k = 1, 2, \ldots, M-1$, where $g_k(n)$ is the kth polyphase component of $p_0(n)$. After optimization, we found that it is best to choose

(a)

(b)

Fig. 3.7. Example 3.2. An image coding example with the linear phase subband coder design in Example 3.1: (a) Image of "Lenna" with 8 bits/pixel; (b) reconstructed version from subbands with PSNR 35.5 dB and the subband bit rate 0.35 bit/pixel (bit allocation followed by entropy coding).

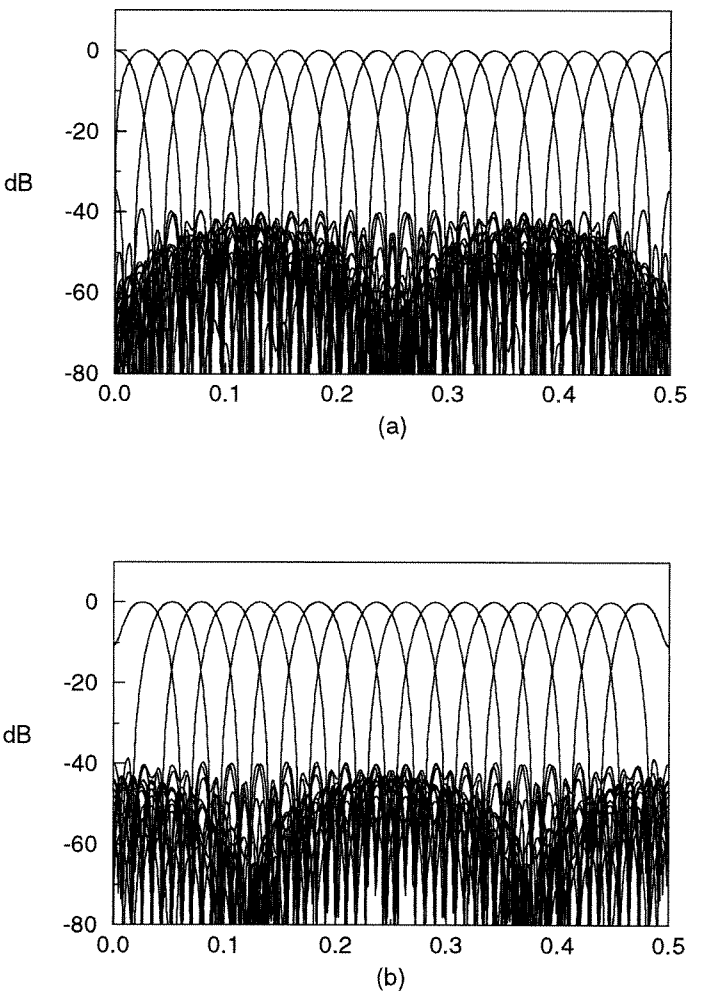

Fig. 3.8. Example 3.3. Cosine modulated PR system: (a) Normalized magnitude responses of the first set of analysis filters: (b) magnitude responses of the second set of analysis filters.

n	M=7	M=8	M=9	M=11	M=13	M=15
0	0.0000000E+00	0.0000000E+00	0.0000000E+00	0.0000000E+00	0.0000000E+00	0.0000000E+00
1	0.0000000E+00	0.0000000E+00	0.0000000E+00	0.0000000E+00	0.0000000E+00	0.0000000E+00
2	0.0000000E+00	0.0000000E+00	0.0000000E+00	0.0000000E+00	0.0000000E+00	0.0000000E+00
3	0.0000000E+00	0.0000000E+00	0.0000000E+00	0.0000000E+00	0.0000000E+00	0.0000000E+00
4	1.8732471E−02	0.0000000E+00	0.0000000E+00	0.0000000E+00	0.0000000E+00	0.0000000E+00
5	3.5665461E−02	1.8383085E−02	1.3193124E−02	0.0000000E+00	0.0000000E+00	0.0000000E+00
6	5.6870395E−02	3.2890536E−02	2.2634022E−02	1.0140769E−02	0.0000000E+00	0.0000000E+00
7	7.8559943E−02	5.1283753E−02	3.4499846E−02	1.6130896E−02	8.2246300E−03	0.0000000E+00
8	9.5441539E−02	7.0416880E−02	4.7970428E−02	2.3511272E−02	1.2364566E−02	6.8684742E−03
9	1.0522026E−01	8.5364224E−02	6.1201399E−02	3.2084683E−02	1.7353344E−02	9.8544667E−03
10	1.0950993E−01	9.3996206E−02	7.2042075E−02	4.1267157E−02	2.3139003E−02	1.3401593E−02
11		9.7873062E−02	7.9378732E−02	5.0105611E−02	2.9520914E−02	1.7506612E−02
12		9.9584507E−02	8.3539952E−02	5.7603527E−02	3.6116001E−02	2.2101899E−02
13			8.5540423E−02	6.3180042E−02	4.2403735E−02	2.7027928E−02
14				6.6845827E−02	4.7872622E−02	3.2028343E−02
15				6.8999556E−02	5.2198363E−02	3.6784105E−02
16				7.0130659E−02	5.5323955E−02	4.0991781E−02
17					5.7402221E−02	4.4448081E−02
18					5.8679392E−02	4.7091898E−02
19					5.9401254E−02	4.8986318E−02
20						5.0264681E−02
21						5.1078668E−02
22						5.1565152E−02

n	M=16	M=17	M=19	M=21	M=24
0	0.0000000E+00	0.0000000E+00	0.0000000E+00	0.0000000E+00	0.0000000E+00
1	0.0000000E+00	0.0000000E+00	0.0000000E+00	0.0000000E+00	0.0000000E+00
2	0.0000000E+00	0.0000000E+00	0.0000000E+00	0.0000000E+00	0.0000000E+00
3	0.0000000E+00	0.0000000E+00	0.0000000E+00	0.0000000E+00	0.0000000E+00
4	0.0000000E+00	0.0000000E+00	0.0000000E+00	0.0000000E+00	0.0000000E+00
5	0.0000000E+00	0.0000000E+00	0.0000000E+00	0.0000000E+00	0.0000000E+00
6	0.0000000E+00	0.0000000E+00	0.0000000E+00	0.0000000E+00	0.0000000E+00
7	0.0000000E+00	0.0000000E+00	0.0000000E+00	0.0000000E+00	0.0000000E+00
8	0.0000000E+00	0.0000000E+00	0.0000000E+00	0.0000000E+00	0.0000000E+00
9	−7.0567914E−03	5.9379618E−03	0.0000000E+00	0.0000000E+00	0.0000000E+00
10	−9.9461336E−03	8.2342790E−03	5.1904905E−03	0.0000000E+00	0.0000000E+00
11	−1.3300380E−02	1.0910574E−02	6.9789570E−03	4.6321577E−03	0.0000000E+00
12	−1.7161896E−02	1.3968583E−02	9.0403012E−03	6.0823399E−03	0.0000000E+00
13	−2.1408026E−02	1.7380301E−02	1.1381438E−02	7.7328479E−03	4.0860508E−03
14	−2.5932379E−02	2.1075551E−02	1.3993922E−02	9.5890298E−03	5.3841990E−03
15	−3.0482434E−02	2.4932616E−02	1.6846952E−02	1.1647991E−02	6.8056680E−03
16	−3.4808738E−02	2.8784655E−02	1.9880926E−02	1.3894873E−02	8.3809124E−03
17	−3.8653819E−02	3.2440869E−02	2.3005024E−02	1.6299068E−02	1.0060428E−02
18	−4.1842661E−02	3.5724832E−02	2.6102687E−02	1.8811663E−02	1.1857825E−02
19	−4.4328241E−02	3.8512137E−02	2.9045232E−02	2.1365729E−02	1.3719700E−02
20	−4.6138550E−02	4.0750965E−02	3.1715938E−02	2.3880869E−02	1.5641153E−02
21	−4.7396165E−02	4.2458746E−02	3.4029691E−02	2.6272669E−02	1.7568068E−02
22	−4.8211730E−02	4.3700099E−02	3.5944399E−02	2.8464194E−02	1.9479842E−02
23	−4.8718561E−02	4.4562085E−02	3.7462398E−02	3.0397564E−02	2.1328626E−02
24	−4.9226990E−02	4.5133321E−02	3.8618922E−02	3.2041030E−02	2.3085849E−02
25		4.5492424E−02	3.9467884E−02	3.3389319E−02	2.4718467E−02
26			4.0068990E−02	3.4459233E−02	2.6200165E−02
27			4.0478947E−02	3.5282156E−02	2.7518646E−02
28			4.0746900E−02	3.5896473E−02	2.8657760E−02
29				3.6341565E−02	2.9625711E−02
30				3.6653941E−02	3.0418824E−02
31				3.6865287E−02	3.1059631E−02
32					3.1554290E−02
33					3.1931110E−02
34					3.2201293E−02
35					3.2391621E−02
36					3.2648321E−02

Table 3.1. The prototype filters with stopband attenuation about 25 dB and order $3M$.

n	M=7	M=9	M=11	M=13	M=15	M=17
0	0.0000000E+00	0.0000000E+00	0.0000000E+00	0.0000000E+00	0.0000000E+00	0.0000000E+00
1	0.0000000E+00	0.0000000E+00	0.0000000E+00	0.0000000E+00	0.0000000E+00	0.0000000E+00
2	0.0000000E+00	0.0000000E+00	0.0000000E+00	0.0000000E+00	0.0000000E+00	0.0000000E+00
3	0.0000000E+00	0.0000000E+00	0.0000000E+00	0.0000000E+00	0.0000000E+00	0.0000000E+00
4	−6.7978138E−04	0.0000000E+00	0.0000000E+00	0.0000000E+00	0.0000000E+00	0.0000000E+00
5	−6.7628801E−04	−5.1424337E−04	0.0000000E+00	0.0000000E+00	0.0000000E+00	0.0000000E+00
6	−4.0454551E−04	−5.5565799E−04	−4.1089306E−04	0.0000000E+00	0.0000000E+00	0.0000000E+00
7	0.0000000E+00	−4.6574969E−04	−4.5550830E−04	−2.3753750E−04	0.0000000E+00	0.0000000E+00
8	−7.6992401E−04	−2.8685604E−04	−4.3325456E−04	−2.6818115E−04	−3.3451450E−04	0.0000000E+00
9	−2.0355803E−03	0.0000000E+00	−3.4597558E−04	−2.6459598E−04	−3.6708079E−04	−2.8913044E−04
10	−3.4812475E−03	−5.3310500E−04	−2.2815828E−04	−2.1799966E−04	−3.7170523E−04	−3.1707660E−04
11	−4.3485166E−03	−1.1604805E−03	0.0000000E+00	−1.3245846E−04	−3.4512883E−04	−3.2738333E−04
12	−4.1820964E−03	−2.0107373E−03	−4.4237113E−04	8.4582874E−05	−2.9116705E−04	−3.1725513E−04
13	−2.7657296E−03	−2.8242451E−03	−7.8913118E−04	0.0000000E+00	−2.2215026E−04	−2.8713764E−04
14	0.0000000E+00	−3.3206044E−03	−1.2985038E−03	−6.0356928E−05	−1.5212153E−04	−2.4166190E−04
15	5.2636888E−03	−3.3414132E−03	−1.8618945E−03	−2.4826199E−04	0.0000000E+00	−1.8912721E−04
16	1.2587822E−02	−2.8254978E−03	−2.3635259E−03	−5.6044074E−04	−2.8745428E−04	−1.3245575E−04
17	2.2269310E−02	−1.6758764E−03	−2.6749144E−03	−9.2668924E−04	−4.3298166E−04	0.0000000E+00
18	3.3964824E−02	0.0000000E+00	−2.7285117E−03	−1.2837077E−03	−6.6823280E−04	−2.7298008E−04
19	4.6897783E−02	3.1145173E−03	−2.5059040E−03	−1.5795348E−03	−9.6850692E−04	−3.7133376E−04
20	6.0046992E−02	7.0401227E−03	−1.9701690E−03	−1.7616044E−03	−1.3016585E−03	−5.3290996E−04
21	7.2291059E−02	1.2091438E−02	−1.0762419E−03	−1.8101016E−03	−1.6320878E−03	−7.4432310E−04
22	8.2524184E−02	1.8236891E−02	0.0000000E+00	−1.7319940E−03	−1.9243028E−03	−9.8761395E−04
23	8.9844578E−02	2.5315655E−02	2.0867021E−03	−1.5293427E−03	−2.1297547E−03	−1.2421812E−03
24	9.3653468E−02	3.3037717E−02	4.4937327E−03	−1.1957418E−03	−2.2244700E−03	−1.4866742E−03
25		4.1034799E−02	7.5104250E−03	−6.1052640E−06	−2.2049230E−03	−1.7003521E−03
26		4.8905760E−02	1.1152817E−02	0.0000000E+00	−2.0540988E−03	−1.8521292E−03
27		5.6230719E−02	1.5386557E−02	−4.3566146E−06	−1.7561930E−03	−1.9280654E−03
28		6.2603026E−02	2.0128782E−02	2.2411346E−03	−1.2950668E−03	−1.9291234E−03
29		6.7681773E−02	2.5246480E−02	3.9316848E−03	−6.5704476E−04	−1.8450335E−03
30		7.1207984E−02	3.0574428E−02	6.0659284E−03	0.0000000E+00	−1.6665926E−03
31		7.3014065E−02	3.5936126E−02	8.6644470E−03	1.2415753E−03	−1.3847337E−03
32			4.1144825E−02	1.1714005E−02	2.5241480E−03	−9.8984707E−04
33			4.6012297E−02	1.5171981E−02	4.0304895E−03	−4.7750042E−04
34			5.0354801E−02	1.8965488E−02	5.7642502E−03	0.0000000E+00
35			5.4018886E−02	2.3001951E−02	7.7213246E−03	9.8408793E−04
36			5.6876247E−02	2.7175943E−02	9.8902761E−03	1.9434730E−03
37			5.8833442E−02	3.1369115E−02	1.2251466E−02	3.0535983E−03
38			5.9828410E−02	3.5456422E−02	1.4779999E−02	4.3201697E−03
39				3.9299808E−02	1.7440394E−02	5.7435820E−03
40				4.2799312E−02	2.0188871E−02	7.3196175E−03
41				4.5808262E−02	2.2982202E−02	9.0401028E−03
42				4.8293471E−02	2.5774117E−02	1.0892218E−02
43				5.0190996E−02	2.8515837E−02	1.2860679E−02
44				5.1470294E−02	3.1157139E−02	1.4923902E−02
45				5.2114185E−02	3.3648561E−02	1.7055081E−02
46					3.5938906E−02	1.9227724E−02
47					3.7987010E−02	2.1414194E−02
48					3.9752809E−02	2.3584936E−02
49					4.1203964E−02	2.5709521E−02
50					4.2314864E−02	2.7756975E−02
51					4.3066456E−02	2.9697395E−02
52					4.3445987E−02	3.1498132E−02
53						3.3135487E−02
54						3.4583767E−02
55						3.5822129E−02
56						3.6833357E−02
57						3.7603806E−02
58						3.8123431E−02
59						3.8385256E−02

(Part I)

Table 3.2. The prototype filters with stopband attenuation about 40 dB and order $7M$.

n	M=19	M=21
0	0.0000000E+00	0.0000000E+00
1	0.0000000E+00	0.0000000E+00
2	0.0000000E+00	0.0000000E+00
3	0.0000000E+00	0.0000000E+00
4	0.0000000E+00	0.0000000E+00
5	0.0000000E+00	0.0000000E+00
6	0.0000000E+00	0.0000000E+00
7	0.0000000E+00	0.0000000E+00
8	0.0000000E+00	0.0000000E+00
9	0.0000000E+00	0.0000000E+00
10	−1.6558991E−04	0.0000000E+00
11	−1.8282560E−04	−1.5293333E−04
12	−1.8876425E−04	−1.7038287E−04
13	−1.8011410E−04	−1.8310268E−04
14	−1.5469053E−04	−1.8959924E−04
15	−1.1192666E−04	−1.8877979E−04
16	−5.4660475E−05	−1.8021234E−04
17	5.5887284E−05	−1.6435662E−04
18	7.2636483E−05	−1.4248425E−04
19	0.0000000E+00	−1.1524764E−04
20	6.0126739E−05	−7.4995432E−05
21	−4.2543141E−05	0.0000000E+00
22	−9.0937729E−05	−2.2376960E−04
23	−2.3797256E−04	−2.7436140E−04
24	−4.1450247E−04	−3.4867946E−04
25	−6.0520828E−04	−4.4487897E−04
26	−7.9667202E−04	−5.5593359E−04
27	−9.7569657E−04	−6.7403513E−04
28	−1.1310135E−03	−7.9140243E−04
29	−1.2469601E−03	−9.0085521E−04
30	−1.3171386E−03	−9.9611584E−04
31	−1.3439718E−03	−1.0719078E−03
32	−1.3251588E−03	−1.1187296E−03
33	−1.2590624E−03	−1.1341471E−03
34	−1.1446079E−03	−1.1219655E−03
35	−9.7784165E−04	−1.0812291E−03
36	−4.4522150E−07	−1.0113093E−03
37	−4.5714288E−04	−9.1131257E−04
38	0.0000000E+00	−7.7954597E−04
39	3.7841191E−04	−6.1328813E−04
40	−3.3891647E−07	−4.0962793E−04
41	1.6268190E−03	−1.7489569E−04
42	2.4336049E−03	0.0000000E+00
43	3.3737325E−03	5.2184964E−04
44	4.4527167E−03	9.7517046E−04
45	5.6721796E−03	1.5008043E−03
46	7.0292544E−03	2.1100678E−03
47	8.5169971E−03	2.8112907E−03
48	1.0126429E−02	3.6108632E−03
49	1.1842074E−02	4.5131371E−03
50	1.3646013E−02	5.5200092E−03
51	1.5519257E−02	6.6306072E−03
52	1.7440829E−02	7.8411619E−03
53	1.9385151E−02	9.1458015E−03
54	2.1327708E−02	1.0534418E−02
55	2.3246652E−02	1.1994196E−02
56	2.5093044E−02	1.3511032E−02
57	2.6858275E−02	1.5068990E−02
58	2.8508104E−02	1.6650708E−02
59	3.0038678E−02	1.8237892E−02
60	3.1372740E−02	1.9811553E−02
61	3.2552236E−02	2.1353022E−02
62	3.3546808E−02	2.2843957E−02
63	3.4349747E−02	2.4267602E−02
64	3.4955258E−02	2.5605235E−02
65	3.5360550E−02	2.6845376E−02
66	3.5563866E−02	2.7974363E−02

n	M=21
67	2.8981500E−02
68	2.9858191E−02
69	3.0597509E−02
70	3.1194316E−02
71	3.1644872E−02
72	3.1946621E−02
73	3.2097969E−02

(Part II)

Table 3.2. The prototype filters with stopband attenuation about 40 dB and order $7M$.

$$g_0(n) = \delta\left(n - \lfloor \tfrac{m_0+1}{2} \rfloor\right),$$
$$g_k(0) = 0, \qquad k = 1, 2, \ldots, \lfloor \tfrac{M-1}{2} \rfloor,$$

where the unit-impulse function $\delta(n)$ is defined in Sec. 3.1. By linear-phase constraint of $P_0(z)$, we have

$$g_M(n) = \delta(n - \left\lceil \frac{m_0 - 1}{2} \right\rceil),$$
$$g_k(m_0) = 0, \qquad k = \left\lceil \frac{M+1}{2} \right\rceil, \ldots, M-1.$$

Those zeros at the beginning of the prototype filters can not be removed without shifting the cosine modulation in (3.12). To be consistent with (3.12), we keep the zeros in the tables. If the quantity $p_0(n)$ is directly used in (3.12) with no modifications, then the set of analysis and synthesis filters have linear phase and give perfect reconstruction.

3.7 Concluding Remarks

In this chapter, we introduced a new class of maximally decimated cosine modulated systems, which have the following properties:

1. Aliasing is canceled exactly or approximately as desired.
2. Amplitude distortion function can be designed to be flat by optimizing over prototype filter coefficients.
3. Each analysis and synthesis filter in the filter bank has linear phase.
4. This new $2M$-channel maximally decimated cosine modulated filter bank has the same design cost and implementation cost as conventional M-channel maximally decimated cosine modulated filter banks. Correspondingly, the coding gain is nearly identical to that of an M-channel paraunitary system.
5. Perfect reconstruction is possible if polyphase components of the prototype filter satisfy the two conditions given in Sec. 3.3. Linear phase property of each analysis and synthesis filter is still preserved in this case.

Summarizing, we have developed a linear phase cosine modulated maximally decimated perfect reconstruction system. Design examples show that very good attenuation characteristics can be obtained as well.

Appendix A.

The quantity $A_i^{(1)}(z)$ in (3.9) is zero if

$$1 + W^{-Mi} = 0 \text{ or } U_k(zW^i)\widetilde{U}_k(z) = 0, \text{ for } k = 1, 2, \ldots, M-1.$$

Since $W^{-Mi} = -1$ for odd i and by (3.5) we have $U_k(zW^i)\widetilde{U}_k(z) \approx 0$, for $i \neq 1$, so $A_i^{(1)}(z)$ in (3.9) is approximately 0. Also $A_i^{(4)}(z) \approx 0$ for the same reason.

Similarly $A_i^{(2)}(z)$ is zero if

$$a_k^{*2} + a_k'^{*2} W^{-Mi} = 0 \text{ or } U_{-k}(zW^i)\widetilde{U}_k(z) \approx 0, \quad \text{for } k = 1, 2, \ldots, M-1.$$

The case when i is even and the case when i is odd are discussed separately.

1. i is even: From Fig. 3.9(a) we observe that only the term $k = i/2$ is the major nonzero part of $A_i(z)$. By choosing $a_k = 1$ and $a_k' = -\sqrt{-1}$, $k = 1, \ldots, M-1$, it can be completely eliminated.

2. 2. i is odd: Consider two cases:

   a) $1 < i < 2M - 1$: By using (3.5) and (3.9), we have

   $$A_i^{(2)}(z) \approx 2U_{-\frac{i-1}{2}}(zW^i)\widetilde{U}_{\frac{i-1}{2}}(z) + 2U_{-\frac{i+1}{2}}(zW^i)\widetilde{U}_{\frac{i+1}{2}}(z). \tag{3.32}$$

   We can also observe the result in (3.32) from Fig. 3.9(b). Since $P_0(z)$ has linear phase,

   $$P_0(e^{j\omega}) = e^{-j\omega N/2} P_R(\omega),$$

   where $P_R(\omega)$ is a real-valued function. We can rewrite (3.32) in terms of $P_R(w)$ as

   $$A_i^{(2)}(z) \approx 2(W^{N/2} + W^{-N/2}) P_R(\omega - \frac{\pi}{M}\frac{i-1}{2}) P_R(\omega - \frac{\pi}{M}\frac{i+1}{2}).$$

   If $N = (2m_0 + 1)M$ for some positive integer m_0, then $(W^{N/2} + W^{-N/2}) = 0$. In this case $A_i^{(2)}(z)$in (3.9) is approximately zero.

   b) $i = 1$ *or* $2M - 1$: When $i = 1$, $A_1^{(2)}(z)$ has a major nonzero term, $2U_{-1}(zW)\widetilde{U}_1(z)$, which cancels the term $2U_0(zW)\widetilde{U}_0(z)$ in Eq. (3.9) with the same choice of N. Similarly for $i = 2M - 1$.

The cancelation of $A_i^{(3)}(z)$ in (3.9) is similar to the cancelation of the $A_i^{(2)}(z)$.

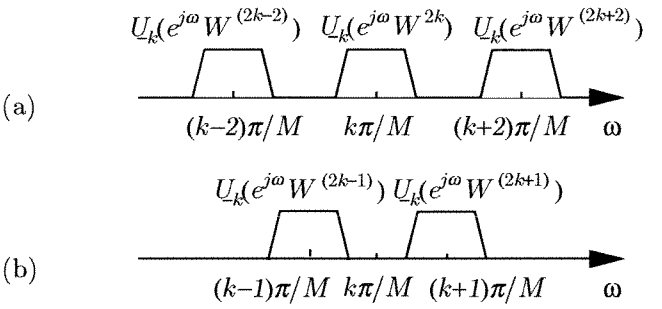

Fig. 3.9. Image copies of $U_{-k}(z)$ due to decimation followed by expansion.

Appendix B. Proof of (3.11).

To derive (3.22), we need to prove the following properties of $\mathbf{C}$ and $\mathbf{S}$:

$$\mathbf{C}^T\mathbf{C} = \tfrac{M}{2}\begin{pmatrix} 2 & \mathbf{0} \\ \mathbf{0} & \mathbf{I}_{M-1} \end{pmatrix} \tag{3.33}$$

$$\mathbf{C}^T\mathbf{\Lambda}_1\mathbf{C} = \tfrac{M}{2}\begin{pmatrix} 0 & \mathbf{0} \\ \mathbf{0} & \mathbf{J}_{M-1} \end{pmatrix} \tag{3.34}$$

$$\mathbf{S}^T\mathbf{S} = \tfrac{M}{2}\begin{pmatrix} 0 & \mathbf{0} \\ \mathbf{0} & \mathbf{I}_{M-1} \end{pmatrix} \tag{3.35}$$

$$\mathbf{S}^T\mathbf{\Lambda}_2\mathbf{S} = \tfrac{M}{2}\begin{pmatrix} 0 & \mathbf{0} \\ \mathbf{0} & \mathbf{J}_{M-1} \end{pmatrix} \tag{3.36}$$

If (3.33)-(3.36) are true, then (3.22) follows.

Matrix $\mathbf{C}$ is very similar to a $(M+1)\times(M+1)$ type I DCT matrix, $\mathbf{C}^I_{M+1}$, and $\mathbf{S}$ is very similar to a $(M-1)\times(M-1)$ type I DST matrix, $\mathbf{S}^I_{M-1}$. (Both $\mathbf{C}^I_{M+1}$ and $\mathbf{S}^I_{M-1}$ are documented in [77].) $\mathbf{C}^I_{M+1}$ and $\mathbf{S}^I_{M-1}$ have entries

$$\begin{aligned} [\mathbf{C}^I_{M+1}]_{mn} &= \kappa_m\kappa_n\sqrt{\tfrac{2}{M}}\cos(\tfrac{\pi}{M}mn), && 0 \le m,n \le M, \\ [\mathbf{S}^I_{M-1}]_{mn} &= \sqrt{\tfrac{2}{M}}\sin(\tfrac{\pi}{M}mn), && 1 \le m,n \le M-1. \end{aligned}$$

Several useful properties of $\mathbf{C}^I_{M+1}$ and $\mathbf{S}^I_{M-1}$ are stated in the following to help proving (3.33)-

(3.36).

$$\mathbf{C}^I_{M+1}{}^T\mathbf{C}^I_{M+1} = \mathbf{I}_{M+1}, \tag{3.37}$$

$$\mathbf{C}^I_{M+1}{}^T\mathbf{\Lambda}_1\mathbf{C}^I_{M+1} = \mathbf{J}_{M+1}, \tag{3.38}$$

$$\mathbf{S}^I_{M-1}{}^T\mathbf{S}^I_{M-1} = \mathbf{I}_{M-1}, \tag{3.39}$$

$$\mathbf{S}^I_{M-1}{}^T\mathbf{\Lambda}_2\mathbf{S}^I_{M-1} = -\mathbf{J}_{M-1}. \tag{3.40}$$

Proof of (3.33)-(3.36)

$\mathbf{C}$ and $\mathbf{S}$ are related to $\mathbf{C}^I_{M+1}$ and $\mathbf{S}^I_{M-1}$ as

$$\sqrt{\frac{M}{2}}\mathbf{C}^I_{M+1} = \begin{pmatrix}\mathbf{C}\Gamma & \mathbf{r}\end{pmatrix}, \quad \mathbf{S} = \begin{pmatrix}\mathbf{0} & \sqrt{\frac{M}{2}}\mathbf{S}^I_{M-1}\end{pmatrix} \tag{3.41}$$

where $\mathbf{r}$ is the last column of $\sqrt{\frac{M}{2}}\mathbf{C}^I_{M+1}$ and $\Gamma = \begin{pmatrix}\sqrt{\frac{1}{2}} & \mathbf{0} \\ \mathbf{0} & \mathbf{I}_{M-1}\end{pmatrix}$ with inverse

$$\Gamma^{-1} = \begin{pmatrix}\sqrt{2} & \mathbf{0} \\ \mathbf{0} & \mathbf{I}_{M-1}\end{pmatrix}.$$

By (3.37), we have

$$\frac{M}{2}\mathbf{C}^I_{M+1}{}^T\mathbf{C}^I_{M+1} = \frac{M}{2}\mathbf{I}_{M+1}. \tag{3.42}$$

and from (3.41) we have

$$\frac{M}{2}\mathbf{C}^I_{M+1}{}^T\mathbf{C}^I_{M+1} = \begin{pmatrix}\Gamma^T\mathbf{C}^T\mathbf{C}\Gamma & \Gamma^T\mathbf{C}^T\mathbf{r} \\ \mathbf{r}^T\mathbf{C}\Gamma & \mathbf{r}^T\mathbf{r}\end{pmatrix}. \tag{3.43}$$

Comparing Eq. (3.42) and (3.43) gives us

$$\Gamma^T\mathbf{C}^T\mathbf{C}\Gamma = \frac{M}{2}\mathbf{I}_M.$$

Relation (3.33) follows the above equation. Similarly for (3.35). Relations (3.34) and (3.36) can be proved in a similar manner.

With (3.33)-(3.36), the right hand side of (3.22) can be written as

$$\frac{M}{2}\begin{pmatrix} \widetilde{\mathbf{g}}_0\begin{pmatrix}2 & \mathbf{0}\\ \mathbf{0} & \mathbf{I}_{M-1}\end{pmatrix}\mathbf{g}_0+\widetilde{\mathbf{g}}_1\begin{pmatrix}0 & \mathbf{0}\\ \mathbf{0} & \mathbf{I}_{M-1}\end{pmatrix}\mathbf{g}_1 & -z\left(\widetilde{\mathbf{g}}_1\begin{pmatrix}0 & \mathbf{0}\\ \mathbf{0} & \mathbf{J}_{M-1}\end{pmatrix}\mathbf{g}_0-z^{-1}\widetilde{\mathbf{g}}_0\begin{pmatrix}0 & \mathbf{0}\\ \mathbf{0} & \mathbf{J}_{M-1}\end{pmatrix}\mathbf{g}_1\right)\\ \widetilde{\mathbf{g}}_1\begin{pmatrix}0 & \mathbf{0}\\ \mathbf{0} & \mathbf{J}_{M-1}\end{pmatrix}\mathbf{g}_0-z^{-1}\widetilde{\mathbf{g}}_0\begin{pmatrix}0 & \mathbf{0}\\ \mathbf{0} & \mathbf{J}_{M-1}\end{pmatrix}\mathbf{g}_1 & \widetilde{\mathbf{g}}_0\begin{pmatrix}0 & \mathbf{0}\\ \mathbf{0} & \mathbf{I}_{M-1}\end{pmatrix}\mathbf{g}_0+\widetilde{\mathbf{g}}_1\begin{pmatrix}2 & \mathbf{0}\\ \mathbf{0} & \mathbf{I}_{M-1}\end{pmatrix}\mathbf{g}_1\end{pmatrix}.$$

The dependence of $\mathbf{g}_i$ on z is dropped for convenience. Notice that the off diagonal elements in the above big matrix is $\mathbf{0}$ if and only if

$$\widetilde{G}_{k+M}(z)G_{M-k}(z)-z^{-1}\widetilde{G}_k(z)G_{2M-k}(z)=0, \qquad k=1,\ldots,M-1. \tag{3.44}$$

Because the prototype filter $P_0(z)$ is of order $N=(2m_0+1)M$ and has linear phase, $G_k(z)$ is related to $G_{M-k}(z)$ and $G_{k+M}(z)$ is related to $G_{2M-k}(z)$, for $k=1,2,\ldots,M-1$.

$$G_k(z)=z^{-m_0}\widetilde{G}_{M-k}(z), \qquad G_{k+M}(z)=z^{-(m_0-1)}\widetilde{G}_{2M-k}(z) \qquad k=1,2,\ldots,M-1.$$

The above property makes Eq. (3.42) automatically satisfied.

Appendix C.

From the definitions of $\mathbf{T}_1$ and $\mathbf{T}_2$, we know

$$\mathbf{d}_1=\mathbf{C}\mathbf{a}_1+\mathbf{\Lambda}_1\mathbf{C}\mathbf{a}_2, \qquad \text{and} \qquad \mathbf{d}_2=\mathbf{S}\mathbf{b}_1+\mathbf{\Lambda}_2\mathbf{S}\mathbf{b}_2. \tag{3.45}$$

Using the relations of (3.41) and (3.33)-(3.36), we can write

$$\mathbf{\Lambda}_1\begin{pmatrix}\mathbf{C}\mathbf{\Gamma} & \mathbf{r}\end{pmatrix}=\begin{pmatrix}\mathbf{C}\mathbf{\Gamma} & \mathbf{r}\end{pmatrix}\mathbf{J}_{M+1} \qquad \text{and} \qquad \mathbf{\Lambda}_2\begin{pmatrix}\mathbf{0} & \mathbf{S}^I_{M-1}\end{pmatrix}=-\mathbf{S}^I_{M-1}\begin{pmatrix}\mathbf{0} & \mathbf{J}_{M-1}\end{pmatrix}.$$

That gives us

$$\mathbf{\Lambda}_1\mathbf{C}=\mathbf{C}\begin{pmatrix}0 & \mathbf{0}\\ \mathbf{0} & \mathbf{J}_{M-1}\end{pmatrix}+\sqrt{2}\begin{pmatrix}\mathbf{r} & \mathbf{0}\end{pmatrix} \qquad \text{and} \qquad \mathbf{\Lambda}_2\mathbf{S}=-\mathbf{S}\begin{pmatrix}0 & \mathbf{0}\\ \mathbf{0} & \mathbf{J}_{M-1}\end{pmatrix}. \tag{3.46}$$

Substituting (3.46) into (3.45), we obtain (3.25).

Chapter 4

Theory and Design of Two-Parallelogram Filter Banks

4.1 Introduction

A one-dimensional (1D) M-channel filter bank (Fig. 1.1) usually has the frequency stacking as shown in Fig. 1.2. The synthesis filters typically have the same passband regions as the corresponding analysis filters. A figure like this showing the passband regions of the filters will be called the *support configuration* of the filter bank. Filter banks with this type of configuration have been successfully designed through many approaches. It is possible to have perfect reconstruction and good individual analysis and synthesis filters (good frequency selectivity) at the same time. It turns out that the support configuration shown in Fig. 1.2 has two features that are necessary for a successful filter bank design. First, the support of each analysis filter does not overlap under modulo $2\pi/M$. Filters with such a support are said to be *AliasFree Supported with respect to M* ($\mathcal{AFS}(M)$). This means that if the filters are ideal, then their outputs allow aliasfree M-fold decimation; that is, no aliasing is created in the subbands. We say a configuration is $\mathcal{AFS}(M)$ if each analysis filter is $\mathcal{AFS}(M)$. The second feature of the support configuration in Fig. 1.2 is a property called permissibility. It is argued in [11] that with certain support configurations in a filter bank, a considerable amount of aliasing will remain uncanceled if the individual filters have good attenuation. In this case, the support configuration is called nonpermissible. The 1D uniform DFT filter bank [98] is known to be an example of this nature. (The notion of configuration permissibility is more involved and will be explained in greater detail in Sec. 4.2.) These two features are desirable for good filter bank design of any dimensions.

Recently, there has been considerable interest in the design of two-dimensional (2D) maximally

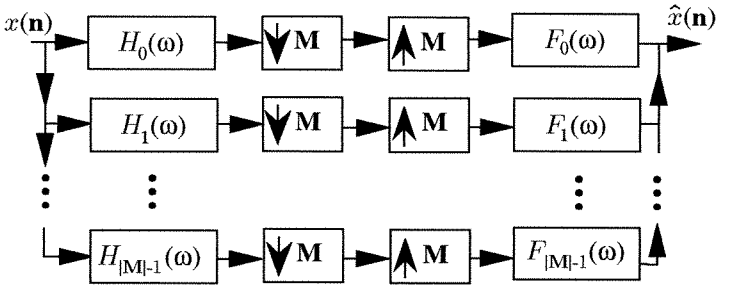

Fig. 4.1. A |M|-channel maximally decimated filter bank, where |M| denotes the absolute value of the determinant of M.

decimated filter banks (Fig. 4.1), [102, 109, 108, 98]. For example, perfect reconstruction is achieved in [2] for a 2D two-channel FIR filter bank with diamond-shaped filters. In [33], transformations are used to design higher dimensional filter banks from filter banks of lower dimensions. In [11], several issues regarding design of multidimensional filter bank are treated. In particular, the concept of support permissibility is introduced and discussed from a pictorial viewpoint. A study of 2D cosine modulated filter bank (CMFB) with rectangular-shaped but nonseparable prototype is made in [8]. The prototype of this type of 2D CMFB has rectangular support but is allowed to be nonseparable. Nonseparable prototype with separable modulation is studied in [40]. Also 2D nonseparable orthonormal wavelets using local cosine or sine bases are obtained in [111, 112, 113]. A nonseparable generalization for 2D CMFB is considered in [30]. However, the support of the 2D filter banks studied therein is nonpermissible in general.

In the construction of 2D filter banks, we have more variety in terms of possible configurations. Even if we impose the condition that all the analysis filters have real coefficients and have only two passbands, it is possible to have more than one configuration for a filter bank with decimation matrix M. Various shapes can be used for the passbands of the individual filters, e.g., triangles [31] and parallelograms [47]. In this chapter, we study the two-parallelogram (*Two-P*) filter banks, the class of 2D filter banks in which the support of each analysis and synthesis filter is the union of two parallelograms. Filters with this type of supports are called *Two-P* filters.

Two-Parallelogram Filter Banks. A typical *Two-P* filter bank has support configuration as shown in Fig. 4.2. This is a natural 2D generalization of the frequency stacking in Fig. 1.2. For a *Two-P* filter bank with decimation matrix M as in Fig. 4.1, we will study the conditions such that the configuration is $\mathcal{AFS}(\mathbf{M})$. For this, we will derive the necessary and sufficient conditions such that a *Two-P* support is $\mathcal{AFS}(\mathbf{M})$. For those $\mathcal{AFS}(\mathbf{M})$ configurations, we will further investigate permissibility of the configurations.

In this context of 1D filter bank design, the cosine modulated filter banks are well-known for low

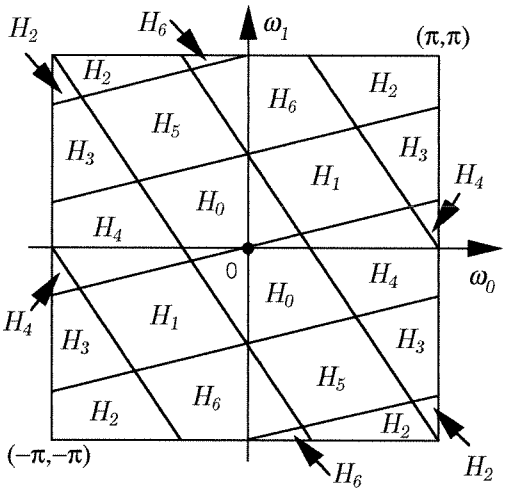

Fig. 4.2. Typical configuration of a two-parallelogram filter bank.

design cost and low complexity. The implementation of *Two-P* filter banks using cosine modulated filter banks yields similar advantage of economy. The *Two-P* CMFB will be constructed and designed in this chapter.

Two-Parallelogram CMFB. In *Two-P* CMFB, each of the two parallelograms of the analysis filters is a shifted version of a real-coefficient prototype, which has a parallelogram support and is in general nonseparable. Each analysis filter is a cosine modulated version of the prototype and each analysis filter consists of two copies of the prototype. The synthesis filters have the same spectral supports as the corresponding analysis filters. The analysis bank will eventually be constrained to be paraunitary; the analysis filter $H_k(\boldsymbol{\omega})$ and the corresponding synthesis filter $F_k(\boldsymbol{\omega})$ are related by $F_k(\boldsymbol{\omega}) = H_k^*(\boldsymbol{\omega})$. All the analysis and synthesis filters have real coefficients. We will present the sufficient conditions such that cancelation of major aliasing (due to overlapping transition bands) can be structurally enforced. Finally, having canceled the major aliasing, we constrain the prototype to ensure perfect reconstruction of the *Two-P* CMFB.

We can conceive that in the more general case of 2D filter banks the individual filters can have any even number of parallelograms. Particularly in the 2D separable filter bank obtained by cascading 1D filter banks, the support of each analysis filter consists of four rectangles. In chapter 5 [54], we will study the *four-parallelogram filter banks* [48], the 2D filter banks in which the supports of the analysis filters consist of four parallelograms. Note that *Two-P* filter banks are fundamentally different from 2D separable filter banks obtained from 1D filter banks. But four-parallelogram filter banks will reduce to separable 2D filter bank in special cases.

Chapter Outline and Chapter Specific Notations

In Sec. 4.2, we explain perfect reconstruction of 1D filter banks from a pictorial viewpoint. This illustration will supply the explanation why $\mathcal{AFS}(\mathbf{M})$ property and permissible configurations are important for good design of analysis and synthesis filters. Sec. 4.3 is devoted to the study of *Two-P* filter banks. For a successful design, the analysis filters should be $\mathcal{AFS}(\mathbf{M})$. Towards this end, we derive the necessary and sufficient conditions such that a *Two-P* filter is $\mathcal{AFS}(\mathbf{M})$. Permissibility of *Two-P* filter bank will also be studied. Using the results developed in Sec. 4.3, we construct $\mathcal{AFS}(\mathbf{M})$ configurations for *Two-P* CMFB (Sec. 4.4). In Sec. 4.5, the analysis and synthesis filters of *Two-P* CMFB are formulated. The necessary and sufficient condition for perfect reconstruction *Two-P* CMFB is presented in Sec. 4.6. Efficient implementation and a design example of *Two-P* CMFB are given in Sec. 4.7. Preliminary versions of this work have been presented at international conferences [47, 51].

Notations in this chapter are as in [98]. The fundamentals of integer matrices and 2D multirate systems are employed frequently in this chapter. A brief review can be found in Chapter 2.

Chapter Specific Notation

- Boldfaced lower case letters are used to represent vectors and boldfaced upper case letters are reserved for matrices. The notations $\mathbf{A}^T$ and $\mathbf{A}^\dagger$ represent the transpose and transpose-conjugate of $\mathbf{A}$.
- Vectors will also be used as subscript, e.g. $P_{\mathbf{k}}(\boldsymbol{\omega})$. If $\mathbf{k} = \begin{pmatrix} k_0 & k_1 \end{pmatrix}^T$, then $P_{\mathbf{k}}(\boldsymbol{\omega})$ and $P_{(k_0,k_1)}(\boldsymbol{\omega})$ will be used interchangeably.
- The notation $\mathbf{I}_k$ denotes a $k \times k$ identity matrix. The subscript k is omitted when the dimension is clear from the context.
- If the support (passband) of a filter $H(\boldsymbol{\omega})$ does not overlap under modulo $2\pi\mathbf{M}^{-T}$, $H(\boldsymbol{\omega})$ is called aliasfree supported with respect to $\mathbf{M}$ ($\mathcal{AFS}(\mathbf{M})$). If, in addition to being $\mathcal{AFS}(\mathbf{M})$, $H(\boldsymbol{\omega})$ is also an ideal filter ($H(\boldsymbol{\omega})$ is 1 in the passband and 0 otherwise), then the output of $H(\boldsymbol{\omega})$ allows aliasfree $\mathbf{M}$-fold decimation [83, 10], and in this case $H(\boldsymbol{\omega})$ is called an aliasfree($\mathbf{M}$) filter. A configuration is referred to as $\mathcal{AFS}(\mathbf{M})$ if all the analysis filters are $\mathcal{AFS}(\mathbf{M})$.

4.2 Basic Consideration of Filter Bank Design

In this section, we explain pictorially how perfect reconstruction is achieved for 1D filter banks. The pictorial illustration will help us identify the roles of $\mathcal{AFS}(\mathbf{M})$ property and permissibility. To explain why these two features are important, we will use the cosine modulated filter banks as an example. An M-band CMFB is a special case of M-band filter banks. It usually has the stacking in Fig. 1.2. The analysis and synthesis filters of CMFB satisfy some additional properties.

In particular, they are the cosine modulated versions of a prototype filter. Although this property has made alias cancelation in CMFB somewhat different from that in a usual filter bank, as the discussion proceeds we will make observations for the more general filter banks. First we review two 1D sampling theorems and verify that the configuration in Fig. 1.2 is indeed $\mathcal{AFS}(M)$.

One-Dimensional Sampling Theorems. Recall the following two types of 1D ideal filter $H(\omega)$ that is known to be aliasfree(M).

Fact 4.1. Suppose $H(\omega)$ has bandwidth $2\pi/N$ as shown Fig. 4.3, then $H(\omega)$ is aliasfree(M) if and only if $N \geq M$. The 2D extension of this fact will be given in Sec. 4.3. To compare with 2D result to be stated later, we define $L = N/M$. In this case, $H(\omega)$ is aliasfree(M) if and only if $L \geq 1$. ■

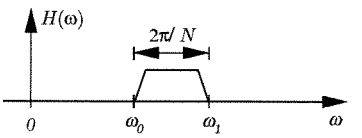

Fig. 4.3. Bandlimited signal with bandwidth $2\pi/N$.

Fact 4.2. One-dimensional bandpass sampling theorem [67]. Suppose a 1D ideal filter $H(\omega)$ has total bandwidth $2\pi/M$ as shown in Fig. 4.4. Then $H(\omega)$ is aliasfree(M) if and only if ω_0 is a multiple of π/M, i.e., $\omega_0 = k\pi/M$, for some integer k. ■

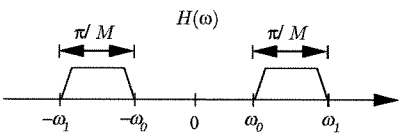

Fig. 4.4. Bandlimited real sequence with total bandwidth $2\pi/M$.

In practice, the filters are not ideal but only $\mathcal{AFS}(M)$. The band edges of the analysis filters in Fig. 1.2 are multiples of π/M; the analysis filters are $\mathcal{AFS}(M)$. So the configuration in Fig. 1.2 is indeed $\mathcal{AFS}(M)$.

One-Dimensional Cosine Modulated Filter Banks (CMFB). Consider the M-channel filter bank in Fig. 1.1. An M-channel CMFB (pseudo-QMF or perfect reconstruction) is typically obtained by starting from a $2M$-channel uniform DFT filter bank, [98]. Each filter in the DFT filter bank is a shifted version of a lowpass prototype $P(\omega)$ (Fig. 4.5(a)) with bandwidth π/M, which is half the total bandwidth of each filter in the desired M-channel system. The filters in the DFT filter bank are then shifted by $\pi/2M$ and paired to obtain real-coefficient analysis filters as in Fig. 4.5(b) for the M-channel CMFB. The shifts of the prototype are denoted by $P_k(\omega)$ in the figure. Each analysis

filter has total bandwidth $2\pi/M$, which is two times that of the prototype. In almost all the designs, the synthesis filters are time-reversed versions of the corresponding analysis filters; the analysis and synthesis filters have the same spectral support.

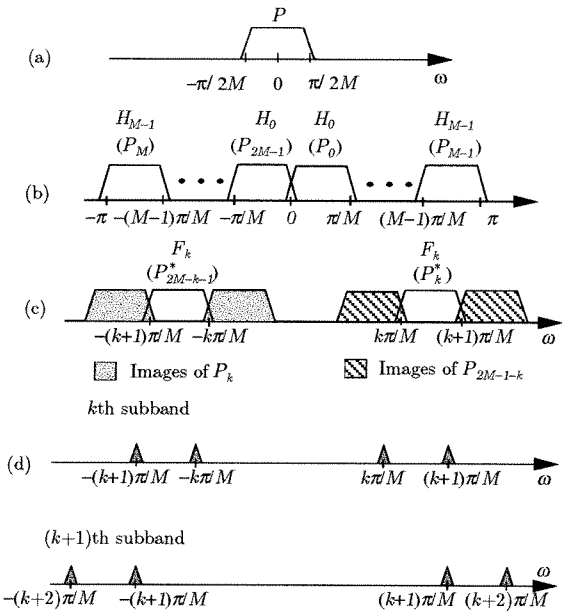

Fig. 4.5. One-dimensional cosine modulated filter bank: (a) The support of the prototype filter $P(\omega)$; (b) the support of the analysis filters $H_k(\omega)$; each analysis filter has two parts, $P_k(\omega)$ and $P_{2M-1-k}(\omega)$; (c) images of the analysis filter $H_k(\omega)$ that are adjacent to the synthesis filter $F_k(\omega)$; (d) the major aliasing in the kth subband and the $(k+1)$th subband.

In the CMFB described above, as each analysis filter consists of two shifted copies of the prototype, each of the two copies has $M-1$ images due to decimation followed by expansion. Due to $\mathcal{AFS}(M)$ property, the images of the analysis filters are adjacent to the support of the corresponding synthesis filters but are not overlapping with the passbands of synthesis filters as shown in Fig. 4.5(c). Thus, if the prototype filter is an ideal brick-wall filter, there is no aliasing and the filter bank has perfect reconstruction. If the prototype filter is not ideal, those images that are adjacent to the synthesis filter result in major aliasing (Fig. 4.5(d)) while those that are not adjacent to the synthesis filters will be attenuated to the stopband level of the prototype filter. In the pseudo QMF CMFB, only the major aliasing errors are canceled and approximate alias cancelation is attained. Approximate reconstruction is then achieved without sophisticated optimization of the lowpass prototype. In the perfect reconstruction CMFB, the prototype is optimized under further constraint (e.g., paraunitariness). The paraunitariness of the CMFB is guaranteed if the polyphase components of the prototype filter satisfy some pairwise power complementary conditions [37]. In both pseudo QMF and perfect reconstruction systems, the design of the whole filter bank is reduced

to the optimization of the lowpass prototype filter. The complexity of the analysis bank is equal to that of a prototype filter plus a DCT matrix.

Main Features of the Configuration in Fig. 1.2

From the preceding discussion, we observe that the support configuration in Fig. 1.2 has the following two features, which are necessary for designing a filter bank with good analysis and synthesis filters.

1. $\mathcal{AFS}(M)$ ***property.*** Each analysis filter is $\mathcal{AFS}(M)$ and the configuration is $\mathcal{AFS}(M)$. This means that if the filters are ideal, they are aliasfree(M) filters; no aliasing is created in the subbands and the filter bank has perfect reconstruction. This feature is indispensable for the design of perfect reconstruction filter banks. For a configuration that is not $\mathcal{AFS}(M)$, severe aliasing will be created in the subbands no matter how good the filters are. Without a $\mathcal{AFS}(\mathbf{M})$ configuration, a filter bank can not have perfect reconstruction even if the analysis and synthesis filters are ideal brick-wall filters.

2. ***Permissibility.*** From the discussion of CMFB, we see that major aliasing errors that contribute to the same aliasing transfer function $A_i(\omega)$ (defined in Chapter 2) appear in pairs. For example, around the frequency $k\pi/M$ (Fig. 4.5(d)) both kth and $(k+1)$th subbands have major aliasing errors and it can be verified that these two aliasing errors contribute to the same aliasing transfer function $A_k(\omega)$. This is essential if alias cancelation is to take place in CMFB. For the more general M-band filter banks, assume the filters are not ideal but have good frequency selectivity. If a certain $A_i(\omega)$ has only one major aliasing term in a particular frequency region, this major aliasing can not be canceled; perfect reconstruction is not possible. So if a perfect reconstruction filter bank has good analysis and synthesis filters, it is necessary that in any frequency region there is more than one major aliasing term contributing to the same aliasing transfer function $A_i(\omega)$. A configuration without this feature will be referred to as *nonpermissible*. Permissibility allows the possibility of canceling major aliasing. If a filter bank has a nonpermissible configuration, the filters can not have good stopband attenuation unless all the filters are ideal brick-wall filters. The one-dimensional uniform DFT filter bank [98] is known to be an example of this nature.

Remarks on Permissibility

1. The issue of permissibility arises only when non ideal filters are considered. Also permissibility is meaningful only when the underlying analysis and synthesis filters have frequency selectivity, i.e., when the notion of passbands and stopbands still makes sense. For example, in delay chain filter bank, the analysis and synthesis filters are allpass functions ($H_k(z) = z^{-k}$ and $F_k(z) = z^k$) and have no frequency selectivity. In this case, discussion of permissibility is

meaningless.

2. To check the $\mathcal{AFS}(M)$ property of a configuration, we can individually examine each analysis filter. But whether a configuration is permissible is determined jointly by all the analysis filters.

3. Permissibility is only a necessary condition for good filter bank designs. It does not suggest any constructive approach to design the filter banks.

4.3 Two-Parallelogram Filter Bank

In this section we study a subclass of 2D filter banks: the *Two-P* filter banks. This is the class of filter banks in which the support of each analysis and synthesis filter is the union of two parallelograms. Before designing any filter bank, we first study the support configuration and see if good analysis and synthesis filters are possible. As a first step towards this, the analysis and synthesis filters should be $\mathcal{AFS}(\mathbf{M})$ for a given decimation matrix $\mathbf{M}$. This calls for a bandpass sampling theorem for *Two-P* filters. For those $\mathcal{AFS}(\mathbf{M})$ configurations, we further investigate permissibility of the configurations.

4.3.1 Sampling Theorems for One- and Two-Parallelogram Filters

A 2D filter $H(\boldsymbol{\omega})$ with a frequency support that consists of k parallelograms is called a k-parallelogram filter. By definition, $H(\boldsymbol{\omega})$ is $\mathcal{AFS}(\mathbf{M})$ if the support of $H(\boldsymbol{\omega})$ does not overlap under modulo $2\pi\mathbf{M}^{-T}$. However, for one-parallelogram or *Two-P* filters, there is no existing simple testing rule as those given in Fact 4.1 and Fact 4.2. The 2D equivalence of Fact 4.1 and Fact 4.2 will be given in this subsection. Due to these 2D extensions, we can easily test $\mathcal{AFS}(\mathbf{M})$ property of one-parallelogram or *Two-P*s filters [50, 55, 56].

One-Parallelogram $\mathcal{AFS}(\mathbf{M})$ Filters

A result related to the multidimensional generalization of Fact 4.1 is as follows. Let $H(\boldsymbol{\omega})$ be a 2D filter with support $SPD(\pi\mathbf{M}^{-T})$ or a shifted version of $SPD(\pi\mathbf{M}^{-T})$ for some integer matrix $\mathbf{M}$. When $H(\boldsymbol{\omega})$ has such a support, $H(\boldsymbol{\omega})$ is $\mathcal{AFS}(\mathbf{M})$ [98]. Now consider the more general case that $H(\boldsymbol{\omega})$ is a one-parallelogram filter with support $SPD(\pi\mathbf{N}^{-T})$ or a shifted version of $SPD(\pi\mathbf{N}^{-T})$. The analysis of $\mathcal{AFS}(\mathbf{M})$ property of one-parallelogram filters is more intricate than that of 1D one-passband case. Let us define

$$\mathbf{L} \triangleq \mathbf{M}^{-1}\mathbf{N},$$

and denote the absolute value of the determinant of $\mathbf{L}$ by $|\mathbf{L}|$. The condition $|\mathbf{L}| \geq 1$ alone does not imply $\mathcal{AFS}(\mathbf{M})$ property [108] and a stronger condition is called for. In particular, the lattice of

$\mathbf{L}^T$ has to satisfy one additional property. More precise statement is given in the theorem to follow.

Theorem 4.1. Let $H(\boldsymbol{\omega})$ be a one-parallelogram signal with frequency support $SPD(\pi\mathbf{N}^{-T})$ or a shifted version of $SPD(\pi\mathbf{N}^{-T})$, where $\mathbf{N}$ is possibly a non integer matrix. Then $H(\boldsymbol{\omega})$ is $\mathcal{AFS}(\mathbf{M})$ if and only if the matrix $\mathbf{L}$ defined as $\mathbf{L} = \mathbf{M}^{-1}\mathbf{N}$ satisfies $LAT(\mathbf{L}^T) \cap (-1,1)^2 = \{\mathbf{0}\}$. ■

This necessary and sufficient condition means that no vector in $LAT(\mathbf{L}^T)$ is inside the square $(-1,1)^2$ except the vector $\mathbf{0}$. For example, let

$$\mathbf{L}^T = \begin{pmatrix} 1 & 0 \\ 0.5 & 2 \end{pmatrix}, \tag{4.1}$$

then $LAT(\mathbf{L}^T)$ is as shown in Fig. 4.6; $LAT(\mathbf{L}^T)$ has only one vector (the vector $\mathbf{0}$) inside the square $(-1,1)^2$. Notice that in 1D case, $|L| \geq 1$ if and only if $LAT(L^T) \cap (-1,1) = \{0\}$. However, this relation does not hold in more than one dimensions.

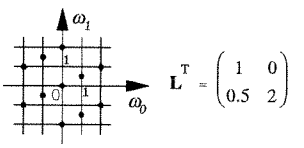

Fig. 4.6. Lattice of $\mathbf{L}^T$.

Proof of Theorem 4.1. Recall that $H(\boldsymbol{\omega})$ is $\mathcal{AFS}(\mathbf{M})$ if and only if the support of $H(\boldsymbol{\omega})$ does not overlap modulo $2\pi\mathbf{M}^{-T}$. So $H(\boldsymbol{\omega})$ is $\mathcal{AFS}(\mathbf{M})$ if and only if, whenever $\mathbf{k}_1 \neq \mathbf{k}_2 \bmod \mathbf{M}^T$,

$$\boldsymbol{\omega}_1 - 2\pi\mathbf{M}^{-T}\mathbf{k}_1 \neq \boldsymbol{\omega}_2 - 2\pi\mathbf{M}^{-T}\mathbf{k}_2, \quad \forall \boldsymbol{\omega}_1, \boldsymbol{\omega}_2 \in SPD(\pi\mathbf{N}^{-T}).$$

Rearranging the above equation, we have $\boldsymbol{\omega}_1 - \boldsymbol{\omega}_2 \neq 2\pi\mathbf{M}^{-T}(\mathbf{k}_1 - \mathbf{k}_2)$. As $\boldsymbol{\omega}_1, \boldsymbol{\omega}_2 \in SPD(\pi\mathbf{N}^{-T})$, $\boldsymbol{\omega}_i$ can be expressed as $\boldsymbol{\omega}_i = \pi\mathbf{N}^{-T}\mathbf{y}_i$, for some 2×1 vectors $\mathbf{y}_i \in [-1,1)^2$, $i = 1,2$. Hence

$$\boldsymbol{\omega}_1 - \boldsymbol{\omega}_2 = 2\pi\mathbf{N}^{-T}\mathbf{y}, \text{ for some } \mathbf{y} \in (-1,1)^2.$$

Using this expression, we have

$$\mathbf{y} \neq \mathbf{L}^T(\mathbf{k}_1 - \mathbf{k}_2), \quad \text{for } \mathbf{k}_1 \neq \mathbf{k}_2 \bmod \mathbf{M}^T.$$

This is satisfied if and only if $LAT(\mathbf{L}^T) \cap (-1,1)^2 = \{\mathbf{0}\}$. ■

This theorem can be generalized for D-dimensional signals. The above technique of the proof can be carried out for signals of any dimensions.

Bandpass Sampling Theorem for Two-Parallelogram Filters

Now consider the case that $H(\boldsymbol{\omega})$ is a *Two-P* filter. The support of $H(\boldsymbol{\omega})$ (Fig. 4.7) consists of two parallelograms, each a shifted version of $SPD(\pi\mathbf{N}^{-T})$. The two passbands can be described as

$$\boldsymbol{\omega}_0 + SPD(\pi\mathbf{N}^{-T}) \text{ and } -\boldsymbol{\omega}_0 + SPD(\pi\mathbf{N}^{-T}).$$

Let $\mathbf{M}$ be an integer matrix with $|\mathbf{M}| = |\mathbf{N}|/2$. For $H(\boldsymbol{\omega})$ to be $\mathcal{AFS}(\mathbf{M})$, the 1D bandpass sampling theorem suggests that the two parallelograms in the support of $H(\boldsymbol{\omega})$ should be properly located. On the other hand, the above sampling theorem for one-parallelogram signals indicates that in higher dimensions the shape of the support also affects whether $\mathcal{AFS}(\mathbf{M})$ property is possible. Indeed, we will see that whether $H(\boldsymbol{\omega})$ is $\mathcal{AFS}(\mathbf{M})$ depends on the matrix $\mathbf{N}$ as well as the relative position of the two parallelograms.

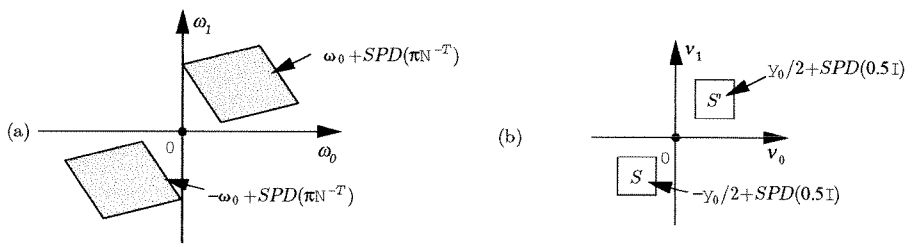

Fig. 4.7. (a) Support of a *Two-P* filter $H(\boldsymbol{\omega})$; (b) support of $H(\boldsymbol{\omega})$ with normalized axes.

Theorem 4.2. Let $H(\boldsymbol{\omega})$ be a 2D filter and let the support of $H(\boldsymbol{\omega})$ be the union of two parallelograms, each a shifted version of $SPD(\pi\mathbf{N}^{-T})$, the matrix $\mathbf{N}$ is possibly a non integer matrix. Let $\mathbf{M}$ be an integer matrix with $|\mathbf{M}| = |\mathbf{N}|/2$. Then $H(\boldsymbol{\omega})$ is $\mathcal{AFS}(\mathbf{M})$ if and only if the following two conditions are satisfied.

1. Define $\mathbf{L} \triangleq \mathbf{M}^{-1}\mathbf{N}$, then $\mathbf{L}^T$ has the form $\mathbf{L}^T = \boldsymbol{\Gamma}\mathbf{U}$, where $\mathbf{U}$ is a unimodular matrix and $\boldsymbol{\Gamma}$ is of one of the following forms,

$$\underset{(a)}{\begin{pmatrix} 1 & \pm p \\ 0 & 2 \end{pmatrix}}, \quad \underset{(b)}{\begin{pmatrix} 2 & 0 \\ \pm p & 1 \end{pmatrix}}, \quad \underset{(c)}{\begin{pmatrix} 2 & \pm p \\ 0 & 1 \end{pmatrix}}, \quad \underset{(d)}{\begin{pmatrix} 1 & 0 \\ \pm p & 2 \end{pmatrix}}, \qquad 0 < p \leq 1. \tag{4.2}$$

   This is equivalent to saying that $|\mathbf{L}| = 2$, $LAT(\mathbf{L}^T) \cap (-1,1)^2 = \{\mathbf{0}\}$ and $\mathbf{L}^T$ has one integer row vector.

2. Let $\boldsymbol{\omega}_0 = \pi\mathbf{N}^{-T}\mathbf{y}_0$, where $\mathbf{y}_0$ is a 2×1 vector. Corresponding to the above four cases of $\mathbf{L}$,

$\mathbf{y}_0$ satisfies,

$$\underset{(a)}{[\mathbf{y}_0]_1 \text{ is odd}} \quad \underset{(b)}{[\mathbf{y}_0]_0 \text{ is odd}} \quad \underset{(c)}{\mathbf{y}_0 = \mathbf{L}^T\mathbf{k} + \begin{pmatrix}1\\0\end{pmatrix}} \quad \underset{(d)}{\mathbf{y}_0 = \mathbf{L}^T\mathbf{k} + \begin{pmatrix}0\\1\end{pmatrix}},$$

$$\text{for some integer vector } \mathbf{k}. \tag{4.3}$$

For example, let $\mathbf{L}$ be as in (4.1). One can verify that the first element of any vector $\mathbf{v} \in LAT(\mathbf{L}^T)$ is an integer and $\mathbf{L}$ satisfies the first condition. Notice the first condition is not necessary in 1D bandpass sampling theorem since $L = 2$ in 1D case and $LAT(L)$ consists of integers only. As indicated by the 1D bandpass sampling theorem in Fact. 4.2, in 1D case only the relative location of the two passbands needs to be constrained.

Proof of Theorem 4.2. We first show that these two conditions are necessary.

Condition 1 is necessary. An equivalent necessary and sufficient condition for $H(\boldsymbol{\omega})$ to be $\mathcal{AFS}(\mathbf{M})$ is that, when $H(\boldsymbol{\omega})$ is decimated and then expanded by $\mathbf{M}$, there is no overlapping in the passbands among $H(\boldsymbol{\omega})$ and the $|\mathbf{M}| - 1$ images. For convenience, we will discuss the decimated and expanded version of $H(\boldsymbol{\omega})$. When $H(\boldsymbol{\omega})$ is decimated and then expanded by $\mathbf{M}$, each of the $|\mathbf{M}| - 1$ images is a shifted version of $H(\boldsymbol{\omega})$; each consists of two parallelograms. For convenience, we normalize the frequency plane by $2\pi\mathbf{N}^{-T}$; the new axes ν_0 and ν_1 are the two entries of $\boldsymbol{\nu} = 2\pi\mathbf{N}^{-T}\boldsymbol{\omega}$. After normalization the support of $H(\boldsymbol{\omega})$ appears as the union of two squares (Fig. 4.7(b)), denoted by S and S' with $S = -\mathbf{y}_0/2 + SPD(0.5\mathbf{I})$ and $S' = \mathbf{y}_0/2 + SPD(0.5\mathbf{I})$.

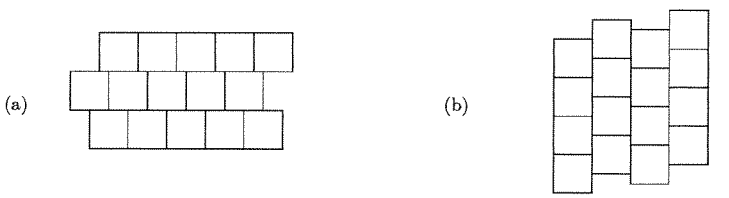

Fig. 4.8. Square tiling with (a) horizontal lines and (b) vertical lines.

As $|\mathbf{N}| = 2|\mathbf{M}|$, this is maximal decimation. So $H(\boldsymbol{\omega})$ and its $|\mathbf{M}| - 1$ images fill the frequency plane; the normalized plane is tiled by the squares of $SPD(0.5\mathbf{I})$. In a square tiling, we can observe at least one set of parallel lines (Fig. 4.8) and all the cells are bounded by these lines. For example in the tiling of Fig. 4.8(a), we can observe one set of horizontal lines and all the squares are bounded by the horizontal lines. An in Fig. 4.8(b), there is one set of vertical lines. So the images of passbands S and S' are confined to these horizontal or vertical lines. Suppose the images of S are located at $-\mathbf{y}_0/2 + \mathbf{c}$ for some vector $\mathbf{c}$. Then $[\mathbf{c}]_1$ must be an integer when the images are bounded by

horizontal lines and $[\mathbf{c}]_0$ must be an integer when the images are bounded by vertical lines. On the other hand observe that the images of S are located at $-\mathbf{y}_0/2 + LAT(\mathbf{L}^T)\mathbf{k}$, for some integer vector $\mathbf{k}$. To have the images of S located between the horizontal or vertical lines, $\mathbf{L}^T$ is necessarily of the form

$$\begin{pmatrix} d_0 & d_1 \\ \times & \times \end{pmatrix} \text{ or } \begin{pmatrix} \times & \times \\ d_0 & d_1 \end{pmatrix} \tag{4.4}$$

for some integers d_0 and d_1, i.e., $\mathbf{L}^T$ has one integer row.

Notice that if a *Two-P* filter with parallelogram prototype $SPD(\pi\mathbf{N}^{-T})$ is $\mathcal{AFS}(\mathbf{M})$, then a one-parallelogram filter with support $SPD(\pi\mathbf{N}^{-T})$ is also $\mathcal{AFS}(\mathbf{M})$. For this, $\mathbf{L}$ must satisfy $LAT(\mathbf{L}^T) \cap (-1,1)^2$. Combining this condition and the fact that $|\mathbf{L}| = 2$, after some row operation we can arrive at (4.2) from (4.4). Conversely, if $\mathbf{L}$ is of the forms in (4.2), then we can verify that $|\mathbf{L}| = 2$, $LAT(\mathbf{L}^T) \cap (-1,1)^2$ and $\mathbf{L}^T$ has one integer row vector. Corresponding to the four cases in 4.2, the passband S and its images are as shown in Fig. 4.9(a)-(d) with $p = 0.25$. Fig. 4.9(e) shows that case when $\mathbf{L}$ is as in (c) of Eq. (4.2) with $p = 1$.

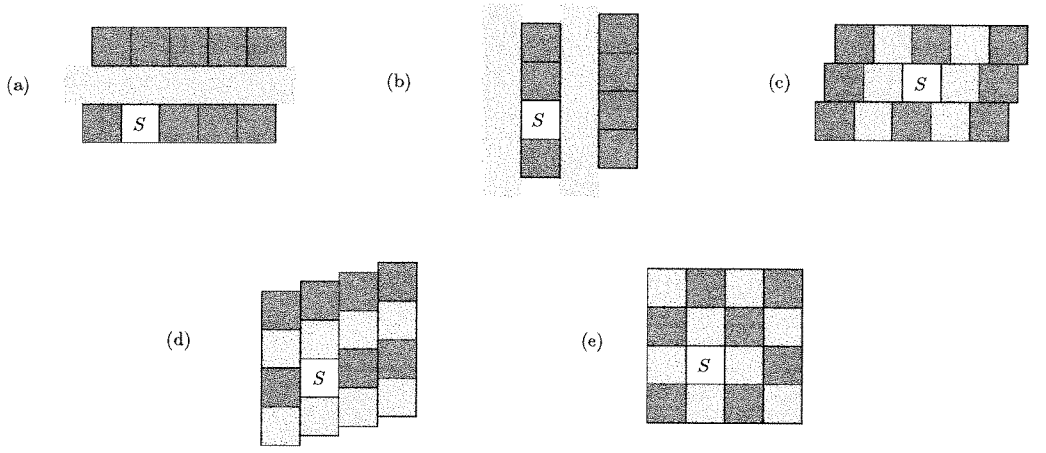

Fig. 4.9. Passband S and relative position to its images (darker shaded squares) for various cases of $LAT(\mathbf{L}^T)$

Condition 2 is necessary. To satisfy the bandpass sampling theorem, the other passband S' must be located in one of the lighter shaded cells that are not occupied yet. In the first case (Fig. 4.9(a)), the second passband can be located anywhere in the lighter shaded stripe; $[\mathbf{y}_0]_1$ is an odd integer. In the third case (Fig. 4.9(c)), lighter shaded cells can be described as

$$-\mathbf{y}_0/2 + \left(\mathbf{L}^T\mathbf{k} + \begin{pmatrix} 1 \\ 0 \end{pmatrix}\right) + SPD(0.5\mathbf{I}), \text{ where } \mathbf{k} \text{ is an integer vector .}$$

When the passband S' is in one of the lighter shaded cells

$$\mathbf{y}_0/2 = -\mathbf{y}_0/2 + \left(\mathbf{L}^T\mathbf{k} + \begin{pmatrix}1\\0\end{pmatrix}\right).$$

So

$$\mathbf{y}_0 = \mathbf{L}^T\mathbf{k} + \begin{pmatrix}1\\0\end{pmatrix}.$$

Similarly, we can verify that the second case and the fourth case.

Conversely, if $\mathbf{L}^T$ is of the form in (4.2) and $\mathbf{y}_0$ is given as in (4.3), we can verify that the passbands of $H(\boldsymbol{\omega})$ and the images are properly interlaced and bandpass sampling theorem is satisfied.

Remarks

1. We would like to point out one necessary condition implied by Theorem 4.2. *The vector* $\mathbf{y}_0$ *has at least one nonzero integer entry.* The importance of this necessary condition will be observed in the next remark.

2. *Continuous time maximal decimation.* Let $H(\boldsymbol{\Omega})$ be the Fourier transform of a 2D continuous time filter $h(\mathbf{t})$. Suppose $H(\boldsymbol{\Omega})$ is an ideal filter and the support of $H(\boldsymbol{\Omega})$ is the union of two parallelograms, each a shifted version of $SPD(\pi\mathbf{N}^{-T})$ and the two parallelograms are separated by $2\pi\mathbf{N}^{-T}\mathbf{y}_0$. The question is what are the conditions such that the output of $H(\boldsymbol{\Omega})$ can be maximally decimated. The necessary and sufficient condition for this is that $\mathbf{y}_0$ has at least one nonzero integer entry. As long as $H(\boldsymbol{\Omega})$ satisfies this condition, we can always find $\mathbf{M}$ with $|\mathbf{M}| = |\mathbf{N}|/2$ such that $H(\boldsymbol{\Omega})$ is aliasfree($\mathbf{M}$). Therefore maximal aliasfree decimation of the output of $H(\boldsymbol{\Omega})$ depends entirely on the relative position of the two passbands. However, in 1D case the condition that y_0 is a nonzero integer is not sufficient. The necessary and sufficient condition in 1D case is that y_0 is an odd integer.

Properties of Two-Parallelogram Filters

In all cases of Fig. 4.9, we observe that S is adjacent to its own images. This is in general true; it can be verified that S is necessarily adjacent to its own images when the bandpass sampling theorem is satisfied. The type of adjacency is determined by $LAT(\mathbf{L}^T)$. More specifically, we have the following three cases.

1. *Complete edge adjacency.* When $\mathbf{L}$ is as in (a) or (b) of Eq. (4.2), S is adjacent to its images on two edges; S and its images form a stripe pattern (Fig. 4.9(a)-(b)).

2. *Partial edge adjacency.* When $\mathbf{L}$ is as in (c) or (d) of Eq. (4.2) with $p \neq 1$, S is partially edge adjacent to its images (Fig. 4.9(c)-(d)).

3. *Vertex adjacency.* When $\mathbf{L}$ is as in (c) or (d) of Eq. (4.2) with $p = 1$, $LAT(\mathbf{L}^T)$ is quincunx (Fig. 4.10). In this case, S is vertex adjacent to its images; S and its images form a check pattern (Fig. 4.9(e)). Notice that this is very different from the 1D case. Recall in 1D case, no passbands of the analysis filters are adjacent to their own images. This observation will help us to study permissibility of *Two-P* filter banks.

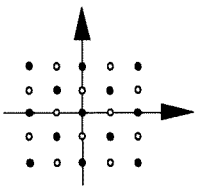

Fig. 4.10. The quincunx lattice.

4.3.2 Permissibility of Two-Parallelogram Filter Banks

Now consider a *Two-P* filter bank. In the subbands, the images of the analysis filters will be attenuated to the stopband level of the synthesis filter except those images that are adjacent to the synthesis filters. Those adjacent images result in major aliasing if the individual filters are assumed to have good frequency selectivity. In 2D case, there are several different types of adjacency, which result in different types of major aliasing. As the notion of permissibility originates from uncancelable major aliasing, we have to consider a finer classification of permissibility. Consider the different cases in Fig. 4.9. Suppose the shaded areas represent the images of S or S'. In all cases, one image is adjacent to S and will result in different major aliasing. For example in Fig. 4.9(a)-(d) the image results in edge aliasing, whereas in Fig. 4.9(e) the image results in vertex aliasing. For an alias transfer function $A_{\mathbf{k}}(\boldsymbol{\omega})$, if in a certain frequency region there is only one particular major aliasing term, then this major aliasing can not be canceled. In this case, when the uncancelable aliasing is edge based or vertex based the support is called edge nonpermissible or vertex nonpermissible respectively. We see that edge adjacency corresponds to band adjacency in 1D case (Fig. 4.5) while vertex adjacency has no 1D correspondence. Comparing these two types of nonpermissibility, edge based aliasing is in general much more serious than vertex based. The filter banks that do not have any type of uncancelable major aliasing is called permissible. We will explain below that the *Two-P* filter banks can have edge permissible but can not have both edge and vertex permissibility.

When the images of S are adjacent to S, major aliasing is created and this major aliasing is

uncancelable. To explain this, suppose

$$\mathbf{L}^T = \begin{pmatrix} 1 & 0 \\ p & 2 \end{pmatrix}$$

as in (d) of Eq. (4.2). As the vector $\begin{pmatrix} 1 & p \end{pmatrix}^T \in LAT(\mathbf{L}^T)$, one image of S will be separated from S by $\begin{pmatrix} 1 & p \end{pmatrix}^T$. This image is edge adjacent to S and creates major aliasing as in Fig. 4.11. The resulting major aliasing contributes to the alias transfer function $A_{(1,0)}(\boldsymbol{\omega})$ since $\begin{pmatrix} 1 & p \end{pmatrix}^T = \mathbf{L}^T \begin{pmatrix} 1 & 0 \end{pmatrix}^T$. In other subbands, the major aliasing errors that contribute to $A_{(1,0)}(\boldsymbol{\omega})$ are not in the the same frequency region; this major aliasing is uncancelable. But from previous subsection, we know images of S will always be adjacent to S. We conclude that *Two-P* filter banks are not permissible in general under the assumption of good analysis and synthesis filters.

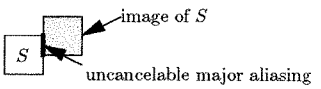

Fig. 4.11. Illustration of uncancelable major aliasing.

On the other hand in Fig. 4.9(e), we observe that images of S are only vertex adjacent to S. So edge permissibility is possible. The *Two-P* cosine modulated filter banks that have edge permissibility will be constructed in the next section.

4.4 Configuration of Two-Parallelogram Cosine Modulated Filter Banks

In view of the construction procedure for 1D cosine modulated filter banks (CMFB) in Sec. 4.2 and the discussion in previous section, there are three important issues to be addressed. First, for a given filter bank with decimation matrix $\mathbf{M}$ as in Fig. 4.1 we ask how to obtain the analysis filters such that the support configuration of the 2D CMFB is an extension of 1D version. The second issue is the analysis and synthesis filters should be $\mathcal{AFS}(\mathbf{M})$ and the configuration should be $\mathcal{AFS}(\mathbf{M})$. Moreover, as the supports of the analysis filters form a tiling of the frequency plane, the filter bank has perfect reconstruction when the prototype filter is an ideal filter. For those that satisfy these two criteria, we further consider support permissibility.

Issue 1. Support Configuration

The general setting of 1D M-channel CMFB can be summarized as follows.

1. Design a $2M$-channel uniform DFT filter bank.

2. Shift the filters in the DFT filter bank by $\pi/2M$ and combine appropriate pairs of filters to yield real-coefficient analysis filters.

We now translate these procedures to 2D case and construct the *Two-P* CMFB. To design a *Two-P* CMFB with decimation matrix $\mathbf{M}$, conceptually we start from a uniform DFT filter bank [98] with decimation matrix $\mathbf{N} = \mathbf{ML}$, where $\mathbf{L}$ is an integer matrix (to be chosen appropriately) with $|\mathbf{L}| = 2$. For example,

$$\text{let } \mathbf{M} = \begin{pmatrix} 7 & -2 \\ 0 & 1 \end{pmatrix} \text{ and } \mathbf{L} = \begin{pmatrix} 1 & 1 \\ 2 & 4 \end{pmatrix}, \text{ then } \mathbf{N} = \begin{pmatrix} 3 & -1 \\ 2 & 4 \end{pmatrix}.$$

As $|\mathbf{N}| = 14$, there are total 14 DFT filters as shown in Fig. 4.12. The DFT filters $P_i(\boldsymbol{\omega})$ are given by

$$P_i(\boldsymbol{\omega}) = P_0(\boldsymbol{\omega} - 2\pi\mathbf{N}^{-T}\mathbf{k}_i), \quad \mathbf{k}_i \in \mathcal{N}(\mathbf{N}^T).$$

Each filter in the DFT filter bank is a shifted version of a prototype $P(\boldsymbol{\omega})$, which has a parallelogram support $SPD(\pi\mathbf{N}^{-T})$. For a given $\mathbf{M}$, the support of the prototype is different for different choice of $\mathbf{L}$. In 1D CMFB, we shift the filters by $\pi/2M$. But in 2D case, the shifts are vector-shifts and we can shift the filters by

$$\pi\mathbf{N}^{-T}\begin{pmatrix}1 & 0\end{pmatrix}^T, \pi\mathbf{N}^{-T}\begin{pmatrix}0 & 1\end{pmatrix}^T, \text{ or } \pi\mathbf{N}^{-T}\begin{pmatrix}1 & 1\end{pmatrix}^T,$$

as shown in Fig. 4.13. Fig. 4.14(a)-(c) shows the results with respect to the three shifts. The filters $Q_{A,i}(\boldsymbol{\omega})$, $Q_{B,i}(\boldsymbol{\omega})$ and $Q_{C,i}(\boldsymbol{\omega})$ are given by

$$\begin{aligned} Q_{A,i}(\boldsymbol{\omega}) &= P_i(\boldsymbol{\omega} - 2\pi\mathbf{N}^{-T}\begin{pmatrix}0.5 & 0\end{pmatrix}^T), \\ Q_{B,i}(\boldsymbol{\omega}) &= P_i(\boldsymbol{\omega} - 2\pi\mathbf{N}^{-T}\begin{pmatrix}0 & 0.5\end{pmatrix}^T), \\ Q_{C,i}(\boldsymbol{\omega}) &= P_i(\boldsymbol{\omega} - 2\pi\mathbf{N}^{-T}\begin{pmatrix}0.5 & 0.5\end{pmatrix}^T). \end{aligned}$$

For all the three cases, filters can be paired to obtain real-coefficient analysis filters. For example, in Fig. 4.14(a), the filter coefficients of $Q_{A,i}(\boldsymbol{\omega})$ and $Q'_{A,i}(\boldsymbol{\omega})$ are complex conjugates of each other. The filters $Q_{A,i}(\boldsymbol{\omega})$ and $Q'_{A,i}(\boldsymbol{\omega})$ can be paired to obtain the analysis filter $H_{A,i}(\boldsymbol{\omega})$,

$$H_{A,i}(\boldsymbol{\omega}) = Q_{A,i}(\boldsymbol{\omega}) + Q'_{A,i}(\boldsymbol{\omega}).$$

The corresponding synthesis filter is $F_{A,i}(\boldsymbol{\omega}) = Q^*_{A,i}(\boldsymbol{\omega}) + Q'^*_{A,i}(\boldsymbol{\omega})$. Similarly in Fig. 4.14(b) and

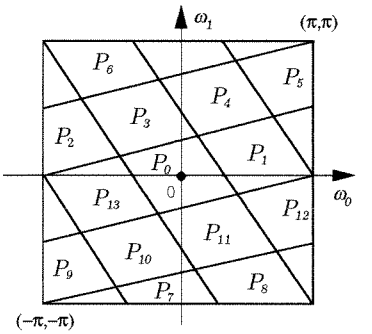

Fig. 4.12. DFT filter bank with decimation matrix $\mathbf{N}$.

(c), $H_{B,i}(\boldsymbol{\omega})$ consists of $Q_{B,i}(\boldsymbol{\omega})$ and $Q'_{B,i}(\boldsymbol{\omega})$, and $H_{C,i}(\boldsymbol{\omega})$ consists of $Q_{C,i}(\boldsymbol{\omega})$ and $Q'_{C,i}(\boldsymbol{\omega})$. (The subscripts A, B and C of the analysis and synthesis filters are only temporary and meant to distinguish the three cases in Fig. 4.14.) Each analysis filter consists of two parallelograms. So the CMFB constructed this way is a subclass of *Two-P* filter banks. We observe that all three support configurations are extension of the 1D version. The three configurations will be referred to as configuration A, B, and C in the discussion to follow. From Fig. 4.14 it seems that configurations A and B are very similar. Indeed as we will see in issue 2 and 3, properties derived for configurations A are also true for configuration B except some minor modifications.

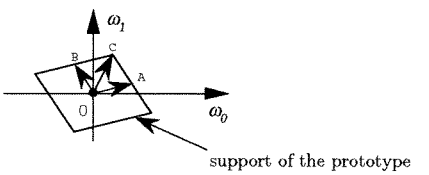

Fig. 4.13. Three possible vector shifts.

Issue 2. $\mathcal{AFS}(\mathbf{M})$ Support Configuration

We now study the conditions such that configurations A, B and C are $\mathcal{AFS}(\mathbf{M})$. As $\mathbf{M}$ is fixed and supports of the analysis filters in each configuration are already determined, Theorem 4.2 implies that $\mathbf{L}$ will completely determine whether the the analysis filters are $\mathcal{AFS}(\mathbf{M})$ in the ideal case. In configuration A, the two passbands of the analysis filters are separated by $2\pi\mathbf{N}^{-T}(2\mathbf{k} + \begin{pmatrix}1 & 0\end{pmatrix}^T)$, for some integer vector $\mathbf{k}$. By Theorem 4.2, the analysis filters are $\mathcal{AFS}(\mathbf{M})$ in ideal case in the following two situations.

1. Choose $\mathbf{L}$ as in (b) of Eq. (4.2) for any $0 < p \leq 1$.

2. Choose $\mathbf{L}$ as in (c) of Eq. (4.2) with $p = 1$, which yields quincunx $LAT(\mathbf{L}^T)$ (Fig. 4.10).

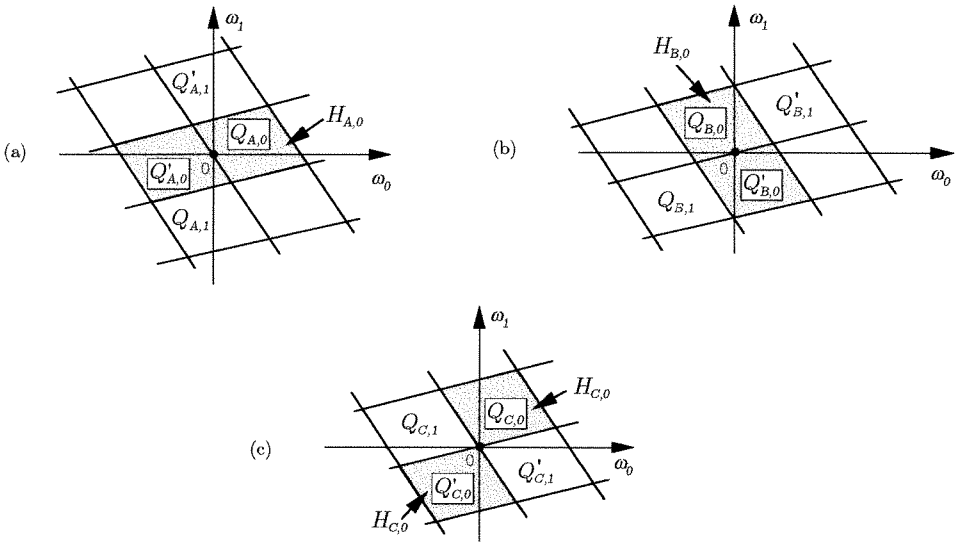

Fig. 4.14. Three possible support configurations of the *Two-P* cosine modulated filter bank, (a) configuration A, (b) configuration B and (c) configuration C.

Similarly, in configurations B and C, the two passbands of the analysis filters are separated respectively by $2\pi\mathbf{N}^{-T}(2\mathbf{k}+\begin{pmatrix}0 & 1\end{pmatrix}^T)$ and $2\pi\mathbf{N}^{-T}(2\mathbf{k}+\begin{pmatrix}1 & 1\end{pmatrix}^T)$. We can verify that configuration B is $\mathcal{AFS}(\mathbf{M})$ if we choose $\mathbf{L}$ as in (a) of Eq. (4.2) for any $0 < p \leq 1$ or we can choose $\mathbf{L}$ as in (c) of Eq. (4.2) with $p = 1$, i.e., quincunx $LAT(\mathbf{L}^T)$. Also configuration C is $\mathcal{AFS}(\mathbf{M})$ if we choose $\mathbf{L}$ as in (a) or (b) of Eq. (4.2) for any $0 < p \leq 1$.

Notice that in all three configurations, the analysis filters form a tiling of the frequency plane. When the configurations are $\mathcal{AFS}(\mathbf{M})$, the filter bank has perfect reconstruction if the prototype is an ideal filter.

Issue 3. Support Permissibility

According to the preceding analysis, each of the three support configurations is $\mathcal{AFS}(\mathbf{M})$ for some $\mathbf{L}$. However not all configurations are valid candidates in terms of support permissibility. From the discussion of *Two-P* filters in Sec. 4.4, we know when $\mathbf{L}^T$ is as in (a) or (b) of Eq. (4.2), one passband is edge adjacent to its own images, which leads to edge nonpermissibility. The 2D CMFB studied in [30] usually has this type of nonpermissible support. From the consideration of support permissibility, any configuration with $\mathbf{L}$ as in (a) or (b) of Eq. (4.2) is not suitable for the development of 2D CMFB. As configuration C is $\mathcal{AFS}(\mathbf{M})$ only for these two types of $\mathbf{L}$, configurations C will not be considered. Also configurations A and B with $\mathbf{L}$ as in (a) and (b) of Eq. (4.2) will not be considered. To design a edge permissible *Two-P* CMFB, the only two possible choices left are configuration A and B with quincunx $LAT(\mathbf{L}^T)$. Indeed, we will explain below that these two choices do lead to edge permissible *Two-P* CMFB.

As we discussed in Sec. 4.4, for *Two-P* filters, each of the two passbands and its images form a check pattern when $LAT(\mathbf{L}^T)$ is quincunx (Fig. 4.9(e)). So each passband is edge adjacent to four images of the other passband, which results in edge aliasing (Fig. 4.15). However, we can show that these edge aliasing appear in pairs and the *Two-P* CMFB is edge permissible. To see this, consider the ith subband in configuration A and only image (a), which is at the support of $Q'_{A,j}(\boldsymbol{\omega})$. The resulting edge aliasing is as shown in Fig. 4.15. On the other hand, four images of $Q_{A,j}(\boldsymbol{\omega})$ will be edge adjacent to $Q'_{A,j}$; one of the four images is at $Q'_{A,i}$ and results in edge aliasing. It turns out that these two edge aliasing errors contribute to the same alias transfer function. So edge aliasing errors appear in pairs and configuration A is edge permissible. The situation for configuration B is similar. In Sec. 4.6, we will discuss in details how those edge aliasing errors can cancel one another.

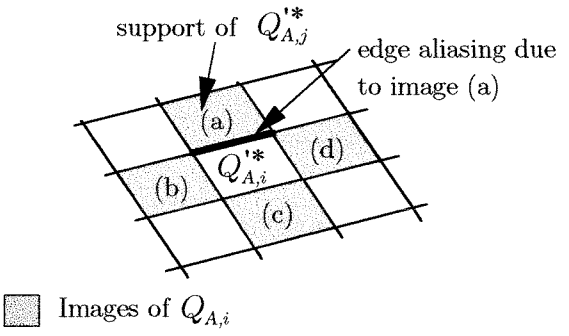

Fig. 4.15. Images of $Q_{A,i}(\boldsymbol{\omega})$ and their positions relative to $Q'^{*}_{A,i}(\boldsymbol{\omega})$; four images of $Q_{A,i}(\boldsymbol{\omega})$ are edge-adjacent to $Q'^{*}_{A,i}(\boldsymbol{\omega})$.

Although configurations A and B can be edge permissible, they are not vertex permissible. For each analysis filter, images of one passband will be vertex adjacent to itself. The analysis in previous section shows that the resulting vertex aliasing is uncancelable under the assumption of good analysis and synthesis filters. Table 4.1 is a summary of the role of $\mathbf{L}$ to the $\mathcal{AFS}(\mathbf{M})$ properly and permissibility of each configuration. We see that configuration C is either violating sampling criterion or edge nonpermissible. Configuration A or B can satisfy the sampling criterion and at the same time is edge permissible if $LAT(\mathbf{L}^T)$ is quincunx (Fig. 4.10). These two cases are more suitable for the construction of *Two-P* CMFB. In this case, the *Two-P* CMFB can have edge-based permissibility but lacks vertex-based permissibility. This imposes limitation on the attenuation of the individual filters in the *Two-P* CMFB.

L / configuration	(a) of Eq. (4.2) $0 < p \leq 1$	(b) of Eq. (4.2) $0 < p \leq 1$	(c) of Eq. (4.2) p=1 (quincunx $LAT(\mathbf{L}^T)$)
A		□	□ ■
B	□		□ ■
C	□	□	■

□ satisfying the sampling criterion

■ edge permissible

Table 4.1. The sampling criterion, edge permissibility and relation to the various cases of $\mathbf{L}$ in Eq. (4.1) for configurations A, B and C.

4.5 Formulation of the Two-Parallelogram Cosine Modulated Filter Banks

We have set up the framework of *Two-P* CMFB in Sec. 4.4. We have also derived two edge permissible support configurations. In this section, we will consider all the design details. For a given 2D filter bank with decimation matrix $\mathbf{M}$, we start from a uniform DFT filter bank with twice the number of channels. By shifting the DFT filters properly, we obtain two edge permissible configurations. We then proceed to formulate the analysis and synthesis filters.

4.5.1 Configuration A and B

Consider the $|\mathbf{M}|$-channel 2D filter bank with decimation matrix $\mathbf{M}$ in Fig. 4.1. We start from a uniform DFT filter bank with decimation matrix $\mathbf{N} = \mathbf{ML}$, where $\mathbf{L}$ is an integer matrix with $|\mathbf{L}| = 2$ and quincunx $LAT(\mathbf{L}^T)$ (for edge permissibility). To be more specific about the formulation of the DFT filter bank, let $\mathbf{M}$ be diagonalized as $\mathbf{M} = \mathbf{U}\mathbf{\Lambda}_\mathbf{M}\mathbf{V}_\mathbf{M}$, where $\mathbf{U}$ and $\mathbf{V}_\mathbf{M}$ are unimodular. The matrix $\mathbf{\Lambda}_\mathbf{M}$ is diagonal with diagonal elements $[\mathbf{\Lambda}_\mathbf{M}]_{00} = \lambda_0 > 0$ and $[\mathbf{\Lambda}_\mathbf{M}]_{11} = \lambda_1 > 0$. For simplicity, we choose

$$\mathbf{L} = \mathbf{V}_\mathbf{M}^{-1} \begin{pmatrix} 1 & 0 \\ 0 & 2 \end{pmatrix} \mathbf{V},$$

for some unimodular $\mathbf{V}$ such that $LAT(\mathbf{L}^T)$ is quincunx. Then the matrix $\mathbf{N}$ given by $\mathbf{N} = \mathbf{ML}$ becomes

$$\mathbf{N} = \underbrace{\mathbf{U}\begin{pmatrix}\lambda_0 & 0\\ 0 & \lambda_1\end{pmatrix}\mathbf{V}_\mathbf{M}}_{\mathbf{M}}\underbrace{\mathbf{V}_\mathbf{M}^{-1}\begin{pmatrix}1 & 0\\ 0 & 2\end{pmatrix}\mathbf{V}}_{\mathbf{L}} \quad \text{or} \quad \mathbf{N} = \underbrace{\mathbf{U}\begin{pmatrix}\lambda_0 & 0\\ 0 & 2\lambda_1\end{pmatrix}}_{\mathbf{\Lambda}}\mathbf{V}. \tag{4.5}$$

Clearly, $|\mathbf{M}| = \lambda_0\lambda_1$, $|\mathbf{L}| = 2$ and $|\mathbf{N}| = 2\lambda_0\lambda_1$. The prototype filter $P(\boldsymbol{\omega})$ in the DFT filter bank has a parallelogram support $SPD(\pi\mathbf{N}^{-T})$. The DFT filters are shifted versions of the prototype by $2\pi\mathbf{N}^{-T}\mathbf{k}_i$, for $\mathbf{k}_i \in \mathcal{N}(\mathbf{N}^T)$.

For referring convenience, we will adopt a particular ordering of $\mathcal{N}(\mathbf{N}^T)$. As $\mathbf{V}^T\mathbf{\Lambda}$ and $\mathbf{N}^T$ have the same lattices, we will consider the ordering of $\mathcal{N}(\mathbf{V}^T\mathbf{\Lambda})$ for simplicity. The ordering is as follows.

$$\mathbf{k}_{k_0+\lambda_0 k_1} = \mathbf{V}^T\begin{pmatrix}k_0\\ k_1\end{pmatrix}, \quad k_0 = 0, 1, \ldots, \lambda_0 - 1,\ k_1 = 0, 1, \ldots, 2\lambda_1 - 1. \tag{4.6}$$

Then $\mathcal{N}(\mathbf{V}^T\mathbf{\Lambda}) = \{\mathbf{k}_0, \mathbf{k}_1, \ldots, \mathbf{k}_{|\mathbf{N}|-1}\}$. Configurations A and B (Fig. 4.14) are obtained by shifting the DFT filters. In particular, the complex filter underlying configurations A and B are

$$Q_\mathbf{k}(\boldsymbol{\omega}) = P\left(\boldsymbol{\omega} - 2\pi\mathbf{N}^{-T}(\mathbf{k} + \mathbf{l})\right), \mathbf{k} \in \mathcal{N}(\mathbf{V}^T\mathbf{\Lambda}),$$

where $\mathbf{l} = \begin{pmatrix}0.5 & 0\end{pmatrix}^T$ for configuration A and $\mathbf{l} = \begin{pmatrix}0 & 0.5\end{pmatrix}^T$ for configuration B. The vector subscript of $Q_\mathbf{k}(\boldsymbol{\omega})$ should be interpreted modulo $\mathbf{N}^T$.

4.5.2 The Analysis and Synthesis Filters

To obtain real-coefficient analysis and synthesis filters, we need to combine two shifted copies of the prototype $P(\boldsymbol{\omega})$. Suppose the impulse response of $Q_\mathbf{k}(\boldsymbol{\omega})$ is $q_\mathbf{k}(\mathbf{n})$. Let $\mathbf{k}'$ be such that $q_{\mathbf{k}'}(\mathbf{n}) = q_\mathbf{k}^*(\mathbf{n})$. Pair $Q_\mathbf{k}(\boldsymbol{\omega})$ and $Q_{\mathbf{k}'}(\boldsymbol{\omega})$, then the analysis filters of the form $Q_\mathbf{k}(\boldsymbol{\omega}) + Q_{\mathbf{k}'}(\boldsymbol{\omega})$ have real coefficients. The pairing procedure is formulated in the following property.

Proposition 4.1. The coefficients of $Q_{\mathbf{k}_{m_0+m_1\lambda_0}}(\boldsymbol{\omega})$ and $Q_{\mathbf{k}_{m_0'+m_1'\lambda_0}}(\boldsymbol{\omega})$ are complex conjugates of each other if m_0, m_0', m_1, and m_1' are related by

$$m_0 + m_0' = b_0 \bmod \lambda_0, \quad \text{and} \quad m_1 + m_1' = b_1 \bmod 2\lambda_1, \text{ where } \begin{pmatrix}b_0\\ b_1\end{pmatrix} = -2\mathbf{V}^{-T}\mathbf{l}. \tag{4.7}$$

Proof: The filter $Q_\mathbf{k}(\boldsymbol{\omega})$ is a shift of the prototype $P(\boldsymbol{\omega})$ by $2\pi\mathbf{N}^{-T}(\mathbf{k} + \mathbf{l})$. If $Q_{\mathbf{k}'}(\boldsymbol{\omega})$ is a shift of the prototype $P(\boldsymbol{\omega})$ by $-2\pi\mathbf{N}^{-T}(\mathbf{k} + \mathbf{l})$, $q_\mathbf{k}(\mathbf{n})$ and $q_{\mathbf{k}'}(\mathbf{n})$ are conjugates of each other. So

$Q_{\mathbf{k}}(\boldsymbol{\omega}) + Q_{\mathbf{k}'}(\boldsymbol{\omega})$ has real coefficients, if $2\pi\mathbf{N}^{-T}(\mathbf{k}' + \mathbf{l}) = -2\pi\mathbf{N}^{-T}(\mathbf{k} + \mathbf{l}) \bmod 2\pi\mathbf{I}$, or equivalently

$$\mathbf{k} + \mathbf{k}' = -2\mathbf{l} \bmod \mathbf{N}^T. \tag{4.8}$$

Next, we would like to relate m and m' such that $\mathbf{k}_m + \mathbf{k}_{m'} = -2\mathbf{l} \bmod \mathbf{N}^T$. Let $m = m_0 + \lambda_0 m_1$ and $m' = m'_0 + \lambda_0 m'_1$, then

$$\mathbf{k}_m = \mathbf{V}^T \begin{pmatrix} m_0 \\ m_1 \end{pmatrix}, \quad \mathbf{k}_{m'} = \mathbf{V}^T \begin{pmatrix} m'_0 \\ m'_1 \end{pmatrix}, \quad \text{and therefore } \mathbf{V}^T \begin{pmatrix} m_0 + m'_0 \\ m_1 + m'_1 \end{pmatrix} \overset{\mathbf{N}^T}{=} -2\mathbf{l}.$$

It follows that

$$Q_{\mathbf{k}_{m_0+m_1\lambda_0}}(\boldsymbol{\omega}) + Q_{\mathbf{k}_{m'_0+m'_1\lambda_0}}(\boldsymbol{\omega})$$

have real coefficients if m_0, m'_0, m_1, and m'_1 are related as in (4.7). ■

If we combine conjugate pairs $Q_{\mathbf{k}}(\boldsymbol{\omega})$ and $Q_{\mathbf{k}'}(\boldsymbol{\omega})$ as described in Proposition 4.1, we get $|\mathbf{M}|$ real-coefficient analysis filters.

$$H_m(\boldsymbol{\omega}) = Q_{\mathbf{k}_{m_0+m_1\lambda_0}}(\boldsymbol{\omega}) + Q_{\mathbf{k}_{m'_0+m'_1\lambda_0}}(\boldsymbol{\omega}), F_m(\boldsymbol{\omega}) = H_m^*(\boldsymbol{\omega}), \quad m = 0, 1, \ldots, |\mathbf{M}| - 1, \tag{4.9}$$

where $m_0 = m \bmod \lambda_0$, $m_1 = b + (m - m_0)/\lambda_0 \bmod 2\lambda_1$, and $b = (b_1 + 1)/2$. Values of m'_0 and m'_1 are given by (4.7). It can be verified that $b = (b_1 + 1)/2$ is an integer and the above enumeration of the analysis filters is complete. It follows from (4.9) that the impulse response of the analysis filter $H_m(\boldsymbol{\omega})$ is

$$h_m(\mathbf{n}) = 2p(\mathbf{n}) \cos(2\pi(\mathbf{k}_{m_0+m_1\lambda_0} + \mathbf{l})^T \mathbf{N}^{-1}\mathbf{n}), \quad m = 0, 1, \ldots, |\mathbf{M}| - 1.$$

We have chosen $F_m(\boldsymbol{\omega}) = H_m^*(\boldsymbol{\omega})$ in the above formulation, as the system is eventually going to be paraunitary. The impulse responses of the analysis and synthesis filters are related by

$$f_k(\mathbf{n}) = h_k(-\mathbf{n}), \text{where } \mathbf{n} \text{ is any } 2 \times 1 \text{ vector.}$$

In a 1D CMFB, each analysis filter has two distinct shifts of the prototype filter. So the total bandwidth of each individual filter is the same. For 2D filters, total bandwidth should be interpreted as the total spectral occupancy. In the *Two-P* CMFB, all analysis filters have the same size of spectral occupancy. Every analysis filter consists of two distinct shifts of the prototype. This follows from the quincunx property of $LAT(\mathbf{L}^T)$ as we will show below.

Proposition 4.2. *The analysis filters have equal size of spectral occupancy.*

Proof: We only need to show that $Q_{\mathbf{k}}(\boldsymbol{\omega})$ and $Q_{\mathbf{k}'}(\boldsymbol{\omega})$ are distinct filters whenever the coefficients

of $Q_{\mathbf{k}}(\boldsymbol{\omega})$ and $Q_{\mathbf{k}'}(\boldsymbol{\omega})$ are complex conjugate of each other. Suppose the contrary is true: the coefficients of $Q_{\mathbf{k}}(\boldsymbol{\omega})$ and $Q_{\mathbf{k}'}(\boldsymbol{\omega})$ are complex conjugate of each other but they are the same filter, i.e., $\mathbf{k} = \mathbf{k}' \bmod \mathbf{N}^T$. By (4.8), we have

$$2\mathbf{k} \overset{\mathbf{N}^T}{=} -2\mathbf{l}.$$

As $LAT(\mathbf{L}^T)$ is quincunx, $2\mathbf{k} = \mathbf{0} \bmod \mathbf{L}^T$. Taking modulo $\mathbf{L}^T$ on both sides of the above equation, we have $\mathbf{0} \overset{\mathbf{L}^T}{=} -2\mathbf{l}$. By the definition of $\mathbf{l}$, $2\mathbf{l} = \begin{pmatrix} 1 & 0 \end{pmatrix}^T$ or $\begin{pmatrix} 0 & 1 \end{pmatrix}^T$. So $2\mathbf{l} \notin LAT(\mathbf{L}^T)$, which leads to a contradiction. We conclude that when the coefficients of $Q_{\mathbf{k}}(\boldsymbol{\omega})$ and $Q_{\mathbf{k}'}(\boldsymbol{\omega})$ are complex conjugate of each other, $Q_{\mathbf{k}}(\boldsymbol{\omega})$ and $Q_{\mathbf{k}'}(\boldsymbol{\omega})$ are not same and each analysis filter consists of two distinct copies of the prototype. ■

4.6 Perfect Reconstruction Two-Parallelogram Cosine Modulated Filter Banks

In this section, we first show how to cancel edge aliasing errors that arise in every subband. Then we present the necessary and sufficient condition for perfect reconstruction of *Two-P* CMFB. In 1D case, the CMFB has perfect reconstruction if and only if the polyphase components of the prototype are pairwise power complementary [37]. We will see that similar necessary and sufficient conditions can be derived for *Two-P* CMFB as well.

4.6.1 Cancelation of Edge Aliasing

In Sec. 4.4, we mention that in each subband (configuration A or B), one passband of each analysis filter is edge adjacent to four images of the other passband. This results in serious edge aliasing. It turns out that these edge aliasing errors from different subband can actually cancel with one another if the prototype has linear phase and satisfies some minor condition. To be more specific, let the impulse response of the prototype be $p(\mathbf{n})$ and

$$p(\mathbf{n}) = p(\mathbf{n}_s - \mathbf{n}), \text{for some integer vector } \mathbf{n}_s. \tag{4.10}$$

Proposition 4.3. Consider a *Two-P* CMFB with analysis and synthesis given as in (4.9). Let $LAT(\mathbf{L}^T)$ be quincunx. Then the followings are true.

1. Edge aliasing errors appear in pairs.

2. Pairwise edge aliasing can cancel with each other if $\mathbf{n}_s$ satisfies

$$\mathbf{n}_s = \mathbf{N} \begin{pmatrix} 0.5 \\ 0.5 \end{pmatrix} \mod \mathbf{N}. \tag{4.11}$$

3. The vector $\mathbf{n}_s$ thus determined is an integer vector and $\mathbf{n}_s$ has the form

$$\mathbf{n}_s \overset{\mathbf{N}}{=} \mathbf{U} \begin{pmatrix} 0 & \lambda_1 \end{pmatrix}^T.$$

■

This is a minor condition because it is always possible to shift the linear-phase prototype such that (4.11) is satisfied.

Proof:

1. Consider the subband that has analysis filter $Q_{\mathbf{k}}(\omega) + Q_{\mathbf{k}'}(\omega)$. The aliasing terms due to edge adjacency of $Q^*_{\mathbf{k}'}(\omega)$ and images of $Q_{\mathbf{k}}(\omega)$ are

$$Q_{\mathbf{k}'+\mathbf{k}_s}(\omega) Q^*_{\mathbf{k}'}(\omega), \text{ where } \mathbf{k}_s \in AS. \tag{4.12}$$

The *Adjacency Set* AS is given by $AS \triangleq \left\{ \begin{pmatrix} 1 \\ 0 \end{pmatrix}, \begin{pmatrix} -1 \\ 0 \end{pmatrix}, \begin{pmatrix} 0 \\ 1 \end{pmatrix}, \begin{pmatrix} 0 \\ -1 \end{pmatrix} \right\}$.

These aliasing terms contribute respectively to the aliasing transfer function

$$A_{\mathbf{L}-\tau(2\mathbf{k}'+2\mathbf{l}+\mathbf{k}_s)}(\omega).$$

Now consider the subband that has analysis filter $Q_{\mathbf{k}-\mathbf{k}_s}(\omega) + Q_{\mathbf{k}'+\mathbf{k}_s}(\omega)$, one image of $Q_{\mathbf{k}-\mathbf{k}_s}(\omega)$ will be located at support of $Q_{\mathbf{k}'}(\omega)$ and results in aliasing error

$$Q^*_{\mathbf{k}'+\mathbf{k}_s}(\omega) Q_{\mathbf{k}'}(\omega), \tag{4.13}$$

which also contributes to $A_{\mathbf{L}-\tau(2\mathbf{k}'+2\mathbf{l}+\mathbf{k}_s)}(\omega)$. So the edge aliasing errors do occur in pairs.

2. Notice that the error in (4.13) is the conjugate of error in (4.12) and they cancel each other if

$$Q^*_{\mathbf{k}'}(\omega) Q_{\mathbf{k}'+\mathbf{k}_s}(\omega) = -Q_{\mathbf{k}'}(\omega) Q^*_{\mathbf{k}'+\mathbf{k}_s}(\omega), \quad \forall \mathbf{k}_s \in AS.$$

In what follows, we show that the above equation holds when $\mathbf{n}_s$ is as in (4.11). By (4.10), $P(\boldsymbol{\omega})$ assumes the form $P(\boldsymbol{\omega}) = e^{-j\boldsymbol{\omega}^T\mathbf{n}_s/2}P_r(\boldsymbol{\omega})$, where $P_r(\boldsymbol{\omega})$ is a real-valued function. Let

$$P_{r,\mathbf{k}}(\boldsymbol{\omega}) = P_r(\boldsymbol{\omega} - 2\pi\mathbf{N}^{-T}(\mathbf{k}+\mathbf{l})),$$

then we can verify

$$Q^*_{\mathbf{k}'}(\boldsymbol{\omega})Q_{\mathbf{k}'+\mathbf{k}_s}(\boldsymbol{\omega}) + Q_{\mathbf{k}'}(\boldsymbol{\omega})Q^*_{\mathbf{k}'+\mathbf{k}_s}(\boldsymbol{\omega}) = (e^{j\pi\mathbf{k}_s^T\mathbf{N}^{-1}\mathbf{n}_s} + e^{-j\pi\mathbf{k}_s^T\mathbf{N}^{-1}\mathbf{n}_s})P_{r,\mathbf{k}'}(\boldsymbol{\omega})P_{r,\mathbf{k}'+\mathbf{k}_s}(\boldsymbol{\omega}).$$

In view of the above equation, the condition for alias cancelation is $e^{j2\pi\mathbf{k}_s^T\mathbf{N}^{-1}\mathbf{n}_s} = -1$, $\forall\mathbf{k}_s \in AS$. Since $e^{j2\pi\mathbf{k}_s^T\mathbf{N}^{-1}\mathbf{n}_s} = e^{-j2\pi\mathbf{k}_s^T\mathbf{N}^{-1}\mathbf{n}_s}$, it is necessary and sufficient that

$$e^{j2\pi\mathbf{k}_s^T\mathbf{N}^{-1}\mathbf{n}_s} = -1, \quad \text{for } \mathbf{k}_s = \begin{pmatrix}1\\0\end{pmatrix} \text{ and } \mathbf{k}_s = \begin{pmatrix}0\\1\end{pmatrix}.$$

That is,

$$2\pi\begin{pmatrix}1 & 0\\ 0 & 1\end{pmatrix}\mathbf{N}^{-1}\mathbf{n}_s = 2\pi\mathbf{d} + \pi\begin{pmatrix}1\\1\end{pmatrix}, \text{for some integer vector } \mathbf{d}.$$

Premultiplying both sides by $\frac{1}{2\pi}\mathbf{N}$, we have $\mathbf{n}_s = \mathbf{N}\mathbf{d} + \mathbf{N}\begin{pmatrix}0.5 & 0.5\end{pmatrix}^T$, or equivalently

$$\mathbf{n}_s = \mathbf{N}\begin{pmatrix}0.5\\0.5\end{pmatrix} \bmod \mathbf{N}.$$

3. The vector $\mathbf{n}_s$ is determined by $\mathbf{n}_s = \mathbf{U}\boldsymbol{\Lambda}\mathbf{V}\begin{pmatrix}0.5 & 0.5\end{pmatrix}^T \bmod \mathbf{N}$. As

$$\mathbf{L}^T = \underbrace{\mathbf{V}^T\begin{pmatrix}1 & 0\\ 0 & 2\end{pmatrix}}_{\mathbf{L}'}\mathbf{V}_{\mathbf{M}}^{-T},$$

$LAT(\mathbf{L}^T)$ is the same as the lattice of $\mathbf{L}'$. Let

$$\mathbf{V} = \begin{pmatrix}v_{00} & v_{01}\\ v_{10} & v_{11}\end{pmatrix}, \text{ then } \mathbf{L}' = \begin{pmatrix}v_{00} & 2v_{10}\\ v_{01} & 2v_{11}\end{pmatrix}.$$

The vector $\begin{pmatrix}v_{00} & v_{01}\end{pmatrix}^T$ is on the lattice of $\mathbf{L}^T$, which is quincunx. Any vector $\mathbf{c}$ on the quincunx lattice has the property that $[\mathbf{c}]_0 + [\mathbf{c}]_1$ is even. This means that $v_{00} + v_{01}$ is even; v_{00} and v_{01} are either both odd or both even. If v_{00} and v_{01} are both even, then $|\mathbf{V}|$ is even, which contradicts with the assumption that $\mathbf{V}$ is unimodular and has $|\mathbf{V}| = 1$. So v_{00} and v_{01}

are both odd. This in turns implies that v_{10} and v_{11} must be one odd, and one even (since $|\mathbf{V}| = 1$). As a result $\mathbf{V}\begin{pmatrix}0.5 & 0.5\end{pmatrix}^T = \begin{pmatrix}c_0 & c_1 + 0.5\end{pmatrix}^T$, for some integers c_0 and c_1. Let $\mathbf{c} = \begin{pmatrix}c_0 & c_1\end{pmatrix}^T$, then $\mathbf{n}_s = \mathbf{U}\mathbf{\Lambda}(\mathbf{c} + \begin{pmatrix}0 & 0.5\end{pmatrix}^T)$ or equivalently

$$\mathbf{n}_s = \mathbf{N}(\mathbf{V}^{-1}\mathbf{c}) + \mathbf{U}\begin{pmatrix}0 & \lambda_1\end{pmatrix}^T.$$

Hence, we have $\mathbf{n}_s \overset{\mathbf{N}}{=} \mathbf{U}\begin{pmatrix}0 & \lambda_1\end{pmatrix}^T$, which is an integer vector. ■

4.6.2 Perfect Reconstruction Conditions

Let the prototype have the following polyphase representation,

$$P(\boldsymbol{\omega}) = \textstyle\sum_{i=0}^{|\mathbf{N}|-1} E_i(\mathbf{N}^T\boldsymbol{\omega})e^{-j\boldsymbol{\omega}^T\mathbf{n}_i}, \tag{4.14}$$

$$\text{where} \quad \mathbf{n}_{n_0+\lambda_0 n_1} = \mathbf{U}\begin{pmatrix}n_0\\ n_1\end{pmatrix}, \quad n_0 = 0,1,\ldots,\lambda_0 - 1,\ n_1 = 0,1,\ldots,2\lambda_1 - 1, \tag{4.15}$$

where $\mathbf{U}$ is as given in (4.5). Then $E_i(\boldsymbol{\omega})$ is the polyphase component of $P(\boldsymbol{\omega})$ with respect to $\mathbf{n}_i$. The paraunitariness of the *Two-P* CMFB can be translated into pairwise power complementary conditions on $E_i(\boldsymbol{\omega})$.

Theorem 4.3. *Necessary and sufficient conditions for paraunitariness.* Consider the filter bank with decimation matrix $\mathbf{M}$ in Fig. 4.1 and the choice of analysis and synthesis filters in (4.9). Let the matrix $\mathbf{N}$ be given by $\mathbf{N} = \mathbf{ML}$, where $LAT(\mathbf{L}^T)$ is quincunx. Also let the prototype be linear-phase with $p(\mathbf{n}) = p(\mathbf{n}_s - \mathbf{n})$ and $\mathbf{n}_s = \mathbf{N}\begin{pmatrix}0.5 & 0.5\end{pmatrix}^T$ mod $\mathbf{N}$. Then the *Two-P* CMFB is paraunitary (i.e., the polyphase matrix is paraunitary) if and only if

$$E_i^*(\boldsymbol{\omega})E_i(\boldsymbol{\omega}) + E_{i+\lambda_0\lambda_1}^*(\boldsymbol{\omega})E_{i+\lambda_0\lambda_1}(\boldsymbol{\omega}) = c, \tag{4.16}$$

where c is some constant. ■

Proof of Theorem 4.3 is given in Appendix A.

Remark on Theorem 4.3. The condition in (4.16) is equivalent to saying that $E_i(\boldsymbol{\omega})$ and $E_{i+\lambda_0\lambda_1}(\boldsymbol{\omega})$ are power complementary in 2D sense. As explained in Sec. 4.5, the *Two-P* CMFB is of configuration A when $\mathbf{l} = \begin{pmatrix}0.5 & 0\end{pmatrix}^T$ and configuration B when $\mathbf{l} = \begin{pmatrix}0 & 0.5\end{pmatrix}^T$. As the theorem is true regardless of choice of $\mathbf{l}$, Theorem 4.3 holds for both configuration A and configuration B.

4.6.3 Polyphase Components of the Prototype

In the 1D CMFB, the polyphase components of the prototype are related in pairs because of linear phase constraint of the prototype. At the same times, there are also power complementary pairs due to paraunitariness. Furthermore if half of the polyphase components are pairwise power complementary, the other half, due to linear phase, are automatically pairwise power complementary as derived in [37]. The situation is similar in the *Two-P* CMFB as we elaborate next.

According to (4.10), the impulse response of the prototype is $p(\mathbf{n}) = p(\mathbf{n}_s - \mathbf{n})$. So the vector $\mathbf{n}_s$ determines the pairwise relations of the polyphase components. More precisely, we will show that the polyphase component are pairwise related by

$$E_{n_0+\lambda_0 n_1}(\boldsymbol{\omega}) = e^{-j\boldsymbol{\omega}^T(\mathbf{d}-\mathbf{V}^{-1}(c_0\ c_1)^T)} E^*_{n'_0+\lambda_0 n'_1}(\boldsymbol{\omega}), \quad n'_0 = -n_0 \bmod \lambda_0, \quad n'_1 = \lambda_1 - n_1 \bmod 2\lambda_1, \tag{4.17}$$

where $\mathbf{d}$ is a vector determined by $\mathbf{n}_s$, and the two quantities c_0 and c_1 are given by

$$c_0 = \begin{cases} 0, & \text{if } n_0 = 0, \\ 1, & \text{otherwise,} \end{cases} \quad \text{and } c_1 = \begin{cases} 0, & \text{if } n_1 \le \lambda_1, \\ 1, & \text{otherwise.} \end{cases}$$

Proof of (4.17). As $\mathbf{n}_s = \mathbf{N}\begin{pmatrix}0.5 & 0.5\end{pmatrix}^T \bmod \mathbf{N}$, we have $\mathbf{n}_s = \mathbf{N}\mathbf{d} + \mathbf{N}\begin{pmatrix}0.5 & 0.5\end{pmatrix}^T$ for some integer vector $\mathbf{d}$. Using the linear phase property of $P(\boldsymbol{\omega})$, we have $P(\boldsymbol{\omega}) = e^{-j\boldsymbol{\omega}^T\mathbf{n}_s}P^*(\boldsymbol{\omega})$. Substituting in the polyphase representation of $P(\boldsymbol{\omega})$ gives us

$$\begin{aligned} & \textstyle\sum_{n_0=0}^{\lambda_0-1}\sum_{n_1=0}^{2\lambda_1-1} E_{n_0+\lambda_0 n_1}(\mathbf{N}^T\boldsymbol{\omega})e^{-j\boldsymbol{\omega}^T\mathbf{U}(n_0\ n_1)^T} \\ = & \textstyle\sum_{n'_0=0}^{\lambda_0-1}\sum_{n'_1=0}^{2\lambda_1-1} E^*_{n'_0+\lambda_0 n'_1}(\mathbf{N}^T\boldsymbol{\omega})e^{-j\boldsymbol{\omega}^T\mathbf{N}\mathbf{d}}e^{-j\boldsymbol{\omega}^T\mathbf{U}(-n'_0\ \lambda_1-n'_1)^T}. \end{aligned}$$

The right hand side of the above equation is equal to

$$\sum_{n'_0=0}^{\lambda_0-1}\sum_{n'_1=0}^{2\lambda_1-1} E^*_{n'_0+\lambda_0 n'_1}(\mathbf{N}^T\boldsymbol{\omega})e^{-j\boldsymbol{\omega}^T\mathbf{N}(\mathbf{d}-\mathbf{V}^{-1}(c_0\ c_1)^T)}e^{-j\boldsymbol{\omega}^T\mathbf{U}(c_0\lambda_0-n'_0\ 2c_1\lambda_1+\lambda_1-n'_1)^T}.$$

So

$$E_{n_0+\lambda_0 n_1}(\mathbf{N}^T\boldsymbol{\omega}) = E^*_{n'_0+\lambda_0 n'_1}(\mathbf{N}^T\boldsymbol{\omega})e^{-j\boldsymbol{\omega}^T\mathbf{N}(\mathbf{d}-\mathbf{V}^{-1}(c_0\ c_1)^T)}$$

if $\begin{pmatrix}n_0 & n_1\end{pmatrix}^T = \begin{pmatrix}c_0\lambda_0 - n'_0 & 2c_1\lambda_1 + \lambda_1 - n'_1\end{pmatrix}^T$. This gives us the pairwise relations given in (4.17). ■

According to the statement of Theorem 4.3, we know the first half and the second half of the polyphase components are power complementary in pairs. Combining these two different pairwise

relations, we observe that if the following pairs

$$\left(E_{n_0+\lambda_0 n_1}(\boldsymbol{\omega}), E_{n_0+(n_1+\lambda_1)\lambda_0}(\boldsymbol{\omega})\right), \text{ for } 0 \le n_0 < \lceil \lambda_0/2 \rceil \text{ and } 0 \le n_1 < \lceil (\lambda_1+1)/2 \rceil,$$

are power complementary, then the others will be pairwise power complementary due to the linear phase property of the prototype. Here the ceiling function $\lceil x \rceil$ is defined as the smallest integer greater than x.

Comment on the Nyquist Property of the Analysis Filters. As in the 1D case, we can define Nyquist filters. A filter $h(\mathbf{m})$ is called a Nyquist($\mathbf{N}$) filter if one polyphase component of $h(\mathbf{m})$ is a delay. From the previous discussion, we observe that while $(E_0(\boldsymbol{\omega}),\ E_{\lambda_0\lambda_1}(\boldsymbol{\omega}))$ is a power complementary pair, these two polyphase components are also related because $P(\boldsymbol{\omega})$ has linear phase. As a result, $E_0(\boldsymbol{\omega})$ and $E_{\lambda_0\lambda_1}(\boldsymbol{\omega})$ are merely delays. So the prototype is a Nyquist($\mathbf{N}$) filter. The analysis filters are cosine modulated versions of the prototype. We conclude that the analysis filters are also Nyquist($\mathbf{N}$) filter.

4.7 Implementation and Design Example of Two-Parallelogram CMFB

Efficient Implementation of the Two-Parallelogram CMFB.

Efficient implementation is one of the reasons that cosine modulated filter banks attract a lot of attention. In the 1D CMFB, the complexity of the analysis bank or the synthesis bank is that of the prototype filter plus a DCT matrix. The DCT matrices are known to be low-complexity matrices. We will show that there also exists efficient implementation for the *Two-P* CMFB. The cost of the analysis bank or the synthesis bank is that of a prototype filter plus a matrix, which has elements resembling that of a nonseparable 2D DCT matrix. Implementation of this DCT-like matrix can be decomposed into 1D DCT matrices of smaller dimensions. Denote the complexity of a λ-point DCT by $C(\lambda)$, then the complexity of $\mathbf{C}$ is roughly $4\lambda_1 C(\lambda_0) + \lambda_0 C(2\lambda_1)$, where λ_0 and λ_1 are the diagonal elements of $\mathbf{\Lambda_M}$.

Using the polyphase representation of the prototype in (4.14), the analysis filters in (4.9) can be rewritten as

$$H_m(\boldsymbol{\omega}) = \sum_{i=0}^{|\mathbf{N}|-1} 2E_i(\mathbf{N}^T\boldsymbol{\omega} - 2\pi\mathbf{b})[\mathbf{C}]_{mi}\exp(-j\boldsymbol{\omega}^T\mathbf{n}_i), \quad m = 0, 1, \ldots, |\mathbf{M}| - 1,$$

where $[\mathbf{C}]_{mi} = \cos(2\pi(\mathbf{k}_{m+b\lambda_0} + \mathbf{b})^T\mathbf{N}^{-1}\mathbf{n}_i), \quad m = 0, 1, \ldots, |\mathbf{M}| - 1, \quad i = 0, 1, \ldots, |\mathbf{N}| - 1.$

The above expression for the analysis filters gives rise to the efficient implementation in Fig. 4.16. The matrix $\mathbf{C}$ is rectangular of dimension $|\mathbf{M}| \times |\mathbf{N}|$. The figure demonstrates that the complexity of the 2D CMFB is that of the prototype plus $\mathbf{C}$. The elements of $\mathbf{C}$ are those of a nonseparable 2D DCT.

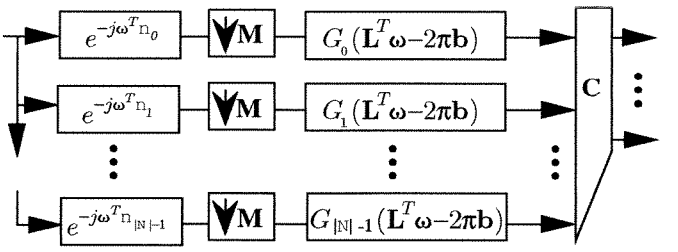

Fig. 4.16. Efficient implementation of the analysis bank of the two-parallelogram cosine modulated filter bank. The matrix C is of dimension $|\mathbf{M}|$ by $2|\mathbf{M}|$.

Decomposition and Complexity of C

We first define the The Kronecker product of two matrices $\mathbf{A}$ and $\mathbf{B}$,

$$\underbrace{\mathbf{A}}_{I\times K} \otimes \underbrace{\mathbf{B}}_{J\times L} = \underbrace{\begin{pmatrix} a_{0,0}\mathbf{B} & \dots & a_{0,K-1}\mathbf{B} \\ \vdots & \dots & \vdots \\ a_{I-1,0}\mathbf{B} & \dots & a_{I-1,K-1}\mathbf{B} \end{pmatrix}}_{IJ\times KL}. \tag{4.18}$$

The matrix $\mathbf{C}$ can be decomposed as (to be shown in Appendix B)

$$\mathbf{C} = \mathbf{C}_1 \otimes \mathbf{C}_0 - \mathbf{S}_1 \otimes \mathbf{S}_0, \tag{4.19}$$

where $\mathbf{C}_0$, $\mathbf{S}_0$ are $\lambda_0 \times \lambda_0$ matrices and $\mathbf{C}_1$, $\mathbf{S}_1$ are $\lambda_1 \times 2\lambda_1$ matrices given by

$$[\mathbf{C}_0]_{k_0 n_0} = \cos(\tfrac{2\pi}{\lambda_0}(k_0 - b_0/2)n_0), \quad [\mathbf{S}_0]_{k_0 n_0} = \sin(\tfrac{2\pi}{\lambda_0}(k_0 - b_0/2)n_0), \qquad 0 \le k_0, n_0 < \lambda_0,$$

$$[\mathbf{C}_1]_{k_1 n_1} = \cos(\tfrac{\pi}{\lambda_1}(k_1 + 0.5)n_1), \quad [\mathbf{S}_1]_{k_1 n_1} = \sin(\tfrac{\pi}{\lambda_1}(k_1 + 0.5)n_1), \quad 0 \le k_1 < \lambda_1, 0 \le n_1 < 2\lambda_1.$$

The implementation of $\mathbf{C}$ is closely related to that of $\mathbf{C}_0, \mathbf{S}_0, \mathbf{C}_1$ and $\mathbf{S}_1$. The matrices $\mathbf{C}_0, \mathbf{S}_0, \mathbf{C}_1$ and $\mathbf{S}_1$ have elements resembling that of DCT and DST matrices. The complexity of these four matrices can be shown to be roughly $C(\lambda_0)$, $C(\lambda_0)$, $\frac{1}{2}C(2\lambda_1)$ and $\frac{1}{2}C(2\lambda_1)$. Using the decomposition in (4.19), we can further show that the complexity of the $\mathbf{C}$ matrix is roughly equal to $4\lambda_1 C(\lambda_0) + \lambda_0 C(2\lambda_1)$. These properties of $\mathbf{C}$, $\mathbf{C}_0, \mathbf{S}_0, \mathbf{C}_1$ and $\mathbf{S}_1$ will be verified in Appendix B.

Example 4.1. *Two-parallelogram CMFB.*

$$\text{Let } \mathbf{M} = \begin{pmatrix} 7 & -2 \\ 0 & 1 \end{pmatrix} = \begin{pmatrix} 1 & -2 \\ 0 & 1 \end{pmatrix} \begin{pmatrix} 7 & 0 \\ 0 & 1 \end{pmatrix}.$$

$$\text{Choose } \mathbf{L} = \begin{pmatrix} 1 & 0 \\ 0 & 2 \end{pmatrix} \begin{pmatrix} 1 & 1 \\ 1 & 2 \end{pmatrix}, \text{ then } \mathbf{N} = \begin{pmatrix} 3 & -1 \\ 2 & 4 \end{pmatrix}.$$

With the above of choice of $\mathbf{L}$, $LAT(\mathbf{L}^T)$ is quincunx. If we choose configuration B, then $\mathbf{l} = \begin{pmatrix} 0 & 0.5 \end{pmatrix}^T$. Fig. 4.2 shows the supports of the analysis filters. By Theorem 4.3, the *Two-P* CMFB has perfect reconstruction if the polyphase components of the prototype satisfy the power complementary condition given in (4.16). Fig. 4.17(a) shows the pairs of polyphase components that are power complementary. As the prototype is linear-phase, the polyphase components are related in pairs. Fig. 4.17(b) shows these pairwise relations. In the figures, we use the notation $E_{n_1}^{n_0}(\boldsymbol{\omega})$ to denote the polyphase component $E_{n_0+n_1\lambda_0}(\boldsymbol{\omega})$. From the discussion for polyphase components in Sec. 4.6.3, if $(E_0^i(\boldsymbol{\omega}),\ E_1^i(\boldsymbol{\omega}))$, for $i = 1, 2, 3$, are power complementary pairs then $(E_0^i(\boldsymbol{\omega}),\ E_1^i(\boldsymbol{\omega}))$, for $i = 4, 5, 6$, are guaranteed to be power complementary pairs. We can optimize $P(\boldsymbol{\omega})$ subject to only the condition that $E_0^i(\boldsymbol{\omega})$ and $E_1^i(\boldsymbol{\omega})$, for $i = 1, 2, 3$, are power complementary. This condition can be satisfied by using the 2D paraunitary lattice, [107].

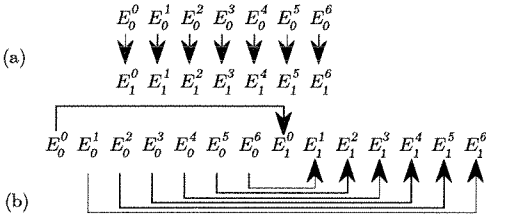

Fig. 19. Example 7.1. Two-parallelogram cosine modulated filter bank. (a) Polyphase components of $P(\omega)$ that are pairwise power complementary. (b) Polyphase components of $P(\omega)$ that are related due to linear phase of $P(\omega)$.

Fig. 4.17. Example 4.1. *Two-P* cosine modulated filter bank; (a) Polyphase components of $P(\boldsymbol{\omega})$ that are pairwise power complementary; (b) polyphase components of $P(\boldsymbol{\omega})$ that are related due to linear phase of $P(\boldsymbol{\omega})$.

Fig. 4.18 shows the support of impulse response of the prototype filter, $p(\mathbf{n})$. The support of $p(\mathbf{n})$ resembles the shape of $SPD(2\mathbf{N})$. Each solid dot represents a possibly non-zero coefficient of $p(\mathbf{n})$. In this optimization, each of the fourteen polyphase components has four coefficients. The corresponding frequency response of the prototype is shown in Fig. 4.19. The stopband attenuation of the prototype is 17 dB. The reason that the prototype can not have good attenuation is due to the lack of vertex permissibility in *Two-P* filter banks (Sec. 4.3).

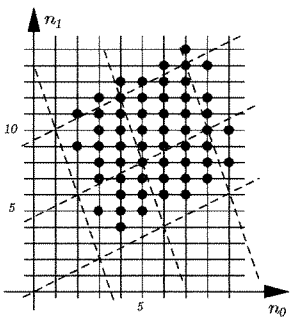

Fig. 4.18. Example 4.1. *Two-P* cosine modulated filter bank. The impulse response support of the prototype. Each solid dot represents a possibly non-zero coefficient of the prototype. (Intersection points of the dashed lines are on the lattice of $\mathbf{N}$. Solid lines represent integers.)

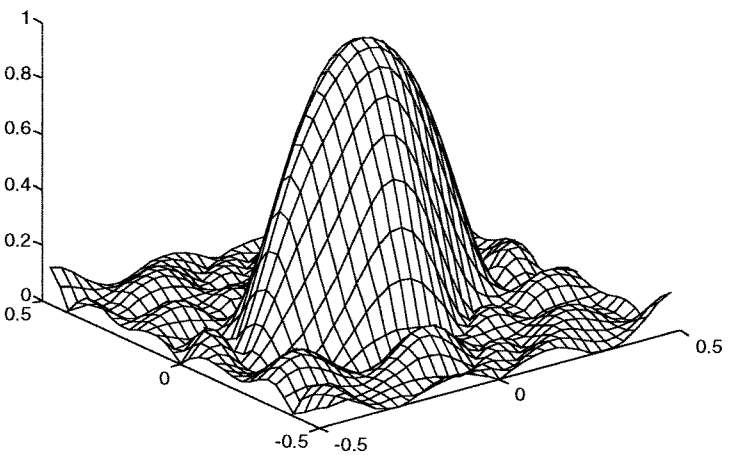

Fig. 4.19. Example 4.1. Two-parallelogram cosine modulated filter bank. The magnitude response of the prototype with frequency normalized by 2π.

Concluding Remarks. In the application of subband coding, the support configuration of the analysis filters on a large scale determines the coding performance of the filter bank. In this chapter we have considered the class of *Two-P* filter bank. The passband of each analysis filter consists of two parallelograms and the frequency plane is partitioned by parallelogram cells. (This type of configurations also has the potential application of extracting directional information like edges.)

To facilitate the analysis, we introduced the notions of edge and vertex permissibility and explained that, although the former one is more important, both types of permissibility are necessary for good filter bank design. As elaborated in Sec. 4.3, the *Two-P* filter banks can possess edge or vertex permissibility but not both. As a consequence, the stopband attenuation of the filters in *Two-P* perfect reconstruction filter banks can not be arbitrary large. Extensions of the discussions of this chapter for the case of linear-phase filters can be found in [51].

Appendix A. Proof of Theorem 4.3

The proof will be done in three steps. In the first step, we formulate the polyphase matrix $\mathbf{E}(\boldsymbol{\omega})$ of the analysis bank. As the 2D CMFB is paraunitary, the filter bank has perfect reconstruction if and only if $\mathbf{E}^\dagger(\boldsymbol{\omega})\mathbf{E}(\boldsymbol{\omega})$ is an identity matrix except some scalar. In the second step, we simplify the product $\mathbf{E}^\dagger(\boldsymbol{\omega})\mathbf{E}(\boldsymbol{\omega})$ as much as possible without using the linear phase property of the prototype $P(\boldsymbol{\omega})$. As elaborated in Sec. 4.6.3, the polyphase components of the prototype are related in pairs due to the linear phase of $P(\boldsymbol{\omega})$. In the final step we use those pairwise relations to show $\mathbf{E}^\dagger(\boldsymbol{\omega})\mathbf{E}(\boldsymbol{\omega}) = \mathbf{I}_{|\mathbf{M}|}$ provided that $E_i(\boldsymbol{\omega})$ are pairwise power complementary as in (4.16).

Notations and preliminaries for Appendix A. For the convenience of derivation, we introduce the following notations.

1. The matrix $\mathbf{J}_k$ denotes a $k \times k$ reversal matrix with non-zero entries $[\mathbf{J}]_{n,k-1-n} = 1$, for $n = 0, 1, \ldots, k-1$.

2. *The DFT matrix.* The $\lambda \times \lambda$ DFT matrix $\mathbf{W}_\lambda$ is given by $[\mathbf{W}_\lambda]_{mn} = W_\lambda^{mn}$, where $W_\lambda = e^{-j2\pi/\lambda}$.

3. Two properties of the Kronecker product (defined in (4.18)) are relevant to our discussion.

$$(1)\quad (\mathbf{A}\otimes\mathbf{B})^\dagger = \mathbf{A}^\dagger \otimes \mathbf{B}^\dagger, \qquad \text{and} \qquad (2)\quad (\underbrace{\mathbf{A}}_{I\times K}\otimes\underbrace{\mathbf{B}}_{J\times L})(\underbrace{\mathbf{C}}_{K\times M}\otimes\underbrace{\mathbf{D}}_{L\times N}) = (\underbrace{\mathbf{AC}}_{I\times M})\otimes(\underbrace{\mathbf{BD}}_{J\times N}).$$

Step 1: *Polyphase matrix $\mathbf{E}(\boldsymbol{\omega})$ of the analysis bank.*

Let $\mathbf{q}(\boldsymbol{\omega})$ be a $|\mathbf{N}| \times 1$ vector $\mathbf{q}(\boldsymbol{\omega}) = \begin{pmatrix} Q_{\mathbf{k}_0}(\boldsymbol{\omega}) & Q_{\mathbf{k}_1}(\boldsymbol{\omega}) & \cdots & Q_{\mathbf{k}_{|\mathbf{N}|-1}}(\boldsymbol{\omega}) \end{pmatrix}^T$ and let $\mathbf{h}(\boldsymbol{\omega})$ be a $|\mathbf{M}| \times 1$ vector $\mathbf{h}(\boldsymbol{\omega}) = \begin{pmatrix} H_0(\boldsymbol{\omega}) & H_1(\boldsymbol{\omega}) & \cdots & H_{|\mathbf{M}|-1}(\boldsymbol{\omega}) \end{pmatrix}^T$, where $H_i(\boldsymbol{\omega})$ is as given in (4.9). In

view of the discussion in Sec. 4.5, we have

$$\mathbf{h}(\boldsymbol{\omega}) = \mathbf{G}\mathbf{q}(\boldsymbol{\omega}),$$

$$\text{where } \mathbf{G} = \begin{pmatrix} \mathbf{I}_{b\lambda_0} & \mathbf{J}_b \otimes \mathbf{J}' & \mathbf{0} & \mathbf{0} \\ \mathbf{0} & \mathbf{0} & \mathbf{I}_{(\lambda_1-b)\lambda_0} & \mathbf{J}_{(\lambda_1-b)} \otimes \mathbf{J}' \end{pmatrix}, \quad \mathbf{J}' = \begin{pmatrix} \mathbf{J}_{b_0+1} & \mathbf{0} \\ \mathbf{0} & \mathbf{J}_{\lambda_0-b_0-1} \end{pmatrix},$$

where the values of b and b_0 are as given in Sec. 4.5. We will first derive the matrix representation of $\mathbf{q}(\boldsymbol{\omega})$ and therefore the matrix representation of $\mathbf{h}(\boldsymbol{\omega})$. From the expression of $\mathbf{h}(\boldsymbol{\omega})$ we can obtain the polyphase matrix $\mathbf{E}(\boldsymbol{\omega})$ of the analysis bank.

Using the polyphase representation of the prototype $P(\boldsymbol{\omega})$ in (4.14), we have

$$Q_{\mathbf{k}_{m_0+\lambda_0 m_1}}(\boldsymbol{\omega} + 2\pi\mathbf{N}^{-T}\mathbf{l}) = \sum_{i_0=0}^{\lambda_0-1}\sum_{i_1=0}^{2\lambda_1-1} e^{j2\pi\mathbf{k}_{m_0+\lambda_0 m_1}^T \mathbf{N}^{-1}\mathbf{n}_{i_0+\lambda_0 i_1}} E_{i_0+\lambda_0 i_1}(\mathbf{N}^T\boldsymbol{\omega}) e^{-j\boldsymbol{\omega}^T\mathbf{n}_{i_0+\lambda_0 i_1}},$$
$$m_0 = 0, 1, \ldots, \lambda_0 - 1,\ m_1 = 0, 1, \ldots, 2\lambda_1 - 1.$$

By the definition of $\mathbf{k}_{m_0+\lambda_0 m_1}$ and $\mathbf{n}_{i_0+\lambda_0 i_1}$ given in (4.6) and (4.15), the term $e^{j2\pi\mathbf{k}_{m_0+\lambda_0 m_1}\mathbf{N}^{-1}\mathbf{n}_{i_0+\lambda_0 i_1}}$ reduces to $W_{\lambda_0}^{-m_0 i_0} W_{2\lambda_1}^{-m_1 i_1}$, where $W_\lambda = e^{-j2\pi/\lambda}$. Then

$$\mathbf{q}(\boldsymbol{\omega} + 2\pi\mathbf{N}^{-T}\mathbf{l}) = \left(\mathbf{W}_{2\lambda_1}^\dagger \otimes \mathbf{W}_{\lambda_0}^\dagger\right) diag(E_0(\mathbf{N}^T\boldsymbol{\omega}), \ldots, E_{|\mathbf{N}|-1}(\mathbf{N}^T\boldsymbol{\omega}))\mathbf{e}_{\mathbf{U}\boldsymbol{\Lambda}}(\boldsymbol{\omega}),$$

where $diag(E_0(\mathbf{N}^T\boldsymbol{\omega}), \ldots, E_{|\mathbf{N}|-1}(\mathbf{N}^T\boldsymbol{\omega}))$ is a $|\mathbf{N}| \times |\mathbf{N}|$ diagonal matrix with the ith diagonal entry $E_i(\mathbf{N}^T\boldsymbol{\omega})$. The matrices $\mathbf{W}_{\lambda_0}$ and $\mathbf{W}_{2\lambda_1}$ are respectively $\lambda_0 \times \lambda_0$ and $2\lambda_1 \times 2\lambda_1$ DFT matrices. The vector $\mathbf{e}_{\mathbf{U}\boldsymbol{\Lambda}}(\boldsymbol{\omega})$ is the 2D delay chain vector with respect to $\mathcal{N}(\mathbf{U}\boldsymbol{\Lambda})$, $\mathbf{e}_{\mathbf{U}\boldsymbol{\Lambda}}(\boldsymbol{\omega}) = \begin{pmatrix} e^{-\boldsymbol{\omega}^T\mathbf{n}_0} & e^{-\boldsymbol{\omega}^T\mathbf{n}_1} \ldots & e^{-\boldsymbol{\omega}^T\mathbf{n}_{|\mathbf{N}|-1}} \end{pmatrix}^T$, where $\mathbf{n}_i$ is as given in (4.15). Since $\mathbf{n}_{i+|\mathbf{M}|} = \mathbf{n}_i + \mathbf{U}(0\ \lambda_1)^T$, for $i = 0, 1, \ldots, |\mathbf{M}| - 1$, $[\mathbf{e}_{\mathbf{U}\boldsymbol{\Lambda}}(\boldsymbol{\omega})]_{i+|\mathbf{M}|} = e^{-j\boldsymbol{\omega}^T\mathbf{U}(0\ \lambda_1)^T}[\mathbf{e}_{\mathbf{U}\boldsymbol{\Lambda}}(\boldsymbol{\omega})]_i$. Let the 2D delay chain with respect to $\mathbf{U}\boldsymbol{\Lambda}_\mathbf{M}$ be

$$\mathbf{e}_{\mathbf{U}\boldsymbol{\Lambda}_\mathbf{M}}(\boldsymbol{\omega}) = \begin{pmatrix} e^{-\boldsymbol{\omega}^T\mathbf{n}_0} & e^{-\boldsymbol{\omega}^T\mathbf{n}_1} \ldots & e^{-\boldsymbol{\omega}^T\mathbf{n}_{|\mathbf{M}|-1}} \end{pmatrix}^T,$$

then $\mathbf{e}_{\mathbf{U}\boldsymbol{\Lambda}}(\boldsymbol{\omega}) = \begin{pmatrix} \mathbf{e}_{\mathbf{U}\boldsymbol{\Lambda}_\mathbf{M}}^T(\boldsymbol{\omega}) & e^{-j\boldsymbol{\omega}^T\mathbf{U}(0\ \lambda_1)^T}\mathbf{e}_{\mathbf{U}\boldsymbol{\Lambda}_\mathbf{M}}^T(\boldsymbol{\omega}) \end{pmatrix}^T$. Then we have

$$\mathbf{h}(\boldsymbol{\omega} + 2\pi\mathbf{N}^{-T}\mathbf{l}) = \underbrace{\mathbf{G}\left(\mathbf{W}_{2\lambda_1}^\dagger \otimes \mathbf{W}_{\lambda_0}^\dagger\right)\begin{pmatrix} \mathbf{E}_0(\mathbf{M}^T\boldsymbol{\omega}) \\ \mathbf{E}_1(\mathbf{M}^T\boldsymbol{\omega}) \end{pmatrix}}_{\mathbf{E}(\mathbf{M}^T(\boldsymbol{\omega}+2\pi\mathbf{N}^{-T}\mathbf{l}))} \mathbf{G}_0\, \mathbf{e}_{\mathbf{U}\boldsymbol{\Lambda}_\mathbf{M}}(\boldsymbol{\omega} + 2\pi\mathbf{N}^{-T}\mathbf{l}), \tag{4.20}$$

where $\mathbf{G}_0$, $\mathbf{E}_0(\boldsymbol{\omega})$ and $\mathbf{E}_1(\boldsymbol{\omega})$ are $|\mathbf{M}| \times |\mathbf{M}|$ diagonal matrices with

$$[\mathbf{G}_0]_{ii} = e^{j2\pi\mathbf{l}^T\mathbf{N}^{-1}\mathbf{n}_i},$$

$$[\mathbf{E}_0(\boldsymbol{\omega})]_{ii} = E_i(\mathbf{L}^T\boldsymbol{\omega}), \qquad i = 0, 1, \ldots, |\mathbf{M}| - 1.$$
$$[\mathbf{E}_1(\boldsymbol{\omega})]_{ii} = e^{-j\boldsymbol{\omega}^T\mathbf{V}_{\mathbf{M}}^{-1}(0\,1)^T} E_{i+\lambda_0\lambda_1}(\mathbf{L}^T\boldsymbol{\omega}),$$

The matrix $\mathbf{E}(\boldsymbol{\omega})$ as indicated in (4.20) is the polyphase matrix of the analysis bank. The 2D CMFB is paraunitary if and only if $\mathbf{E}(\boldsymbol{\omega})$ is paraunitary. For simplicity, we will prove the paraunitariness of $\mathbf{E}(\boldsymbol{\omega} + 2\pi\mathbf{L}^{-T}\mathbf{l})$, i.e., $\mathbf{E}^\dagger(\boldsymbol{\omega} + 2\pi\mathbf{L}^{-T}\mathbf{l})\mathbf{E}(\boldsymbol{\omega} + 2\pi\mathbf{L}^{-T}\mathbf{l}) = \mathbf{I}_{|\mathbf{M}|}$.

Step 2: *Simplification of the product* $\mathbf{E}^\dagger(\boldsymbol{\omega} + 2\pi\mathbf{L}^{-T}\mathbf{l})\mathbf{E}(\boldsymbol{\omega} + 2\pi\mathbf{L}^{-T}\mathbf{l})$.

$$\begin{aligned}&\mathbf{E}^\dagger(\boldsymbol{\omega} + 2\pi\mathbf{L}^{-T}\mathbf{l})\mathbf{E}(\boldsymbol{\omega} + 2\pi\mathbf{L}^{-T}\mathbf{l})\\ =\ & \mathbf{G}_0^\dagger(\mathbf{E}_0^\dagger(\boldsymbol{\omega})\ \mathbf{E}_1^\dagger(\boldsymbol{\omega}))\underbrace{(\mathbf{W}_{2\lambda_1}\otimes\mathbf{W}_{\lambda_0})\mathbf{G}^T\mathbf{G}(\mathbf{W}_{2\lambda_1}^\dagger\otimes\mathbf{W}_{\lambda_0}^\dagger)}_{\mathbf{G}_1}\begin{pmatrix}\mathbf{E}_0(\boldsymbol{\omega})\\ \mathbf{E}_1(\boldsymbol{\omega})\end{pmatrix}\mathbf{G}_0.\end{aligned}$$

By the definition of $\mathbf{G}$, we can verify that the product $\mathbf{G}^T\mathbf{G}$ is

$$\mathbf{G}^T\mathbf{G} = \mathbf{I}_{|\mathbf{N}|} + \begin{pmatrix}\mathbf{J}_{2b} & \mathbf{0}\\ \mathbf{0} & \mathbf{J}_{2(\lambda_1-b)}\end{pmatrix}\otimes\mathbf{J}'.$$

It can be shown that the DFT matrix $\mathbf{W}_\lambda$ has the following property

$$\mathbf{W}_\lambda\begin{pmatrix}\mathbf{J}_c & \mathbf{0}\\ \mathbf{0} & \mathbf{J}_{\lambda-c}\end{pmatrix}\mathbf{W}_\lambda^\dagger = \begin{pmatrix}1 & \mathbf{0}\\ \mathbf{0} & \mathbf{J}_{\lambda-1}\end{pmatrix}\boldsymbol{\Gamma}_\lambda^{c-1},$$

where $\boldsymbol{\Gamma}_\lambda$ is a $\lambda\times\lambda$ diagonal matrices with $[\boldsymbol{\Gamma}_\lambda]_{kk} = e^{j2\pi k/\lambda}$, $k = 0, 1, \ldots, \lambda - 1$. Using this relation and the second property of Kronecker product, we have

$$\mathbf{G}_1 = \mathbf{I}_{|\mathbf{M}|} + \left\{\begin{pmatrix}1 & \mathbf{0}\\ \mathbf{0} & \mathbf{J}_{2\lambda_1-1}\end{pmatrix}\otimes\begin{pmatrix}1 & \mathbf{0}\\ \mathbf{0} & \mathbf{J}_{\lambda_0-1}\end{pmatrix}\right\}(\boldsymbol{\Gamma}_{2\lambda_1}^{b_1}\otimes\boldsymbol{\Gamma}_{\lambda_0}^{b_0}).$$

It follows that

$$\mathbf{E}^\dagger(\boldsymbol{\omega} + 2\pi\mathbf{L}^{-T}\mathbf{l})\mathbf{E}(\boldsymbol{\omega} + 2\pi\mathbf{L}^{-T}\mathbf{l}) = \mathbf{E}_0^\dagger(\boldsymbol{\omega})\mathbf{E}_0(\boldsymbol{\omega}) + \mathbf{E}_1^\dagger(\boldsymbol{\omega})\mathbf{E}_1(\boldsymbol{\omega}) + \mathbf{G}_0^\dagger\widehat{\mathbf{G}}(\boldsymbol{\omega})\mathbf{G}_0$$

where $$\widehat{\mathbf{G}}(\boldsymbol{\omega}) = \begin{pmatrix}\mathbf{E}_0^\dagger(\boldsymbol{\omega})\ \mathbf{E}_1^\dagger(\boldsymbol{\omega})\end{pmatrix}\left\{\begin{pmatrix}1 & \mathbf{0}\\ \mathbf{0} & \mathbf{J}_{2\lambda_1-1}\end{pmatrix}\otimes\begin{pmatrix}1 & \mathbf{0}\\ \mathbf{0} & \mathbf{J}_{\lambda_0-1}\end{pmatrix}\right\}\begin{pmatrix}\boldsymbol{\Gamma}_{2\lambda_1}^{b_1}\otimes\boldsymbol{\Gamma}_{\lambda_0}^{b_0}\end{pmatrix}\begin{pmatrix}\mathbf{E}_0(\boldsymbol{\omega})\\ \mathbf{E}_1(\boldsymbol{\omega})\end{pmatrix}.$$

In the next step, $\widehat{\mathbf{G}}(\boldsymbol{\omega})$ will be shown to be equal to the $|\mathbf{M}|\times|\mathbf{M}|$ zero matrix. Since both $\mathbf{E}_0(\boldsymbol{\omega})$ and $\mathbf{E}_1(\boldsymbol{\omega})$ are both diagonal, $\mathbf{E}(\boldsymbol{\omega} + 2\pi\mathbf{L}^{-T}\mathbf{l})$ is paraunitary if and only if $[\mathbf{E}_0(\boldsymbol{\omega})]_{ii}$ and $[\mathbf{E}_1(\boldsymbol{\omega})]_{ii}$ are power complementary. Or equivalently, $(E_i(\boldsymbol{\omega}), E_{i+\lambda_0\lambda_1}(\boldsymbol{\omega}))$ is a power complementary pair in 2D sense.

Step 3: *Proof of* $\widehat{\mathbf{G}}(\omega) = \mathbf{0}$.

As mentioned in Sec. 4.5, b_1 is odd. So

$$[\mathbf{\Gamma}_{2\lambda}^{b_1}]_{k+\lambda_1,k+\lambda_1} = -[\mathbf{\Gamma}_{2\lambda}^{b_1}]_{kk}, \text{ for } k = 0, 1, \ldots, \lambda_1 - 1$$

and hence

$$[\mathbf{\Gamma}_{2\lambda_1}^{b_1} \otimes \mathbf{\Gamma}_{\lambda_0}^{b_0}]_{k+\lambda_0\lambda_1,k+\lambda_0\lambda_1} = -[\mathbf{\Gamma}_{2\lambda_1}^{b_1}\mathbf{\Gamma}_{\lambda_0}^{b_0}]_{kk}, \text{ for } k = 0, 1, \ldots, \lambda_0\lambda_1 - 1.$$

Let

$$\mathbf{\Gamma}_{2\lambda_1}^{b_1} \otimes \mathbf{\Gamma}_{\lambda_0}^{b_0} = \begin{pmatrix} \mathbf{\Gamma} & \mathbf{0} \\ \mathbf{0} & -\mathbf{\Gamma} \end{pmatrix}.$$

We observe that

$$(\mathbf{\Gamma}_{2\lambda_1}^{b_1} \otimes \mathbf{\Gamma}_{\lambda_0}^{b_0}) \begin{pmatrix} \mathbf{E}_0(\omega) \\ \mathbf{E}_1(\omega) \end{pmatrix} = \begin{pmatrix} \mathbf{E}_0(\omega) \\ -\mathbf{E}_1(\omega) \end{pmatrix} \mathbf{\Gamma}.$$

Consider the partition $\begin{pmatrix} 1 & \mathbf{0} \\ \mathbf{0} & \mathbf{J}_{2\lambda_1-1} \end{pmatrix} = \begin{pmatrix} \mathbf{A} & \mathbf{B} \\ \mathbf{B} & \mathbf{A} \end{pmatrix}$, then $\mathbf{A} = \begin{pmatrix} 1 & \mathbf{0} \\ \mathbf{0} & \mathbf{0} \end{pmatrix}$, and $\mathbf{B} = \begin{pmatrix} 0 & \mathbf{0} \\ \mathbf{0} & \mathbf{J}_{\lambda_0-1} \end{pmatrix}$.

As a result,

$$\begin{aligned} &\widehat{\mathbf{G}}(\omega)\mathbf{\Gamma}^\dagger \\ = \; &\underbrace{\mathbf{E}_0^\dagger(\omega)(\mathbf{A} \otimes \widehat{\mathbf{J}})\mathbf{E}_0(\omega) - \mathbf{E}_1^\dagger(\omega)(\mathbf{A} \otimes \widehat{\mathbf{J}})\mathbf{E}_1(\omega)}_{\widehat{\mathbf{G}}_1(\omega)} + \underbrace{\mathbf{E}_1^\dagger(\omega)(\mathbf{B} \otimes \widehat{\mathbf{J}})\mathbf{E}_0(\omega) - \mathbf{E}_0^\dagger(\omega)(\mathbf{B} \otimes \widehat{\mathbf{J}})\mathbf{E}_1(\omega)}_{\widehat{\mathbf{G}}_2(\omega)}, \end{aligned}$$

where

$$\widehat{\mathbf{J}} = \begin{pmatrix} 1 & \mathbf{0} \\ \mathbf{0} & \mathbf{J}_{\lambda_0-1} \end{pmatrix}.$$

By the definition of $\mathbf{A}$ and $\widehat{\mathbf{J}}_0$, we can verify that $\widehat{\mathbf{G}}_1(\omega) = \mathbf{0}$ if

$$\begin{aligned} E_0^*(\omega)E_0(\omega) &= E_{\lambda_0\lambda_1}^*(\omega)E_{\lambda_0\lambda_1}(\omega), \\ E_{i_0}^*(\omega)E_{\lambda_0-i_0}(\omega) &= E_{i_0+\lambda_0\lambda_1}^*(\omega)E_{\lambda_0-i_0+\lambda_0\lambda_1}(\omega), 0 < i_0 < \lambda_0. \end{aligned} \tag{4.21}$$

Similarly, $\widehat{\mathbf{G}}_2(\omega) = \mathbf{0}$ if

$$\begin{aligned} e^{j\omega^T\mathbf{V}^{-1}(0\;1)^T}E_{(i_1+\lambda_1)\lambda_0}^*(\omega)E_{(\lambda_1-i_1)\lambda_0}(\omega) &= E_{i_1\lambda_0}^*(\omega)E_{(2\lambda_1-i_1)\lambda_0}(\omega), 0 < i_1 < \lambda_1, \\ e^{j\omega^T\mathbf{V}^{-1}(0\;1)^T}E_{i_0+(i_1+\lambda_1)\lambda_0}^*(\omega)E_{\lambda_0-i_0+(\lambda_1-i_1)\lambda_0}(\omega) &= E_{i_0+i_1\lambda_0}^*(\omega)E_{\lambda_0-i_0+(2\lambda_1-i_1)\lambda_0}(\omega), \\ 0 < i_0 < \lambda_0, 0 < i_1 < \lambda_1. \end{aligned} \tag{4.22}$$

Eq. (4.21) and (4.22) can be verified by using the the relation of the polyphase components in (4.17).

Appendix B. Decomposition and Complexity of the Matrix C

1. **Decomposition of the matrix C.** Substitute in

$$\mathbf{k}_{k_0+\lambda_0 k_1} = \mathbf{V}^T (k_0\ k_1)^T, \text{ and } \mathbf{n}_{n_0+\lambda_0 n_1} = \mathbf{V}^T (n_0\ n_1)^T,$$

we have

$$[\mathbf{C}]_{k_0+\lambda_0 k_1, n_0+\lambda_0 n_1} = \cos(\frac{2\pi}{\lambda_0}(k_0 - b_0/2)n_0 + \frac{\pi}{\lambda_1}(k_1 + 0.5)n_1),$$

$$\text{or } [\mathbf{C}]_{k_0+\lambda_0 k_1, n_0+\lambda_0 n_1} = [\mathbf{C}_1]_{k_1 n_1} [\mathbf{C}_0]_{k_0 n_0} - [\mathbf{S}_1]_{k_1 n_1} [\mathbf{S}_0]_{k_0 n_0}.$$

Then we have $\mathbf{C} = \mathbf{C}_1 \otimes \mathbf{C}_0 - \mathbf{S}_1 \otimes \mathbf{S}_0$.

2. **The complexity of the matrices $\mathbf{C}_0, \mathbf{S}_0, \mathbf{C}_1$ and $\mathbf{S}_1$.** The DCT and DST matrices are categorized into four types in [77]. The matrix $\mathbf{C}_1$ has the first λ_1 rows of a $2\lambda_1 \times 2\lambda_1$ type II DCT. In some implementation methods, $\mathbf{C}_1$ requires only half the computation of a $2\lambda_1$ point DCT. Likewise, $\mathbf{S}_1$ is the upper half of a $2\lambda_1 \times 2\lambda_1$ type II DST and needs half the complexity of a $2\lambda_1$ point DST. When b_0 is odd, $\mathbf{C}_0$ is a rearrangement of a type II DCT matrix. Computation of $\mathbf{C}_0$ is equivalent to that of a λ_0 point DCT. Similarly, $\mathbf{S}_0$ can be obtained by rearranging a type II DST matrix and the computation of $\mathbf{S}_0$ is equivalent to that of a λ_0 point DST. However, when b_0 is even, $\mathbf{C}_0$ and $\mathbf{S}_0$ become respectively rearrangement of type I DCT and type I DST. Complexity of $\mathbf{C}_0$ and $\mathbf{S}_0$ are comparable to that of a $\lambda_0 + 1$ point type I DCT and $\lambda_0 - 1$ point type I DST.

3. **The complexity of the matrix C.** The matrix $\mathbf{C}$ has two parts, namely $\mathbf{C}_1 \otimes \mathbf{C}_0$ and $\mathbf{S}_1 \otimes \mathbf{S}_0$. We will look into details of computing $\mathbf{C}_1 \otimes \mathbf{C}_0$. The implementation of $\mathbf{S}_1 \otimes \mathbf{S}_0$ is similar. Suppose the input of $\mathbf{C}$ is $\mathbf{x}$, a $|\mathbf{N}| \times 1$ vector. Let

$$\mathbf{y} = (\mathbf{C}_1 \otimes \mathbf{C}_0)\,\mathbf{x},$$

a $|\mathbf{M}| \times 1$ vector. By the property of Kronecker product, we can also write $\mathbf{C}_1 \otimes \mathbf{C}_0$ as

$$(\mathbf{C}_1 \otimes \mathbf{I}_{\lambda_0})\,(\mathbf{I}_{2\lambda_1} \otimes \mathbf{C}_0)\,.$$

The vector $\mathbf{y}$ can be obtained in two steps: (i) computation of $\mathbf{I}_{2\lambda_1} \otimes \mathbf{C}_0$ and (ii) computation of $\mathbf{C}_1 \otimes \mathbf{I}_{\lambda_0}$. We analyze these two operations as follows.

(i) Partition $\mathbf{x}$ into $2\lambda_1$ vectors, each of size λ_0, i.e., $\mathbf{x} = \begin{pmatrix} \mathbf{x}_0^T & \mathbf{x}_1^T & \dots & \mathbf{x}_{2\lambda_1-1}^T \end{pmatrix}^T$. Let

$$\mathbf{w} = (\mathbf{I}_{2\lambda_1} \otimes \mathbf{C}_0)\,\mathbf{x}$$

be the output of the first step, then $\mathbf{w} = \left((\mathbf{C}_0\mathbf{x}_0)^T \quad (\mathbf{C}_0\mathbf{x}_1)^T \quad \dots \quad (\mathbf{C}_0\mathbf{x}_{2\lambda_1-1})^T\right)^T$. The computation of $\mathbf{w}$ requires $2\lambda_1 C(\lambda_0)$.

(ii) It can be verified that after some row exchanges and column exchanges $\mathbf{C}_1 \otimes \mathbf{I}_{\lambda_0}$ assumes the form $\mathbf{I}_{\lambda_0} \otimes \mathbf{C}_1$. Namely, $\mathbf{C}_1 \otimes \mathbf{I}_{\lambda_0} = \mathbf{P}_1(\mathbf{I}_{\lambda_0} \otimes \mathbf{C}_1)\mathbf{P}_2$, where $\mathbf{P}_1$ and $\mathbf{P}_2$ are permutation matrices. Partition $\mathbf{P}_2\mathbf{w}$ into λ_0 vectors, $\mathbf{P}_2\mathbf{w} = \left(\mathbf{w}_0^T \quad \mathbf{w}_1^T \quad \dots \quad \mathbf{w}_{\lambda_0-1}^T\right)^T$. Each of $\mathbf{w}_i's$ is a $2\lambda_1 \times 1$ vector. Then,

$$\mathbf{y} = \mathbf{P}_1 \left((\mathbf{C}_1\mathbf{w}_0)^T \quad (\mathbf{C}_1\mathbf{w}_1)^T \quad \dots \quad (\mathbf{C}_1\mathbf{w}_{\lambda_0-1})^T\right)^T.$$

As $\mathbf{P}_1$ and $\mathbf{P}_2$ are permutation matrices and require no computation, operation $\mathbf{C}_1 \otimes \mathbf{I}_{\lambda_0}$ can be completed with complexity $\frac{\lambda_0}{2}C(2\lambda_1)$.

So the computation needed for $\mathbf{C}_1 \otimes \mathbf{C}_0$ is $2\lambda_1 C(\lambda_0) + \frac{\lambda_0}{2}C(2\lambda_1)$. The matrix $\mathbf{S}_1 \otimes \mathbf{S}_0$ has the same complexity. This verifies that complexity of $\mathbf{C}$ is $4\lambda_1 C(\lambda_0) + \lambda_0 C(2\lambda_1)$.

Chapter 5

Four-Parallelogram Filter Banks

5.1 Introduction

In Chapter 4, we studied two-dimensional two-parallelogram filter banks. This is the class of systems in which the supports (passbands) of the analysis filters consist of two parallelograms, each a shifted version of a parallelogram prototype. Fig. 5.1 (a) and (b) show respectively a parallelogram prototype and the support (passband) of a typical analysis filter in a two parallelogram filter bank. The analysis filters have real coefficients; the supports are symmetric with respect to the origin. Consider the two-dimensional (2D) filter bank with decimation matrix M in Fig. 1.1. It is explained in [53] that for successful design of the analysis and synthesis filters, it is necessary that the configuration of the filter bank be $\mathcal{AFS}(\mathbf{M})$ and permissible. More specific description of these two properties are given below.

Recall that a filter $H(\boldsymbol{\omega})$ is called *AliasFree Supported with respect to* M ($\mathcal{AFS}(\mathbf{M})$) if the support of $H(\boldsymbol{\omega})$ does not overlap under modulo $2\pi\mathbf{M}^{-T}$. When $H(\boldsymbol{\omega})$ is an ideal filter, the output of $H(\boldsymbol{\omega})$

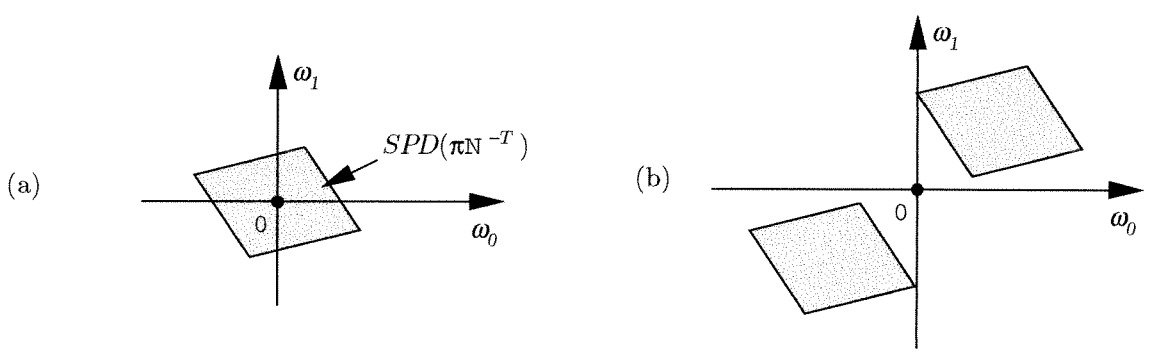

Fig. 5.1. Two-parallelogram filter bank: (a) Parallelogram prototype and (b) typical support of an analysis filter.

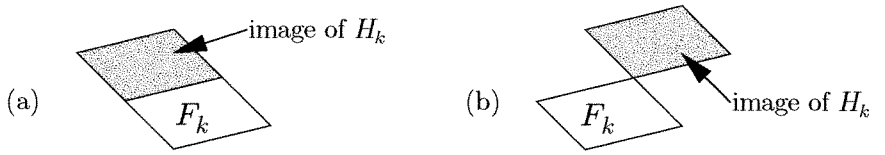

Fig. 5.2. (a) Image of the kth analysis filter is edge adjacent to the kth synthesis filter; (b) image of the kth analysis filter is vertex adjacent to the kth synthesis filter.

would allow aliasfree M-fold decimation. When all the analysis filters are $\mathcal{AFS}(\mathbf{M})$, the configuration is referred to as $\mathcal{AFS}(\mathbf{M})$. If a filter bank has a $\mathcal{AFS}(\mathbf{M})$ configuration then, in ideal case no aliasing is created in the subbands and the filter bank has perfect reconstruction. In practice, the non-ideal roll-off of the filter causes aliasing in the subband. When the analysis filters are decimated and then expanded by $\mathbf{M}$, each has $|\mathbf{M}| - 1$ images, where the notation $|\mathbf{M}|$ denotes the absolute value of the determinant of $\mathbf{M}$. All the images are attenuated to the stopband level of the synthesis filters except those images that are adjacent to the passband of the synthesis filters. These adjacent images result in different types of major aliasing depending on the type of adjacency involved. For example, in Fig. 5.2(a) one image of the analysis filter $H_k(\boldsymbol{\omega})$ is edge adjacent to the synthesis filter $F_k(\boldsymbol{\omega})$ and results in edge aliasing and similarly the image in Fig. 5.2(b) results in vertex aliasing. A perfect reconstruction filter bank enjoys complete alias cancelation, so major aliasing of one subband is canceled largely by major aliasing of other subbands. However, when the configurations are not constructed properly, it is possible that some edge aliasing can not be canceled if the analysis and synthesis filters have good frequency selectivity. Such configurations are called edge nonpermissible. Similarly, if some vertex aliasing in a configuration are uncancelable when the filters have good frequency selectivity, the configuration is called vertex nonpermissible. For the individual filters to have good frequency selectivity, it is necessary that the configuration have permissibility [11, 31], which includes edge and vertex permissibility [53]. In this case, the importance of edge permissibility is much greater than vertex permissibility. Notice that permissibility is determined jointly by all the analysis filters. To have a permissible configuration, the support of one analysis filter will affect the choice of other filters.

Although the two-parallelogram filter banks can not possess both edge and vertex permissibility in general, the two-parallelogram filter banks can have edge permissibility. Edge permissible two-parallelogram cosine modulated filter banks are constructed and designed in [47, 53]. However, lack of permissibility leads to limitation in the stopband attenuation of the individual filters in the two-parallelogram cosine modulated filter banks.

Four-Parallelogram Filter Banks

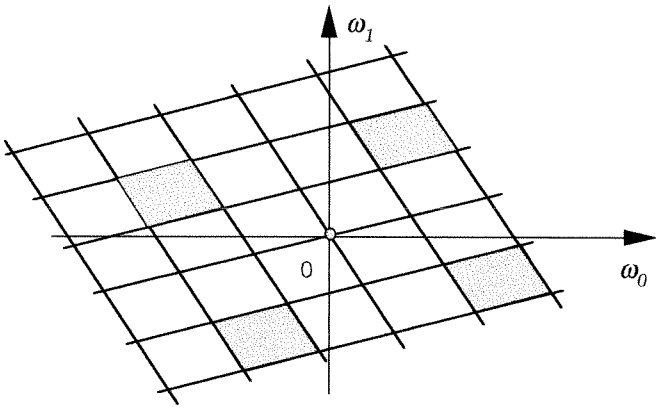

Fig. 5.3. Typical support of an analysis filter in a *Four-P* filter bank.

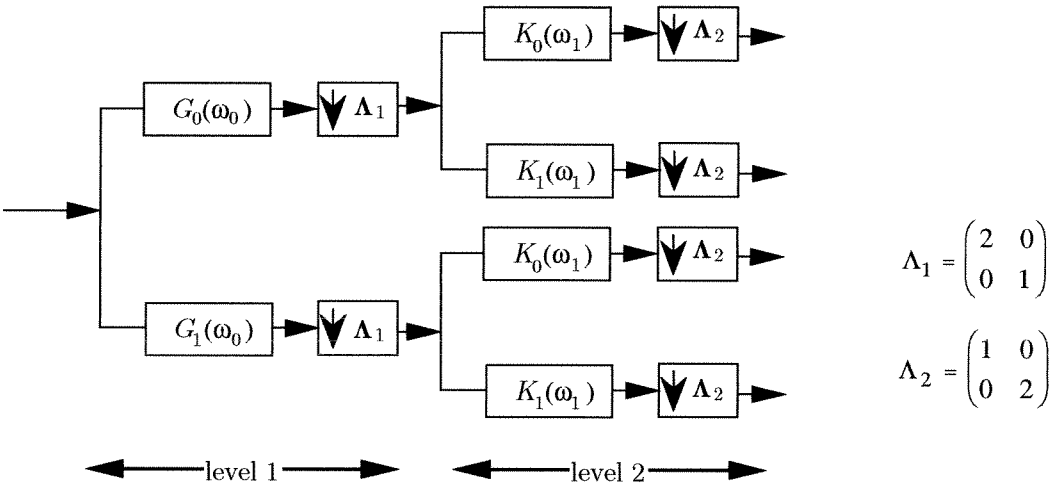

Fig. 5.4. A four-channel tree structured filter bank obtained by cascading two 1D two-channel filter banks.

In this chapter, we study four parallelogram filter banks [48], the class of filter banks in which the supports of the analysis filters consist of four parallelograms as shown in Fig. 5.3. The simplest way to design four-parallelogram (*Four-P*) filter banks is by using separable filter banks [109]. A separable 2D filter bank can be obtained by cascading two one-dimensional (1D) filter banks in a tree structure. For example, the tree structured filter bank in Fig. 5.4 is obtained by using two 1D two-channel filter banks. The resulting 2D analysis and synthesis filters are products of two 1D filters and are separable; the support of each analysis filter is the union of four rectangles (Fig. 5.5). The 2D analysis and synthesis filters can have good frequency selectivity if the 1D filters have good frequency selectivity. Therefore the separable 2D filter banks are both edge and vertex permissible. In this chapter we will pursue edge and vertex permissibility for *Four-P* filter banks.

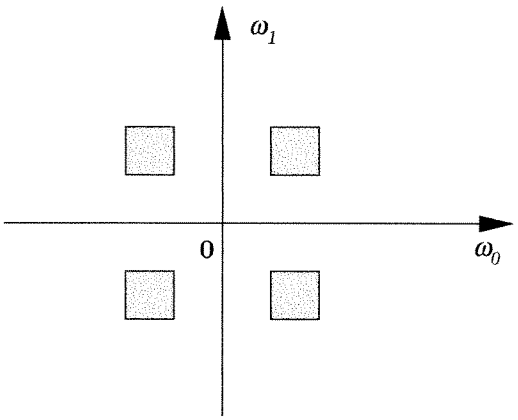

Fig. 5.5. Separable filter bank. Typical support of an analysis filter.

To obtain a support configuration for *Four-P* filter bank, we first construct a parallelogram prototype. Then we shift the parallelogram prototype properly and combine four shifted parallelograms to obtain the support of each analysis filter. The synthesis filters have the same supports as the corresponding analysis filters. As the support of each analysis filter consists of four shifted versions of the parallelogram prototype, the area of the parallelogram prototype is one fourth the area of the support of an analysis filter. In a $|\mathbf{M}|$-channel filter bank, the area of an analysis filter support is usually the same as $SPD(\pi\mathbf{M}^{-T})$, where $SPD(\cdot)$ is defined in Chapter 2. Let the parallelogram prototype be $SPD(\pi\mathbf{N}^{-T})$, where $\mathbf{N} = \mathbf{ML}$, for some integer matrix $\mathbf{L}$ with $|\mathbf{L}| = 4$. Due to the integer matrix constraint on $\mathbf{L}$, the *Four-P* filter banks considered in this chapter are only a subclass of *Four-P* filter banks. Since $|\mathbf{N}| = 4|\mathbf{M}|$, the area of $SPD(\pi\mathbf{N}^{-T})$ is one fourth that of $SPD(\pi\mathbf{M}^{-T})$. For a given decimation matrix $\mathbf{M}$, the choice of $\mathbf{L}$ will determine the parallelogram prototype and indirectly affect the supports of the analysis filters. Then we combine four shifted versions of the parallelogram prototype to obtain the supports of the analysis filters.

For *Four-P* filter banks, there are a variety of possible configurations. For example, consider the lowpass analysis filter $H_0(\boldsymbol{\omega})$. Fig. 5.6 (a) and (b) show two of the possible supports for $H_0(\boldsymbol{\omega})$. The support of $H_0(\boldsymbol{\omega})$ is different when the four parallelograms in the support of $H_0(\boldsymbol{\omega})$ are glued in different manners. Notice that in the two-parallelogram filter banks, the analysis filters have only two passbands; when the filters have real coefficients, the location of one passband will determine the location of the other passband. This is not true in the *Four-P* filter bank case as we can see from Fig. 5.6. The preceding construction indicates that for a given decimation matrix $\mathbf{M}$, the support configuration is determined by the following two steps. Step one, choose $\mathbf{L}$ and hence the parallelogram prototype. Step two, shift the parallelogram prototype properly and combine four shifted copies to obtain the support for each analysis filter. We will construct various types of configurations for the *Four-P* filter banks and discuss permissibility of these configurations.

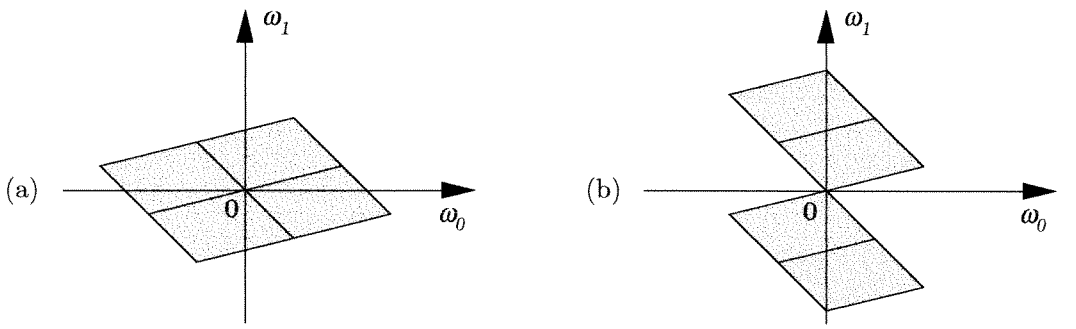

Fig. 5.6. Two of the possible supports for the 0th analysis filter.

It turns out that permissibility is only possible for a special class of *Four-P* filter banks, the simplistic *Four-P* filter banks. We will see that in permissible simplistic *Four-P* filter banks, the decimation matrix $\mathbf{M}$ is necessarily of the form $\mathbf{Q}\mathbf{\Lambda}$, where $\mathbf{Q}$ is an integer matrix with $|\mathbf{Q}| = 1$ or 2, and $\mathbf{\Lambda}$ is a diagonal integer matrix. This gives rise to the implementation of simplistic *Four-P* filter banks of low design cost. In particular, when $|\mathbf{Q}| = 1$ simplistic *Four-P* filter banks can be implemented by using a separable filter bank with decimation matrix $\mathbf{\Lambda}$ followed by a so called unimodular transformation [97]. When $|\mathbf{Q}| = 2$, the desired configuration can be achieved by concatenating a separable 2D filter banks with a 2D two-channel filter bank in the form of a tree. In Chapter 4, we discuss cosine modulated implementation of two-parallelogram filter banks. For *Four-P* filter banks, we will not do it because attractive implementation can be obtained with little loss of generality as we will show.

Chapter Outline

All notations and conventions are precisely as in Chapter 4. The sections are organized as follows. In Sec. 5.2, we will consider a special class of *Four-P* filter banks, the simplistic *Four-P* filter banks. For a given decimation matrix $\mathbf{M}$, we say a *Four-P* filter bank is simplistic if the support of the lowpass analysis filter is the parallelogram $SPD(\pi\mathbf{M}^{-T})$. The other filters in the simplistic filter banks will be constructed such that the configuration of the filter bank is permissible. We will see that, in this case the decimation matrix needs to be properly constrained. In Sec. 5.3, we make connection between permissible simplistic *Four-P* filter banks to other existing filter banks. Via this connection, permissible simplistic *Four-P* filter banks can be achieved by cascading filter banks of low design cost. Other types of *Four-P* filter banks (other than the simplistic *Four-P* filter banks) are studied in Sec. 5.4.

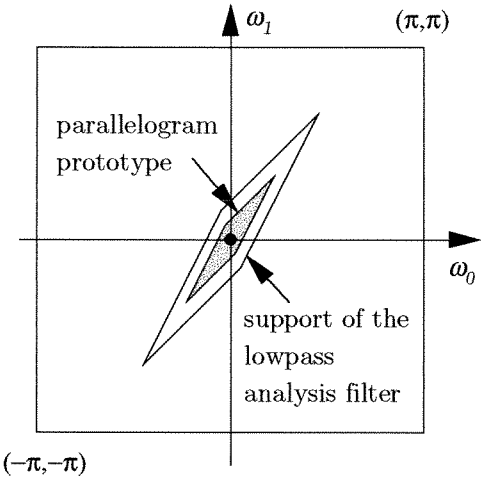

Fig. 5.7. Simplistic four-parallelogram filter bank. The parallelogram prototype $SPD(\pi \mathbf{N}^{-T})$ and the support of the lowpass analysis filter $SPD(\pi \mathbf{M}^{-T})$.

5.2 The Simplistic Four-Parallelogram Filter Banks

Consider the filter bank with decimation matrix $\mathbf{M}$ in Fig. 1.1. In this section, we consider simplistic *Four-P* filter banks, a special type of *Four-P* filter banks that are completely characterized by the support of the lowpass analysis filter $H_0(\boldsymbol{\omega})$. A *Four-P* filter bank with decimation matrix $\mathbf{M}$ is called simplistic if the support of $H_0(\boldsymbol{\omega})$ is $SPD(\pi \mathbf{M}^{-T})$. Recall that in a separable filter bank with diagonal decimation matrix $\boldsymbol{\Lambda}$, the support of the lowpass analysis filter is $SPD(\pi \boldsymbol{\Lambda}^{-T})$. So, the lowpass analysis filter in simplistic filter banks is the natural nonseparable generalization of the lowpass analysis filter in a separable filter bank.

We can verify that in simplistic filter banks, the matrix $\mathbf{L}$ is

$$\mathbf{L} = \begin{pmatrix} 2 & 0 \\ 0 & 2 \end{pmatrix}.$$

The matrix $\mathbf{N}$ that determines the parallelogram prototype $SPD(\pi \mathbf{N}^{-T})$ is $\mathbf{N} = 2\mathbf{M}$. For example,

$$\text{let } \mathbf{M} = \begin{pmatrix} 8 & -5 \\ -4 & 5 \end{pmatrix}, \text{ then } \mathbf{N} = 2 \begin{pmatrix} 8 & -5 \\ -4 & 5 \end{pmatrix}.$$

The parallelogram prototype $SPD(\pi \mathbf{N}^{-T})$ and the support of the lowpass analysis filter $SPD(\pi \mathbf{M}^{-T})$ are as shown in Fig. 5.7.

Frequency Normalization. All the frequency planes in previous figures are shown with ω_0 and ω_1 as two axes, e.g., Fig. 5.7. For the convenience of illustration, we will use a new set of axes. On the

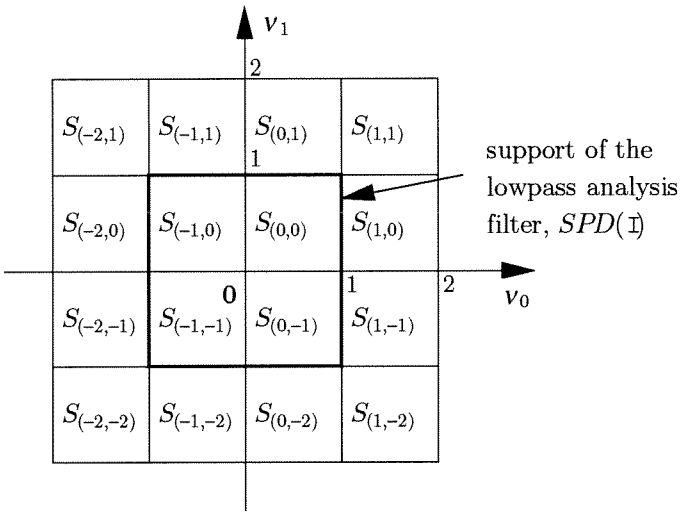

Fig. 5.8. The simplistic four-parallelogram filter bank. The support of the lowpass analysis filter.

new frequency plane, the parallelogram prototype would appear the same for any chosen $\mathbf{N}$. More specifically, we will normalize the frequency plane by $2\pi\mathbf{N}^{-T}$; we define

$$\boldsymbol{\nu} = \begin{pmatrix} \nu_0 \\ \nu_1 \end{pmatrix} = \frac{1}{2\pi}\mathbf{N}^T \begin{pmatrix} \omega_0 \\ \omega_1 \end{pmatrix}$$

and use ν_0 and ν_1 as the two axes. On the normalized frequency plane, the parallelogram prototype will always appear as the square $SPD(0.5\mathbf{I})$ (Fig. 5.8). In the simplistic filter bank case, the support of $H_0(\boldsymbol{\omega})$ becomes $SPD(\mathbf{I})$ as shown in Fig. 5.8. In Fig. 5.8 the notation $S_{(k_0,k_1)}$ denotes the square

$$SPD(0.5\mathbf{I}) + \begin{pmatrix} k_0 + 0.5 \\ k_1 + 0.5 \end{pmatrix},$$

where the vector subscript of S should be interpreted modulo $\mathbf{N}^T$. The support of $H_0(\boldsymbol{\omega})$ is the union of the four squares

$$S_{(0,0)}, S_{(-1,0)}, S_{(0,-1)}, \text{ and } S_{(-1,-1)}.$$

Notice that to have real-coefficient filters, whenever $S_{(k_0,k_1)}$ belongs to a certain analysis filter, $S_{(-k_0-1,-k_1-1)}$ must be part of the same analysis filter. We will call $(S_{(k_0,k_1)}, S_{(-k_0-1,-k_1-1)})$ a conjugate pair. The support of each analysis filter consists of two conjugate pairs.

Necessary Condition for Permissibility. So far, only the support of the lowpass analysis filter is determined. As permissibility is jointly determined by all the analysis filters, the supports of the analysis filters in other subbands have to be constrained properly. We would like to construct the

other filters such that the configuration has edge and vertex permissibility at the same time. With this premise, we can derive the following necessary condition.

Proposition 5.1. If a simplistic *Four-P* filter bank is permissible, the supports of the other analysis filters $H_m(\boldsymbol{\omega})$ must contain

$$\text{the conjugate pair } \left(S_{(k_0,k_1)}, S_{(-k_0-1,-k_1-1)}\right), \text{ and the conjugate pair } \left(S_{(-k_0-1,k_1)}, S_{(k_0,-k_1-1)}\right). \tag{5.1}$$

■

Corollary 5.1. The condition in Proposition 5.1 in terms implies decimation matrix $\mathbf{M}$ is restricted to the following form.

$$\mathbf{M} = \mathbf{Q}\boldsymbol{\Lambda}, \tag{5.2}$$

where $\mathbf{Q}$ is an integer matrix with $|\mathbf{Q}| = 1$ or 2 and $\boldsymbol{\Lambda}$ is a diagonal integer matrix. ■

Proposition 5.1 and Corollary 5.1 will be shown in Sec. 5.2.1 and 5.2.2 respectively.

5.2.1 Edge and Vertex Permissible Simplistic Four-Parallelogram Filter Banks

Recall that the $\mathbf{M}$-fold decimated and expanded version of $H_0(\boldsymbol{\omega})$ contains $|\mathbf{M}|$ copies, which are shifted copies of $H_0(\boldsymbol{\omega})$ by

$$2\pi\mathbf{M}^{-T}\mathbf{m}, \mathbf{m} \in \mathcal{N}(\mathbf{M}^T).$$

With axes normalization, the images of passband $S_{\mathbf{k}}$ are at

$$S_{\mathbf{k}+2\mathbf{m}}, \quad \mathbf{m} \in \mathcal{N}(\mathbf{M}^T),\ \mathbf{m} \neq \mathbf{0}. \tag{5.3}$$

Fig. 5.9 illustrates the locations of the images of $S_{\mathbf{k}}$. The images of $S_{\mathbf{k}}$ are neither edge adjacent nor vertex adjacent to $S_{\mathbf{k}}$. It follows from (5.3) that a particular $S_{\mathbf{n}}$ is occupied by an image of $S_{\mathbf{k}}$ if $\frac{1}{2}(\mathbf{n}-\mathbf{k})$ is an integer vector. Furthermore, the aliasing resulting from the image at $S_{\mathbf{n}}$ contributes to the aliasing transfer function $A_{\frac{1}{2}(\mathbf{n}-\mathbf{k})}(\boldsymbol{\omega})$ (see Chapter 2 for the definition of aliasing transfer functions). In the equations to follow, the vector subscript $\mathbf{n}$ of $S_{\mathbf{n}}$ should be interpreted modulo $\mathbf{N}^T$ while the vector subscript $\mathbf{k}$ of $A_{\mathbf{k}}(\boldsymbol{\omega})$ should be interpreted modulo $\mathbf{M}^T$.

From Fig. 5.9, we see that three images of $S_{(0,0)}$ will be at $S_{(-2,0)}$, $S_{(0,-2)}$ and $S_{(-2,-2)}$ as shown in Fig. 5.10. The images at $S_{(-2,0)}$, $S_{(0,-2)}$ are edge adjacent to $H_0(\boldsymbol{\omega})$ and result in edge aliasing while the image at $S_{(-2,-2)}$ is vertex adjacent to $H_0(\boldsymbol{\omega})$ and results in vertex aliasing. We discuss

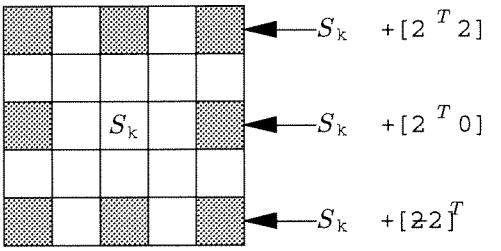

Fig. 5.9. The location of the images of S.

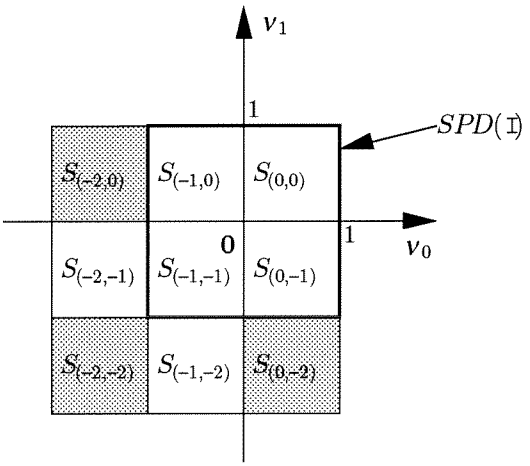

Fig. 5.10. The simplistic four-parallelogram filter bank. The image of $S_{(0,0)}$.

respectively the cancelation of aliasing on account of the three images mentioned above. We will argue that due to the presence of the images at $S_{(-2,0)}$ and $S_{(0,-2)}$, the supports of two other analysis filters will become determined.

1. *The image at* $S_{(-2,0)}$: From Fig. 5.9, we see that this image is edge adjacent to $S_{(-1,0)}$. The aliasing term contributes to the aliasing transfer function $A_{(-1,0)}(\boldsymbol{\omega})$. Let the support of the analysis filter $H_1(\boldsymbol{\omega})$ contain $S_{(-2,0)}$. Then, this is the only subband that can provide an aliasing term to cancel the aliasing error in the first subband. To be able to contribute to the aliasing transfer function $A_{(-1,0)}(\boldsymbol{\omega})$, the support of $H_1(\boldsymbol{\omega})$ must contain $S_{(1,0)}$. As the analysis filters have real coefficients, the support of $H_1(\boldsymbol{\omega})$ must contain the conjugate pairs $(S_{(1,0)}, S_{(-2,-1)})$ and $(S_{(-2,0)}, S_{(1,-1)})$ (Fig. 5.8). Summarizing, the support of $H_1(\boldsymbol{\omega})$ is the union of

$$S_{(1,0)}, S_{(-2,-1)}, S_{(-2,0)}, \text{ and } S_{(1,-1)},$$

as shown in Fig. 5.11.

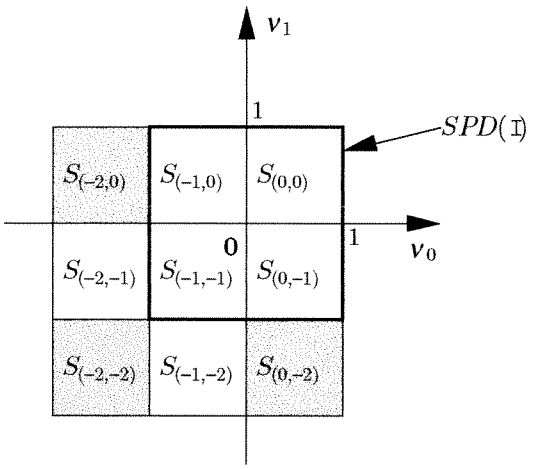

Fig. 5.11. The second and third analysis filters in the simplistic four-parallelogram filter bank.

2. *The image at* $S_{(0,-2)}$: Similarly to the previous case, this image is edge adjacent to $S_{(0,-1)}$ and creates an aliasing term that contributes to the aliasing transfer function $A_{(0,-1)}(\boldsymbol{\omega})$. Let the support of the analysis filter $H_2(\boldsymbol{\omega})$ contain $S_{(0,-2)}$. To be able to cancel the edge aliasing error in the 0th subband, the support of $H_2(\boldsymbol{\omega})$ must also contain $S_{(0,1)}$. As the analysis filters are real-coefficient, the support of $H_2(\boldsymbol{\omega})$ is the union of

$$S_{(0,1)}, S_{(-1,-2)}, S_{(0,-2)}, \text{ and } S_{(-1,1)},$$

as shown in Fig. 5.11.

3. *The image at* $S_{(-2,-2)}$: This image is vertex adjacent to $S_{(-1,-1)}$. This will result in aliasing error that contributes to $A_{(-1,-1)}(\boldsymbol{\omega})$. Similarly, it is necessary that $S_{(-2,-2)}$ and $S_{(-1,-1)}$ are parts of the same analysis filter. As the analysis filters are real-coefficient, $S_{(-2,-2)}$ and $S_{(-1,-1)}$ always belong to the same analysis filter.

We can verify that the cancelation of aliasing caused by the images of $S_{(0,-1)}$, $S_{(-1,0)}$ and $S_{(-1,-1)}$ require the same choice of support for the second and third subbands. Repeating the same argument, we conclude that for the purpose of alias cancelation or support permissibility the analysis filters are necessarily of the form in (5.1).

In a typical 1D M-channel filter bank, each analysis filter has total bandwidth $2\pi/M$. In 2D case, total bandwidth should be interpreted as total area of spectral occupancy. When the filters are not constructed properly, some filters would have less area than the others. The following result shows that this situation can be avoided.

Proposition 5.2. *When the supports of the analysis filters are chosen according to (5.1), all analysis filters*

have the same area of spectral occupancy. ■

Proof. We only need to show that the four squares are distinct under modulo $\mathbf{N}^T$. For this we will show that $S_{(k_0,k_1)}$ is not the same as the other three terms in (5.1). Suppose that $S_{(k_0,k_1)}$ and $S_{(-k_0-1,k_1)}$ are identical for some k_0 and k_1. Then

$$\begin{pmatrix} k_0 \\ k_1 \end{pmatrix} = \begin{pmatrix} -k_0 - 1 \\ k_1 \end{pmatrix} \bmod \mathbf{N}^T,$$

which implies $\begin{pmatrix} 2k_0+1 & 0 \end{pmatrix}^T = \mathbf{0} \bmod \mathbf{N}^T$, i.e., $\begin{pmatrix} 2k_0+1 & 0 \end{pmatrix}^T$ is on the lattice of $\mathbf{N}^T$. But $\mathbf{N}^T = 2\mathbf{M}^T$ and $\begin{pmatrix} 2k_0+1 & 0 \end{pmatrix}^T$ can not be a vector of $LAT(\mathbf{N}^T)$. So $S_{(k_0,k_1)}$ and $S_{(-k_0-1,k_1)}$ are distinct $\forall k_0, k_1$. In a similar manner, we can show that $S_{(k_0,k_1)}$ and $S_{(k_0,-k_1-1)}$ are distinct and also that $S_{(k_0,k_1)}$ and $S_{(-k_0-1,-k_1-1)}$ are distinct $\forall k_0, k_1$. ■

5.2.2 Proof of Corollary 5.1

We first show that support permissibility will imply the matrix $\mathbf{K}$ given by

$$\mathbf{K} = \mathbf{M}^{-T} \underbrace{\begin{pmatrix} 1 & 0 \\ 0 & -1 \end{pmatrix}}_{\mathbf{\Lambda}_0} \mathbf{M}^{-T} \tag{5.4}$$

is an integer matrix, which in turns will give us (5.2).

By (5.1), the analysis filter that contains the pair $(S_{(k_0,k_1)}, S_{(-k_0-1,-k_1-1)})$ should also contain $(S_{(-k_0-1,k_1)}, S_{(k_0,-k_1-1)})$.

$$\text{Suppose } \begin{pmatrix} k_0 \\ k_1 \end{pmatrix} = \begin{pmatrix} k_0' \\ k_1' \end{pmatrix} \bmod \mathbf{N}^T, \text{ then } \begin{pmatrix} k_0 - k_0' \\ k_1 - k_1' \end{pmatrix} = \mathbf{0} \mod \mathbf{N}^T. \tag{5.5}$$

The conjugate pair $(S_{(k_0,k_1)}, S_{(-k_0-1,-k_1-1)})$ should be the same as the pair $(S_{(k_0',k_1')}, S_{(-k_0'-1,-k_1'-1)})$. It follows that $(S_{(-k_0-1,k_1)}, S_{(k_0,-k_1-1)})$ is the same as the pair $(S_{(-k_0'-1,k_1')}, S_{(k_0',-k_1'-1)})$. With $\mathbf{N} = 2\mathbf{M}$, we can verify that $[-k_0 - 1, k_1]^T \neq [k_0', -k_1' - 1]^T \bmod \mathbf{N}^T$, for all k_0 and k_1. So we have $S_{(-k_0-1,k_1)} = S_{(-k_0'-1,k_1')}$ and hence

$$\begin{pmatrix} k_0' - k_0 \\ k_1 - k_1' \end{pmatrix} = \mathbf{0} \mod \mathbf{N}^T. \tag{5.6}$$

Combining (5.5) and (5.6), we have $\mathbf{\Lambda}_0 \mathbf{N}^T \mathbf{d} = \mathbf{0} \bmod \mathbf{N}^T$, $\forall \mathbf{d} \in \mathcal{Z}^2$, where $\mathbf{\Lambda}_0$ is as defined in (5.4) and $\mathcal{Z}^2$ is the set of all 2×1 integer vectors. Let $\mathbf{d}_0 = \begin{pmatrix} 1 & 0 \end{pmatrix}^T$ and $\mathbf{d}_1 = \begin{pmatrix} 0 & 1 \end{pmatrix}^T$, then

$\mathbf{\Lambda}_0\mathbf{N}^T\begin{pmatrix}\mathbf{d}_0 & \mathbf{d}_1\end{pmatrix} = \mathbf{N}^T\begin{pmatrix}\mathbf{k}_0 & \mathbf{k}_1\end{pmatrix}$, for some integer vectors $\mathbf{k}_0$ and $\mathbf{k}_1$. If we define $\mathbf{K} = \begin{pmatrix}\mathbf{k}_0 & \mathbf{k}_1\end{pmatrix}$, then $\mathbf{K}$ is a 2×2 integer matrix. Since $\begin{pmatrix}\mathbf{d}_0 & \mathbf{d}_1\end{pmatrix}$ is the 2×2 identity matrix and $\mathbf{N} = 2\mathbf{M}$, we have $\mathbf{\Lambda}_0\mathbf{M}^T = \mathbf{M}^T\mathbf{K}$ and we conclude that $\mathbf{K} = \mathbf{M}^{-T}\mathbf{\Lambda}_0\mathbf{M}^T$ is an integer matrix. In fact, as $|\mathbf{M}^{-T}\mathbf{\Lambda}_0\mathbf{M}^T| = 1$, $\mathbf{K}$ is unimodular.

Let the decimation matrix $\mathbf{M}$ have Smith form $\mathbf{M} = \mathbf{U}_s\mathbf{\Lambda}_s\mathbf{V}_s$, where $[\mathbf{\Lambda}_s]_{00} = \beta$ and $[\mathbf{\Lambda}_s]_{11} = \alpha\beta$ (see Chapter 2 for the definition of the Smith form of integer matrices).

$$\text{Let } \mathbf{V}_s^T = \begin{pmatrix} v_{00} & v_{01} \\ v_{10} & v_{11} \end{pmatrix}, \text{ then } \mathbf{K} = |\mathbf{V}_s^T| \begin{pmatrix} v_{00}v_{11} + v_{10}v_{01} & 2\alpha v_{01}v_{11} \\ -\frac{2}{\alpha}v_{00}v_{10} & -v_{00}v_{11} - v_{10}v_{01} \end{pmatrix}.$$

The matrix $\mathbf{K}$ is unimodular if α divides $2v_{00}v_{10}$.

(i) α is odd: Suppose $\alpha = \alpha_1\alpha_2$, then α_1 divides v_{00} and α_2 divides v_{10}. So

$$\mathbf{M} = \underbrace{\mathbf{U}_s \begin{pmatrix} v_{00}/\alpha_1 & v_{10}/\alpha_2 \\ \alpha_2 v_{01} & \alpha_1 v_{11} \end{pmatrix}}_{\mathbf{Q}} \underbrace{\beta \begin{pmatrix} \alpha_1 & 0 \\ 0 & \alpha_2 \end{pmatrix}}_{\mathbf{\Lambda}},$$

where the matrix $\mathbf{Q}$ has $|\mathbf{Q}| = 1$.

(ii) α is even: Suppose $\alpha = 2\alpha_1\alpha_2$, α_1 divides v_{00} and α_2 divides v_{10}. Then

$$\mathbf{M} = \underbrace{\mathbf{U}_s \begin{pmatrix} 1 & 0 \\ 0 & 2 \end{pmatrix} \begin{pmatrix} v_{00}/\alpha_1 & v_{10}/\alpha_2 \\ \alpha_2 v_{01} & \alpha_1 v_{11} \end{pmatrix}}_{\mathbf{Q}} \underbrace{\beta \begin{pmatrix} \alpha_1 & 0 \\ 0 & \alpha_2 \end{pmatrix}}_{\mathbf{\Lambda}_2},$$

where $\mathbf{Q}$ has $|\mathbf{Q}| = 2$. Notice that in the special case of two-channel 2D filter bank, $\alpha = 2$ and $\beta = 1$, the matrix $\mathbf{K}$ is always unimodular and (5.6) is satisfied. ■

Example 5.1. *Decimation matrix* $\mathbf{M}$ *not satisfying (5.2).* This example illustrates that some edge aliasing errors will remain uncanceled when (5.1) is not satisfied. Consider the decimation matrix

$$\mathbf{M} = \begin{pmatrix} 1 & 1 \\ -1 & 2 \end{pmatrix},$$

which is not of the form in (5.2) and hence the analysis filters can not be of the form in (5.1). The supports of the analysis filters consist of four parallelograms, each a shifted version of $SPD(\pi\mathbf{N}^{-T})$,

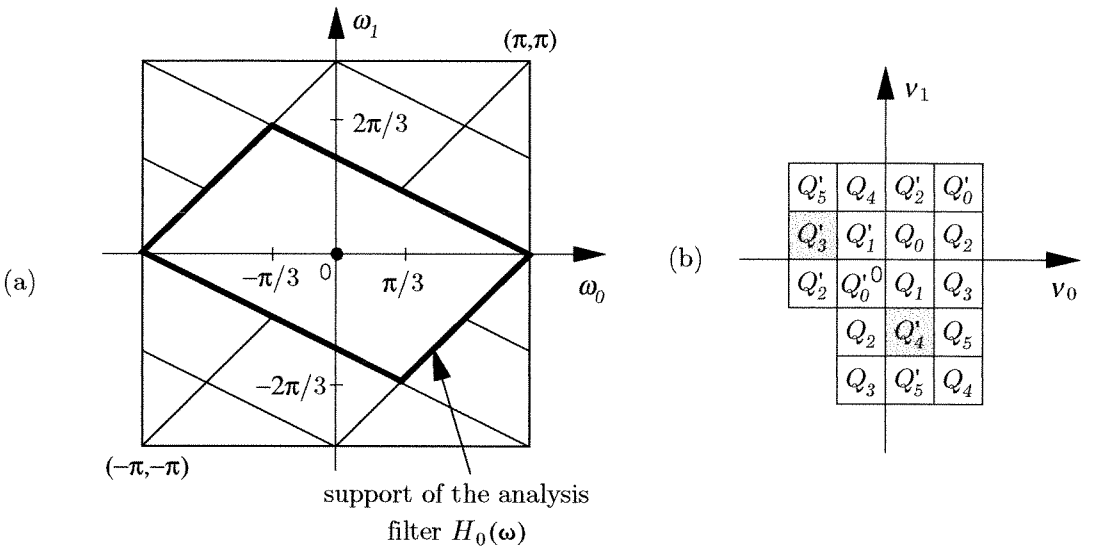

Fig. 5.12. Example 5.1. (a) Support of the 0th analysis filter; (b) pertaining to the illustration of alias cancelation.

where

$$\mathbf{N} = 2\begin{pmatrix} 1 & 1 \\ -1 & 2 \end{pmatrix}.$$

The support of the lowpass analysis filter $H_0(\boldsymbol{\omega})$ is as shown in Fig. 5.12(a). With axis normalization the support of $H_0(\boldsymbol{\omega})$ becomes $SPD(\mathbf{I})$ as shown in Fig. 5.12(b). We have labeled all the cells in Fig. 5.12(b) by Q_k and Q_k' with (Q_k, Q_k') denoting a conjugate pair. As $|\mathbf{N}| = 12$, there are total 6 conjugate pairs (Q_k, Q_k'), for $k = 0, 1, \ldots, 5$.

The lowpass filter $H_0(\boldsymbol{\omega})$ contains the pair (Q_0, Q_0') and the pair(Q_1, Q_1'). The two images of Q_0 are at Q_3' and Q_4'. The image at Q_3' is edge adjacent to Q_1'. To cancel the aliasing from this image, it is necessary that the analysis filter contain both Q_3' and Q_2. Let this analysis filter be $H_1(\boldsymbol{\omega})$, then $H_1(\boldsymbol{\omega})$ consists of the pairs (Q_2, Q_2') and the pair (Q_3, Q_3'). In this case, the two pairs left for the last analysis filter $H_2(\boldsymbol{\omega})$ are (Q_4, Q_4') and (Q_5, Q_5'). However, the image of Q_0 at Q_4' is edge adjacent to Q_1 and results in edge based aliasing error. Cancelation of this aliasing requires that Q_4' and Q_2' belong to the same analysis filter, i.e. (Q_2, Q_2') and (Q_4, Q_4') belong to the same analysis filter. As the support of $H_2(\boldsymbol{\omega})$ consists of (Q_4, Q_4') and (Q_5, Q_5'), this aliasing *cannot be canceled.*

5.3 Design of the Simplistic Four-Parallelogram Filter Banks

The results presented in the previous section show that for permissibility of simplistic *Four-P* filter banks, the decimation matrix $\mathbf{M}$ has the special form $\mathbf{M} = \mathbf{Q}\boldsymbol{\Lambda}$, where $\mathbf{Q}$ is an integer matrix with

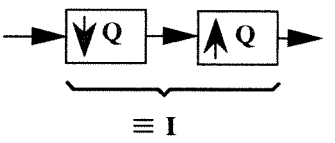

Fig. 5.13. A cascade of a unimodular decimator $\mathbf{Q}$ and a unimodular expander $\mathbf{Q}$.

$|\mathbf{Q}| = 1$ or 2 and $\mathbf{\Lambda}$ is a diagonal integer matrix. As a result, the support described in (5.1) can always be obtained by cascading systems of low design cost. In particular, when the matrix $\mathbf{Q}$ has $|\mathbf{Q}| = 1$, the support configurations can be obtained by designing two 1D perfect reconstruction filter banks and performing a unimodular transformation [97]. When the matrix $\mathbf{Q}$ has $|\mathbf{Q}| = 2$, the desired configuration can be achieved by concatenating a separable 2D filter banks with a 2D two-channel filter bank in the form of a tree structure. We now explain both of these in greater detail.

Case 1, $|\mathbf{Q}| = 1$

Consider a 2D $|\mathbf{M}|$-channel perfect reconstruction filter bank obtained by cascading two 1D filter banks using tree structure. The first level and second level of the tree are 1D filter banks with $[\mathbf{\Lambda}]_{00}$ channels and $[\mathbf{\Lambda}]_{11}$. The overall system, having decimation matrix $\mathbf{\Lambda}$, will be denoted by $\mathcal{FB}_{\mathbf{\Lambda}}$. Let the analysis and synthesis filters of $\mathcal{FB}_{\mathbf{\Lambda}}$ be defined as $G_m(\boldsymbol{\omega})$ and $T_m(\boldsymbol{\omega})$ respectively. Then the support of $G_m(\boldsymbol{\omega})$ is the union of four rectangles of $SPD(\pi\frac{1}{2}\mathbf{\Lambda}^{-1})$. Recall that a unimodular decimator or a unimodular expander only permutes the input and the cascade of a unimodular decimator $\mathbf{Q}$ followed by a unimodular expander $\mathbf{Q}$ is an identity system Fig. 5.13. Now if we insert a unimodular decimator $\mathbf{Q}$ before $\mathcal{FB}_{\mathbf{\Lambda}}$ and insert a unimodular expander $\mathbf{Q}$ after $\mathcal{FB}_{\mathbf{\Lambda}}$, the new system (Fig. 5.14(a)) remains a perfect reconstruction system. This is equivalent to inserting a decimator $\mathbf{Q}$ before each analysis filter and an expander $\mathbf{Q}$ after each synthesis filter (Fig. 5.14(b)). We can redraw Fig. 5.14(b) as Fig. 5.14(c). Denote the new filter bank with decimation matrix $\mathbf{M} = \mathbf{Q}\mathbf{\Lambda}$ by $\mathcal{FB}_{\mathbf{M}}$, which will be called the unimodular transformation of $\mathcal{FB}_{\mathbf{\Lambda}}$ by $\mathbf{Q}$. The analysis and synthesis filters of $\mathcal{FB}_{\mathbf{M}}$ are $G_m(\mathbf{Q}^T\boldsymbol{\omega})$ and $T_k(\mathbf{Q}^T\boldsymbol{\omega})$. Observe that the support of $G_m(\mathbf{Q}^T\boldsymbol{\omega})$ is the union of four shifted copies of $SPD(\pi\frac{1}{2}\mathbf{Q}^{-T}\mathbf{\Lambda}^{-1})$. One can verify that the filter bank $\mathcal{FB}_{\mathbf{M}}$ with analysis filters $H_m(\boldsymbol{\omega})$ and synthesis filters $F_m(\boldsymbol{\omega})$ given by

$$H_m(\boldsymbol{\omega}) = G_m(\mathbf{Q}^T\boldsymbol{\omega}), \quad F_m(\boldsymbol{\omega}) = T_m(\mathbf{Q}^T\boldsymbol{\omega}), \tag{5.7}$$

is a simplistic *Four-P* filter bank. This result is identical to those found earlier in [97].

Example 5.2. *Simplistic Four-P filter banks.* Consider a 20-channel filter bank with decimation

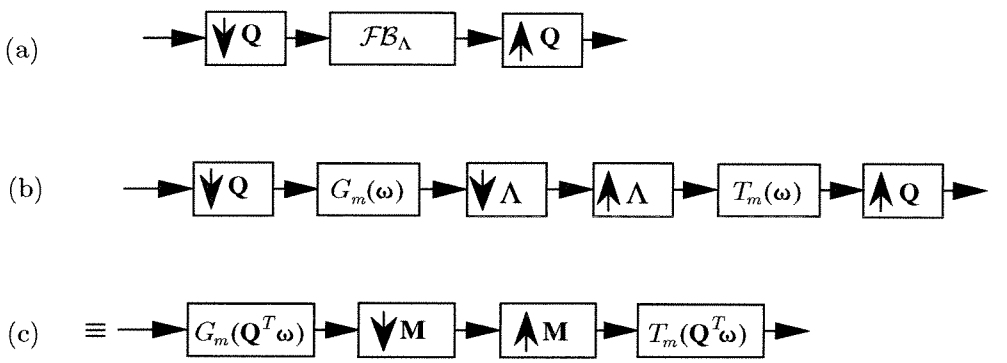

Fig. 5.14. Pertaining to the illustration of the unimodular transformation.

matrix

$$\mathbf{M} = \begin{pmatrix} 8 & -5 \\ -4 & 5 \end{pmatrix},$$

which can be factorized as

$$\begin{pmatrix} 2 & -1 \\ -1 & 1 \end{pmatrix} \begin{pmatrix} 4 & 0 \\ 0 & 5 \end{pmatrix}.$$

The matrix $\mathbf{M}$ has the form in case 1 of (5.1). Design a separable filter bank by concatenating a 1D four-channel filter bank and a 1D five-channel filter bank. Using the substitution in (5.7), the new nonseparable filter bank has the desired configuration as described in (5.1). The parallelogram prototype is as shown in Fig. 5.7. Fig. 5.15(a) shows the support configuration of the the analysis filters. Fig. 5.15(b) shows the magnitude response of the lowpass analysis filter.

Case 2, $|\mathbf{Q}| = 2$

Consider a tree structured filter bank with two levels in Fig. 5.16. The first level of the tree is a two-channel filter bank with decimation matrix $\mathbf{Q}$. The lowpass analysis filter of the two-channel system has support $SPD(\pi\mathbf{Q}^{-T})$. For the second level of the tree, we use a separable $|\mathbf{\Lambda}|$-channel filter bank ($\mathcal{FB}_\mathbf{\Lambda}$) that is obtained by cascading two 1D filter banks of $[\mathbf{\Lambda}]_{00}$ channels and $[\mathbf{\Lambda}]_{11}$ channels in the form of a tree. Then the overall filter bank has the desired configuration of *Four-P* filter banks.

Example 5.3. *Simplistic Four-P filter banks.* Consider a 8-channel *Four-P* filter bank with decimation matrix

$$\mathbf{M} = \underbrace{\begin{pmatrix} 1 & 1 \\ -1 & 1 \end{pmatrix}}_{\mathbf{Q}} \underbrace{\begin{pmatrix} 2 & 0 \\ 0 & 2 \end{pmatrix}}_{\mathbf{\Lambda}}.$$

The matrix $\mathbf{M}$ has the form in case 2 of (5.1). We can obtain a *Four-P* filter bank by using a tree

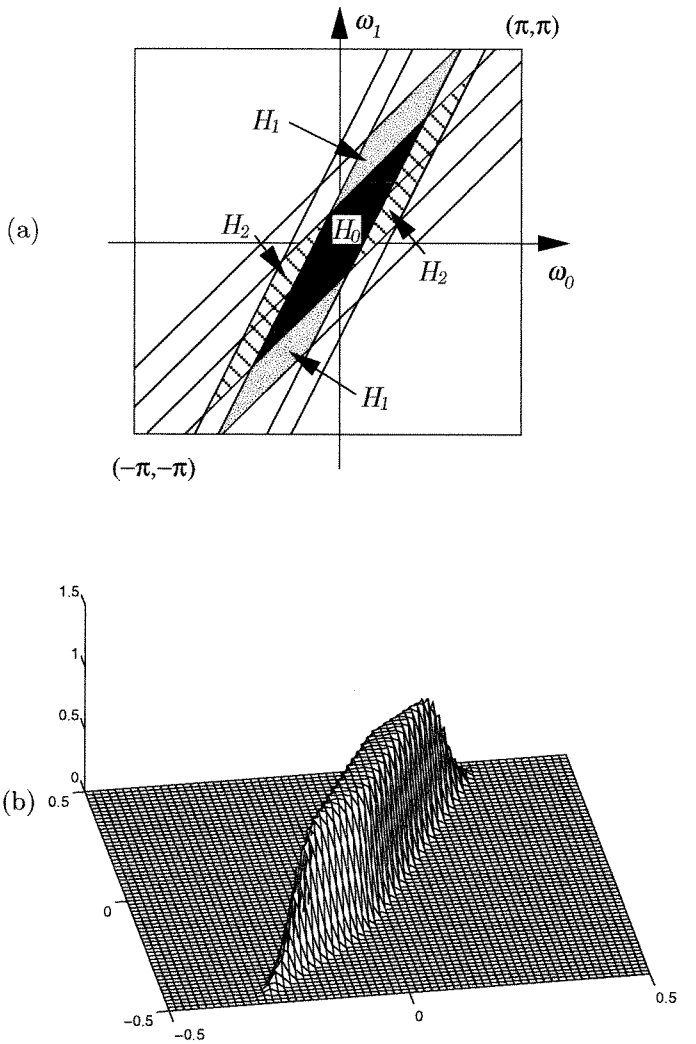

Fig. 5.15. Example 5.2. Simplistic *Four-P* filter bank: (a) Spectral support of the analysis filters and (b) the magnitude response of the lowpass analysis filter with frequency normalized by 2π.

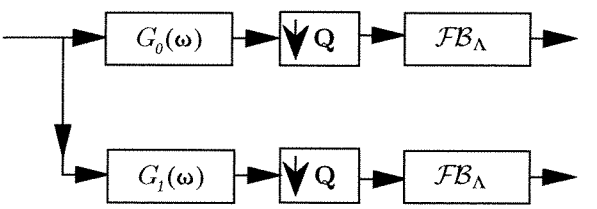

Fig. 5.16. A two-level tree structured filter bank. The first level is a two-dimensional two-channel filter bank with decimation matrix $\mathbf{Q}$ and the second level is a two-dimensional separable filter bank with decimation matrix $\mathbf{\Lambda}$.

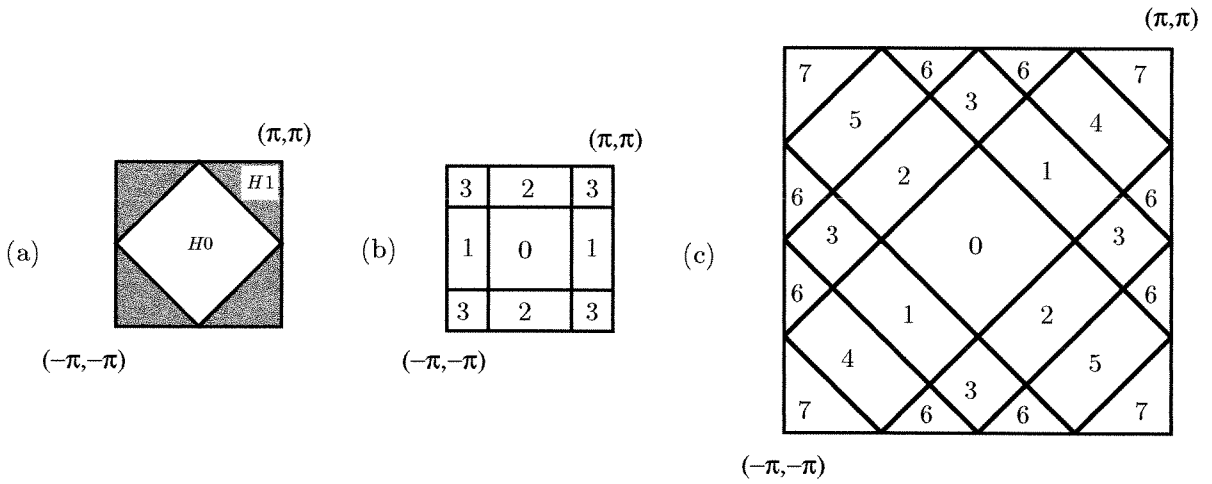

Fig. 5.17. Example 5.3. The simplistic four-parallelogram filter bank: (a) The two-channel diamond filter bank; (b) the supports of the analysis filters in a four-channel separable filter bank (with the support of the kth filter denoted by k); (c) the supports of the eight analysis filters in the overall system (with the support of the kth analysis filter denoted by k).

structure filter bank with two levels (Fig. 5.16). For the first level of the tree, we use the diamond filter bank [102, 2]. The diamond filter bank is a two-channel system with decimation matrix

$$\mathbf{Q} = \begin{pmatrix} 1 & 1 \\ -1 & 1 \end{pmatrix}.$$

The supports of the analysis filters in the diamond filter bank are as shown in Fig. 5.17(a). For the second level, we use a separable system with decimation matrix $\mathbf{\Lambda} = 2\mathbf{I}_2$ (Fig. 5.17(b)), which can be obtained as a tree structure of two 1D two-channel filter banks. Then the resulting analysis filters of the *Four-P* filter banks have supports as shown Fig. 5.17(c). Each analysis filter $H_m(\boldsymbol{\omega})$ consists of *Four-P*s. We can verify that the four squares in each analysis filter are located as in (5.1).

Remark on Cosine Modulated Implementation. Cosine modulated filter banks enjoy the advantages of low design cost and low complexity. This motivates us to consider cosine modulated implementation for *Four-P* filters. In the first case $|\mathbf{Q}| = 1$, if the two 1D filter banks are cosine modulated, then the resulting 2D nonseparable filter bank will also be cosine modulated. In the second case $|\mathbf{Q}| = 2$, even if the two systems are cosine modulated, the tree structured system is not cosine modulated in general. However, in both cases the overall systems have the desired configurations.

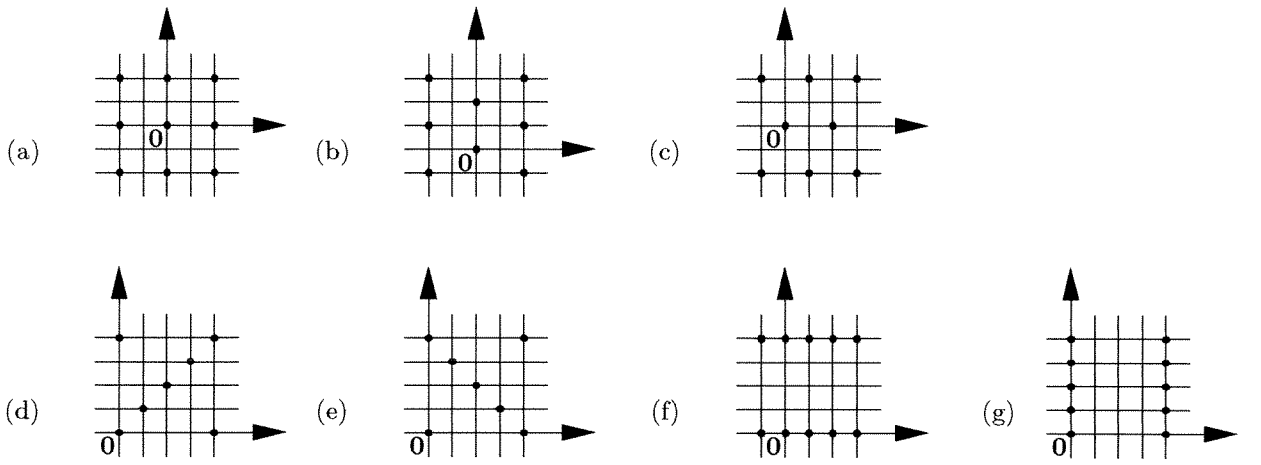

Fig. 5.18. Possible lattices of integer matrix $\mathbf{L}^T$, where $\mathbf{L}$ has $|\mathbf{L}| = 4$.

5.4 Other Possible Four-Parallelogram Filter Banks

In the simplistic *Four-P* filter banks, we have constrained $\mathbf{L}$ to be $2\mathbf{I}_2$ and the support of lowpass filter $H_0(\boldsymbol{\omega})$ to be a parallelogram of twice the size of the prototype parallelogram. However, for the more general *Four-P* filter banks, the only requirement is that each filter contains four parallelograms of identical shapes. The matrix $\mathbf{L}$ can be any integer matrix with $|\mathbf{L}| = 4$. As $\mathbf{L}$ is an integer matrix and $|\mathbf{L}| = 4$, there are 7 possible $LAT(\mathbf{L}^T)$ as shown in Fig. 5.18(a)-(g). Also the support of the lowpass analysis filter is not necessarily a parallelogram as in simplistic *Four-P* filter banks. Several possible supports of the first analysis filter are given in Fig. 5.19. In all cases of Fig. 5.19, the support of $H_0(\boldsymbol{\omega})$ consists of four connected parallelograms. In fact, any one of the four parallelograms is edge adjacent or vertex adjacent to another parallelogram. One can verify that Fig. 5.19 is also a complete list of connected supports for $H_0(\boldsymbol{\omega})$ that has $\mathcal{AFS}(\mathbf{M})$ property. This follows from the fact that $\mathbf{L}$ is an integer matrix.

Suppose we choose $\mathbf{L}$ to be an integer matrix and choose the support of $H_0(\boldsymbol{\omega})$ from one of the choices in Fig. 5.19. In this case, it can be verified that the filter bank can not possess both edge and vertex permissibility, except for the class of simplistic *Four-P* filter banks in Sec. 5.2 and some special cases. We have not been able to analyze these special cases in a unified manner. However, exhaustive case study shows that in these special cases, the decimation matrix $\mathbf{M}$ is rather restricted and the determinant of $\mathbf{M}$ can not be arbitrarily large. We will look at one such example.

Example 5.4. *Permissible but not simplistic Four-P filter bank.* Consider the filter bank in Fig. 1.1. Let the decimation matrix be

$$\mathbf{M} = \begin{pmatrix} 1 & 1 \\ -2 & 2 \end{pmatrix}.$$

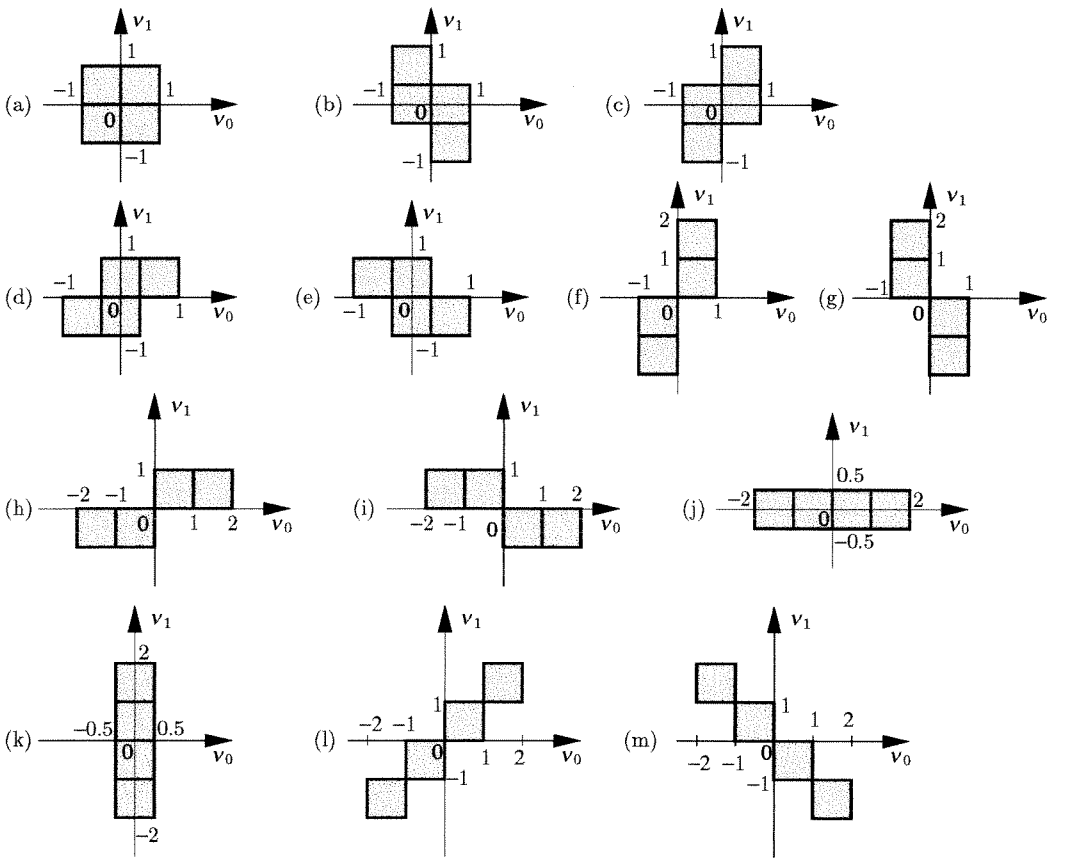

Fig. 5.19. Possible supports of the lowpass analysis filter.

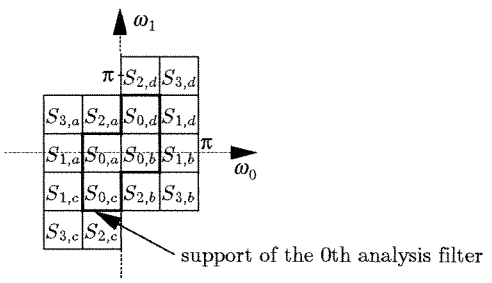

Fig. 5.20. Example 5.4. The support configuration of a permissible four-parallelogram filter bank that is not simplistic.

As $|\mathbf{M}| = 4$, the filter bank has 4 channels. If we choose

$$\mathbf{L} = \begin{pmatrix} 2 & -1 \\ 2 & 1 \end{pmatrix},$$

the lattice of $\mathbf{L}^T$ is as shown in Fig. 5.18(b). In this case, the matrix $\mathbf{N} = 4\mathbf{I}$. We choose the configuration for the four analysis filters as in Fig. 5.20. Observe that the support of $H_0(\boldsymbol{\omega})$ is as in Fig. 5.19(c). The four passbands of $H_k(\boldsymbol{\omega})$ are labeled as $S_{k,a}$, $S_{k,b}$, $S_{k,c}$, and $S_{k,d}$, for $k = 0, 1, 2, 3$. When decimated and expanded by $\mathbf{M}$, each passband has 3 images. These images result in edge and vertex aliasing. However, we will show that these edge and vertex aliasing errors appear in pairs and the configuration in Fig. 5.20 is edge and vertex permissible. Towards this end, we will verify following. Whenever there is edge or vertex aliasing error induced by $S_{0,a}$ in a certain frequency region, we can find a similar edge or vertex aliasing error in another subband.

When the 0th analysis filter is decimated and then expanded by $\mathbf{M}$, the three images of $S_{0,a}$ are at $S_{0,a} + \mathbf{L}^T\mathbf{k}$, for $\mathbf{k} \in \mathcal{N}(\mathbf{M}^T)$ and $\mathbf{k} \neq \mathbf{0} \bmod \mathbf{M}^T$. One can verify that the three images are actually at $S_{2,c}$, $S_{1,d}$, and $S_{3,d}$ as shown in Fig. 5.21(a). In what follows, we discuss the aliasing errors induced by these three images.

(1) *Image of $S_{0,a}$ at $S_{2,c}$.* This image is edge adjacent to $S_{0,c}$ and results in edge aliasing. As $S_{0,a}$ and $S_{2,c}$ are separated by $\begin{pmatrix} 0 & -2 \end{pmatrix}^T = \mathbf{L}^T \begin{pmatrix} 1 & -1 \end{pmatrix}^T$, this edge aliasing term contributes to aliasing transfer function $A_{(-1,1)}(\boldsymbol{\omega})$. Observe that in the second subband, passband $S_{2,a}$ has one image at $S_{0,c}$ (Fig. 5.21(b)), which is edge adjacent to $S_{2,c}$ and create edge aliasing similar to that in the 0th subband.

(2) *Image of $S_{0,a}$ at $S_{1,d}$.* This image is edge adjacent to $S_{0,d}$ (Fig. 5.21(a)) and results in edge aliasing that contributes to $A_{(1,0)}(\boldsymbol{\omega})$. In the first subband, passband $S_{1,a}$ has one image at $S_{0,d}$ (Fig. 5.21(c)). This image is edge adjacent to $S_{1,d}$ and a similar edge aliasing contributing to $A_{(1,0)}(\boldsymbol{\omega})$ is created. On the other hand, the image of $S_{0,a}$ at $S_{1,d}$ is also vertex adjacent to

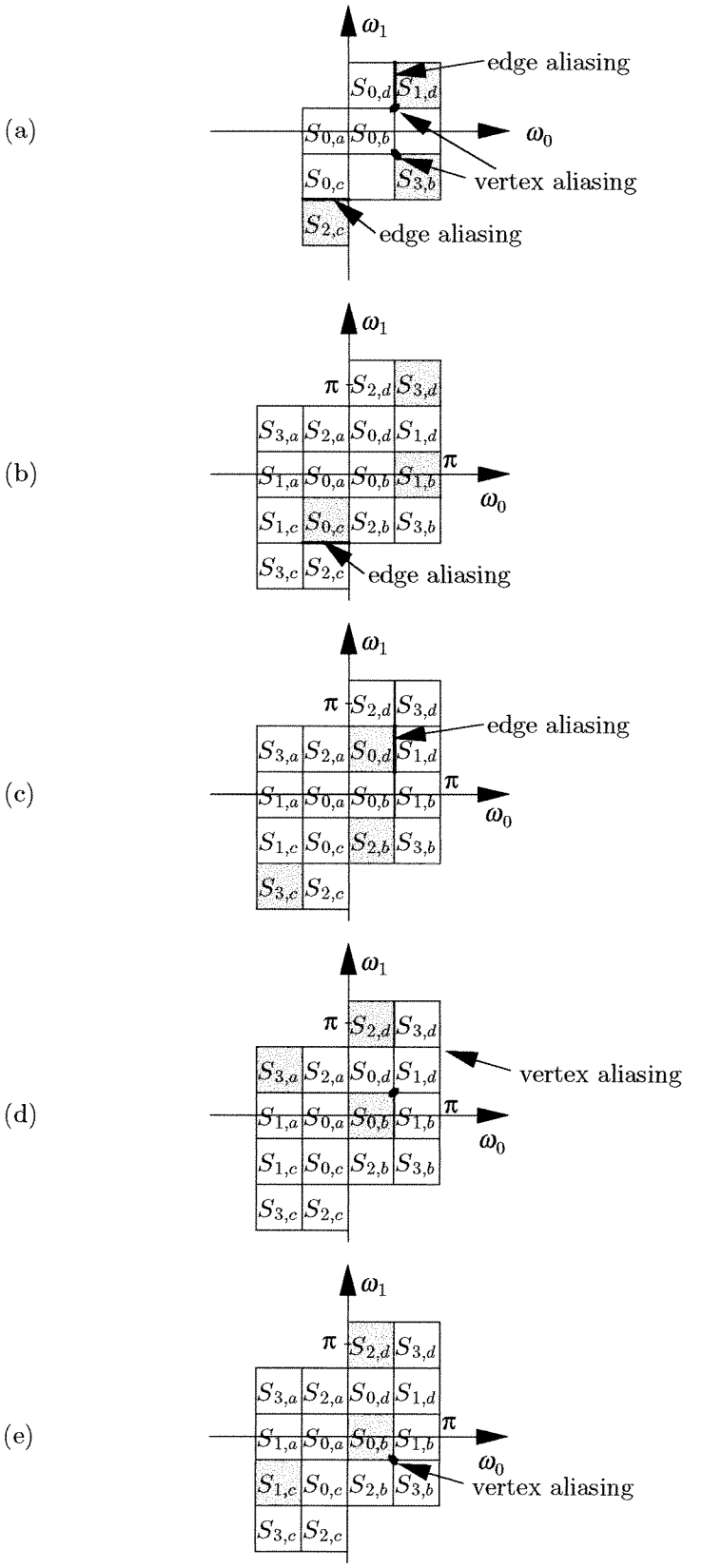

Fig. 5.21. Example 5.4. (a) Images of $S_{0,a}$, (b) images of $S_{2,a}$, (c) images of $S_{1,a}$, (d) images of $S_{1,c}$, and (e) images of $S_{3,a}$.

$S_{0,b}$ and results in vertex aliasing (Fig. 5.21(a)). But we see that one image of $S_{1,c}$ is at $S_{0,b}$ (Fig. 5.21(d)) and creates aliasing similar to the vertex aliasing in the 0th subband.

(3) *Image of* $S_{0,a}$ *at* $S_{3,b}$. This image is vertex adjacent to $S_{0,b}$ (Fig. 5.21(a)) and results in vertex aliasing that contributes to $A_{(0,1)}(\boldsymbol{\omega})$. We see that in the third subband, passband $S_{3,a}$ has one image at $S_{0,b}$ (Fig. 5.21(e)). As this image is vertex adjacent to $S_{3,b}$, it results in vertex aliasing similar to that in the 0th subband.

In a similar manner, we can analyze the edge and vertex aliasing caused by the other passbands of $H_0(\boldsymbol{\omega})$ and also the major aliasing in the other three subbands. One can show that in this example edge and vertex aliasing always appear in pairs and the configuration in Fig. 5.20 is permissible.

Concluding Remarks

The construction procedure of the configurations for the *Four-P* filter banks suggests that the configurations vary with the following two factors, (1) the choice of integer matrix $\mathbf{L}$ and (2) the location of the four parallelograms in the support of each analysis filter. By changing these two factors, we can obtain various types of configurations. We have investigated permissibility for all those types of configuration in which the support of $H_0(\boldsymbol{\omega})$ is connected. In this case, the study shows that if such *Four-P*s filter banks can possess both edge permissibility and vertex permissibility, then the decimation matrix $\mathbf{M}$ is not arbitrary. In particular, $\mathbf{M}$ is either of the form $\mathbf{Q\Lambda}$ for some integer matrix $\mathbf{Q}$ with $|\mathbf{Q}| = 1$ or 2 and some diagonal matrix $\mathbf{\Lambda}$ (Eq. (5.2)) or $\mathbf{M}$ is limited to some special cases (elaborated in Sec. 5.4). In the former event, *Four-P* filter banks can be obtained by designing separable systems and (when $|\mathbf{Q}| = 2$) 2D two-channel filter banks.

In our construction of the parallelogram prototype, we constrain $\mathbf{L}$ to be an integer matrix. It is possible that a non integer matrix $\mathbf{L}$ will provide more flexibility in the design of *Four-P* filter banks. Research in this regard is still open.

Bibliography

[1] R. Ansari, A. E. Cetin and S. H. Lee, "Sub-band coding of images using nonrectangular filter banks," Proc. SPIE, vol. 974, pp. 315-323, 1988.

[2] R. Ansari and C. Guillemot, "Exact reconstruction filter banks using diamond FIR filters," Proc. Int. Conf. on new trends in Comm. Control, and Signal Proc., Turkey, July 1990.

[3] J. Backus, *The acoustical foundations of music*, W. W. Norton & Company, Inc., 1977.

[4] R. H. Bamberger and M. J. T. Smith, "A filter bank for the directional decomposition of images: theory and design," *IEEE Trans. on Signal Processing,* vol. SP-40, April 1992.

[5] M. G. Bellanger and J. L. Daguet, "TDM-FDM transmultiplexer: digital polyphase and FFT," *IEEE Trans. on Communications,* vol. COM-22, no. 9, pp. 1199-1204, Sep. 1992.

[6] H. Bolcskei and F. Hlawatsch, "Oversampled Wilson-type cosine modulated filter banks with linear phase," Proc. of the 30th Annual Asilomar Conference on Signals, Systems and Computers, 1996.

[7] N. K. Bose, *Applied multidimensional systems theory,* Van Nostrand Reinhold, 1982.

[8] S. C. Chan, "Two dimensional non-separable modulated filter banks," Proc. International Conf. on Acoustic, Speech, and Signal Processing, April 1994.

[9] T. Chen and P. P. Vaidyanathan, "The role of integer matrices in multidimensional multirate systems," *IEEE Trans. on Signal Processing,* vol. SP-41, March 1993.

[10] T. Chen and P. P. Vaidyanathan, "Recent developments in multidimensional multirate systems," *IEEE Trans. on Circuits And Systems For Video Technology,* vol. 3, April 1993.

[11] T. Chen and P. P. Vaidyanathan, "Consideration in multidimensional filter bank design," Proc. of International Symposium on Circuits and Systems, May 1993.

[12] P. L. Chu, "Quadrature mirror filter design for an arbitrary number of equal bandwidth channels," *IEEE Trans. on Acoustic, Speech and Signal Processing*, pp. 203-218, Feb. 1985.

[13] A. Cohen, I. Daubechies, and J. C. Feauveau, "Biorthogonal bases of compactly supported wavelets," *Communications on Pure and Applied Mathematics*, vol. 45, pp. 485-560, 1992.

[14] P. C. Cosman, R. M. Gray, and M. Vetterli "Vector quantization of image subbands - a survey review," *IEEE Trans. on Image Processing*, pp. 202-225, Feb. 1996.

[15] R. V. Cox, "The design of uniformly and nonuniformly spaced pseudo QMF," *IEEE Trans. on Acoustic, Speech and Signal Processing*, vol. ASSP-34, pp. 1090-1096, Oct. 1986.

[16] R. V. Cox, D. E. Bock, K. B. Bauer J. D. Johnston and J. H. Snyder, "The analog voice privacy system," *AT& T Tech. J.*, vol. 66, pp. 119-131, Jan.-Feb. 1987.

[17] R. E. Crochiere, S. A. Waber, and J. L. Flanagan, "Digital coding of speech in subbands,"*Bell Sys. Tech. Jour.*, vol. 55, pp. 1069-1085, Oct. 1976.

[18] R. E. Crochiere and L. R. Rabiner, *Multirate digital signal processing*, Englewood Cliffs, Prentice Hall, 1983.

[19] I. Djokovic and P. P. Vaidyanathan, "On optimal analysis synthesis filters for coding gain maximization," *IEEE Trans. on Signal Processing*, vol. 44, no. 5, pp. 1276-1279, May 1996.

[20] E. Dubois, "The sampling and reconstruction of time-varying imagery with application in video systems," *Proc. IEEE*, vol. 73, no. 4, pp. 502-522, April 1985.

[21] D. E. Dudgeon and R. M. Mersereau, *Multidimensional digital signal processing*, Englewood Cliffs, Prentice Hall, 1984.

[22] B. L. Evans, R. H. Bamberger, and J. H. McClellan, "Rules for multidimensional multirate structures," *IEEE Trans. on Signal Processing*, vol. SP-42, pp. 762-771, April 1994.

[23] N. J. Fliege, "Computational efficiency of modified DFT polyphase filter banks," Proc. of the 27th Annual Asilomar Conference on Signals, Systems and Computers, 1993.

[24] R. A. Gopinath and C. S. Burrus, "Theory of modulated filter banks and modulated tight frames," Proc. IEEE Int. Conf. Acoustic, Speech and Signal Processing, 1993.

[25] R. A. Gopinath and C. S. Burrus, "On upsampling, downsampling, and rational sampling rate filter banks," *IEEE Trans. on Signal Processing*, vol. 42, pp. 812-824, April 1994.

[26] R. A. Gopinath and C. S. Burrus, "Factorization approach to unitary time-varying filter banks trees and wavelets," *IEEE Trans. on Signal Processing*, vol. 43, no. 3, pp. 666-680, March 1995.

[27] R. A. Gopinath, "Modulated filter banks and wavelets–a general unified theory," Proc. IEEE Int. Conf. Acoustic, Speech and Signal Processing, pp. 1585-1588, May, 1996.

[28] C. Herley and M. Vetterli, "Wavelets and filter banks - theory and design," *IEEE Trans. on Signal Processing*, vol. 40, no. 9, pp. 2207-2232, Sep. 1992.

[29] C. Herley, "Boundary filters for finite length signals and time-varying filter banks," *IEEE Trans. on Circuits and Systems*, vol. 42, no. 2, pp. 102-114, Feb. 1995.

[30] M. Ikehara, "Cosine-modulated 2 dimensional FIR filter banks satisfying perfect reconstruction," Proc. International Conf. on Acoustic, Speech, and Signal Processing, April 1994.

[31] M. Ikehara, "Modulated 2 dimensional perfect reconstruction FIR filter banks with permissible passbands," Proc. International Conf. on Acoustic, Speech, and Signal Processing, pp. 1468-1471, May 1995.

[32] N. Jayant, J. Johnston and R. Safranek, "Signal compression based on models of human perception," *Proc. IEEE*, vol. 81, no. 10, pp. 1385-1422, Oct. 1993.

[33] T. A. C. M. Kalker, "Commutativity of up/down sampling," *Electron. Lett.*, vol. 28, no. 6, pp. 567-569, March 1992.

[34] T. A. C. M. Kalker and I. A. Shah, "A group theoretic approach to multidimensional filter banks: theory and application," *IEEE Trans. on Signal Processing*, vol. 44, no. 6, pp. 1392-1405, June 1996.

[35] C. W. Kim and R. Ansari, "FIR/IIR exact reconstruction filter banks with applications to subband coding of images," Midwest CAS Symposium, May 1991.

[36] R. D. Koilpillai, T. Q. Nguyen and P. P. Vaidyanathan, "Some results in the theory of cross-talk free transmultiplexers," *IEEE Trans. on Signal Processing*, vol. SP-39, pp. 2174-2183, Oct. 1991.

[37] R. D. Koilpillai and P. P. Vaidyanathan, "Cosine-modulated FIR filter banks satisfying perfect reconstruction," *IEEE Trans. on Signal Processing*, vol. SP-40, pp. 770-783, April 1992.

[38] J. Kovacevic and M. Vetterli "The commutativity of up/downsampling in two dimensions," *IEEE Trans. on Information Theory*, vol. 37, no. 4 pp. 695-698, May 1991.

[39] J. Kovacevic and M. Vetterli "Non-separable multidimensional perfect reconstruction filter banks and wavelet bases for R^n," *IEEE Trans. on Information Theory*, vol. 38, no. 2 pp. 533-555, March 1992.

[40] J. Kovacevic, "Local cosine bases in two dimensions," Proc. International Conf. on Acoustic, Speech, and Signal Processing, vol. IV, pp. 2125-2128, May 1995.

[41] M. Kunt, A. Ikonomopoulos and M. Kocher, "Second generation image coding techniques," *Proc. IEEE*, vol. 73, pp. 549-574, April 1985.

[42] J. S. Lim, *Two-dimensional signal and image processing*, Englewood Cliffs, Prentice Hall, 1990.

[43] Y.-P. Lin and P. P. Vaidyanathan, "Linear phase cosine modulated maximally decimated filter banks with perfect reconstruction," Proc. International Symposium on Circuits and Systems, pp. 2.17-2.20, June 1994.

[44] Y.-P. Lin and P. P. Vaidyanathan, "Application of DFT filter banks and cosine modulated filter banks in filtering," Proc. IEEE Asia-Pacific Conference on Circuits and Systems, Dec. 1994.

[45] Y.-P. Lin and P. P. Vaidyanathan, "On the application of under-decimated filter banks," *The Telecommunications and Data Acquisition Progress Report 42-119*, Jet Propulsion Lab., Caltech, Nov. 1994.

[46] Y.-P. Lin, S.-M. Phoong, and P. P. Vaidyanathan, "New results on multidimensional Chinese remainder theorem," *IEEE Signal Processing Letters*, vol. 1, no. 11, pp. 176-178, Nov. 1994.

[47] Y.-P. Lin and P. P. Vaidyanathan, "Two-dimensional paraunitary cosine modulated perfect reconstruction filter banks," Proc. International Symposium on Circuits and Systems, pp. 752-755, April 1995.

[48] Y.-P. Lin and P. P. Vaidyanathan, " Two-dimensional four-parallelogram filter banks," Proc. of the 29th Annual Asilomar Conf. on Signals, Systems and Computers, Oct. 1995.

[49] Y.-P. Lin and P. P. Vaidyanathan, "Linear phase cosine modulated maximally decimated filter banks with perfect reconstruction," vol. 42, no. 11, pp. 2525-2539, *IEEE Trans. on Signal Processing*, Nov. 1995.

[50] Y. Lin and P. P. Vaidyanathan, "Sampling theorems of two-dimensional signals," Proc. International Conf. on Acoustic, Speech, and Signal Processing, April 1996.

[51] Y.-P. Lin and P. P. Vaidyanathan, "Two-dimensional linear-phase cosine modulated filter banks," Proc. International Symposium on Circuits and Systems, May 1996.

[52] Y.-P. Lin and P. P. Vaidyanathan, "Theory and design of two-dimensional filter banks: a review," *Multidimensional Systems and Signal Processing*, Academic Press, July. 1996.

[53] Y.-P. Lin and P. P. Vaidyanathan, "Theory and design of two-parallelogram filter banks," *IEEE Trans. on Signal Processing*, Nov. 1996.

[54] Y.-P. Lin and P. P. Vaidyanathan, "On the study of four parallelogram filter banks," *IEEE Trans. on Signal Processing*, Nov. 1996.

[55] Y.-P. Lin and P. P. Vaidyanathan, "One-dimensional and two-dimensional periodically nonuniform sampling," Technical report, Caltech, Aug. 1996.

[56] Y.-P. Lin and P. P. Vaidyanathan, "Periodically nonuniform sampling of a new class of bandpass signals," Signal Processing Work Shop, Leon, Norway, Sep. 1996.

[57] Y.-P. Lin and P. P. Vaidyanathan, "On efficient design of prototype filters for cosine modulated filter banks," in preparation.

[58] S. G. Mallat, "A theory for multiresolution signal decomposition - the wavelet representation," *IEEE Trans. on Pattern Analysis and Machine Intelligence,* vol. 11, no. 7, pp. 674-693, 1989.

[59] H. S. Malvar, *Signal processing with lapped transforms,* Artech House, Norwood, MA, 1992.

[60] H. S. Malvar, "Extended lapped transforms - properties, applications, and fast algorithms," *IEEE Trans. on Signal Processing,* vol. 40, no. 11, pp. 2703-2714, Nov. 1992.

[61] J. L. Mannos and D. J. Sakrison, "The effects of a visual fidelity criterion on the encoding of images," *IEEE Trans. on Information Theory,* vol. 20, no. 4, pp. 525-536, July 1974.

[62] J. Masson and Z. Picel, "Flexible design of computationally efficient nearly perfect QMF filter banks," Proc. IEEE Int. Conf. Acoustic, Speech and Signal Processing, pp. 14.7.1-14.7.4, Tempa, FL, March, 1985.

[63] D. L. Neuhoff and T. N. Pappas, 'Perceptual coding of images for halftone display," *IEEE Trans. on Image Processing*, vol. 3, pp. 341-354, 1994.

[64] T. Q. Nguyen, "A class of generalized cosine-modulated filter bank," IEEE Int. Symposium on Circuits and Systems, 1992.

[65] T. Q. Nguyen, "Near-perfect-reconstruction pseudo-QMF banks," *IEEE Trans. on Signal Processing*, vol. 42, no. 1, pp. 65-76, Jan. 1994.

[66] H. J. Nussbaumer, "Pseudo QMF filter bank," *IBM Tech. disclosure Bulletin,* vol. 24, pp. 3081-3087, Nov. 1981.

[67] A. V. Oppenheim, A. S. Willsky, and I. Young, *Signals and systems*, Englewood Cliffs, Prentice Hall, 1983.

[68] M. G. Perkins and T. Lookabaugh, "A psychophysically justified bit allocation algorithm for subband image coding systems," Proc. IEEE Int. Conf. Acoustic, Speech and Signal Processing, 1989.

[69] S. Phoong and P. P. Vaidyanathan, "One- and two-level filter bank convolvers," *IEEE Trans. on Signal Processing*, vol. 43, no. 1, pp. 116-133, Jan. 1995.

[70] S. Phoong, C. W. Kim, P. P. Vaidyanathan, and R. Ansari, "A new class of two-channel biorthogonal filter banks and wavelet bases," *IEEE Trans. on Signal Processing*, vol. 43, no. 3, pp. 649-665, March 1995.

[71] S. Phoong and P. P. Vaidyanathan, "Time-varying lapped orthogonal transforms," Proc. Int. Conf. Digital Signal Processing, Limassol, Cyprus, June 1995.

[72] W. H. Press, B. P. Flannery, S. A. Teukolsky and W. T. Vetterling, *Numerical recipes,* Cambridge Univ. Press, 1989.

[73] J. P. Princen and A. B. Bradley, "Analysis/synthesis filter bank design based on time domain aliasing cancellation," *IEEE Trans. on Acoustic, Speech and Signal Processing*, Vol. 34, pp. 1153-1161, 1986.

[74] A. Papoulis, *Signal analysis*, McGraw-Hill, Inc., 1965.

[75] K. Ramchandran and M. Vetterli, "Best wavelet packet bases in a rate distortion sense," *IEEE Trans. on Image Processing,* vol. 2, no. 2, pp. 160-175, April 1993.

[76] T. A. Ramstad, "Cosine modulated analysis-synthesis filter banks with critical sampling and perfect reconstruction," Proc. IEEE Int. Conf. Acoustic, Speech and Signal Processing, pp. 1789-1792, Toronto, Canada, May 1991.

[77] K. R. Rao and J. J. Hwang, *Techniques and standards for image, video, and audio coding*, Prentice Hall, 1996.

[78] J. H. Rothweiler, "Polyphase quadrature filters, a new subband coding technique," Proc. of the IEEE Int. Conf. on Acoustic, Speech and Signal Processing, pp. 1280-1283, April, 1983.

[79] R. J. Safranek and J. D. Johnston, "A perceptually tuned sub-band image coder with image-dependent quantization and post-quantization data compression," Proc. IEEE Int. Conf. Acoustic, Speech and Signal Processing, 1989.

[80] A. Said and W. A. Pearlman, "Image compression using the spatial orientation tree," Proc. IEEE Inter. Symposium on Circuits and Systems, May 1993.

[81] A. Said and W. A. Pearlman, "A new, fast and efficient image codec based on set partitioning in hierarchical trees," *IEEE Trans. on Circuits and Systems for Video Technology,* vol. 6, no. 3, pp. 243-250, June 1996.

[82] V. Sathe and P. P. Vaidyanathan, "Effects of multirate systems on the statistical properties of random inputs," *IEEE Trans. on Signal Processing,* vol. 41, no. 1, pp. 131-146, Jan. 1993.

[83] J. M. Shapiro, "Embedded image coding using zerotrees of wavelet coefficients," *IEEE Trans. on Signal Processing,* vol. 41, no. 12, pp. 3445-3462, Dec. 1993.

[84] E. P. Simoncelli and E. H. Adelson, "Nonseparable extensions of quadrature mirror filters to multiple dimensions," *Proc. IEEE*, vol. 78, pp. 652-664, April 1990.

[85] M. J. T. Smith and III. T. P. Barnwell."A new filter bank theory for time-frequency representation," *IEEE Trans. on Acoustic, Speech and Signal Processing*, vol. ASSP-35, pp. 314-327, March 1987.

[86] M. J. T. Smith and S. L. Eddins, "Analysis/synthesis techniques for subband image coding," *IEEE Trans. on Acoustic, Speech and Signal Processing*, vol. 38, no. 8, pp. 1446-1456, 1990.

[87] M. J. T. Smith and W. C.-L. Chung, "Recursive time-varying filter banks for subband image coding," *IEEE Trans. on Image Processing*, vol. 4, no. 7, pp. 885-895, July 1995.

[88] A. K. Soman, P. P. Vaidyanathan, and T. Q. Nguyen, "Linear phase paraunitary filter banks: theory, factorizations and applications," *IEEE Trans. on Signal Processing*, vol. SP-41, no. 12, pp. 3480-3496, Dec. 1993.

[89] G. Strang and T. Q. Nguyen, *Wavelets and filter banks,* Wellesley-Cambridge Press, 1996.

[90] D. B. H. Tay and N. G. Kingsbury, "Flexible design of multidimensional perfect reconstruction FIR 2-band filters using transformation of variables," *IEEE Trans. on Image Processing*, vol. 2, no. 4, pp. 466-480, Oct. 1993.

[91] M. K. Tsatsanis and G. B. Giannakis, "Principle component filter banks for optimum multiresolution analysis," *IEEE Trans. on Signal Processing*, vol. 43, no. 8, pp. 1766-1777, Aug. 1995.

[92] M. Unser, "On the optimality of ideal filters for pyramid and wavelet signal approximation," *IEEE Trans. on Signal Processing*, vol. 41, no. 12, pp. 3591-3596, Dec. 1993.

[93] P. P. Vaidyanathan, "Theory and design of M-channel maximally decimated quadrature mirror filters with arbitrary M, having the perfect-reconstruction property," *IEEE Trans. on Acoustics Speech and Signal Processing*, vol. SP-35, vol. 4, pp. 476-492, April 1987.

[94] P. P. Vaidyanathan, "Quadrature mirror filter banks, M-band extensions and perfect reconstruction techniques," *IEEE ASSP magazine*, vol. 4, pp. 4-20, June 1987.

[95] P. P. Vaidyanathan, "Fundamentals of multidimensional multirate digital signal processing," *Sadahana*, vol. 15, pp. 157-176, Nov. 1990.

[96] P. P. Vaidyanathan, "New results in multidimensional multirate systems," Proc. International Symposium on Circuits and Systems, 1991.

[97] P. P. Vaidyanathan, *Multirate systems and filter banks*, Englewood Cliffs, Prentice Hall, 1993.

[98] P. P. Vaidyanathan, "Theory of optimal orthonormal filter banks," Proc. Inter. Conf. Acoustic, Speech and Signal Processing, pp. 1487-1490, May 1996.

[99] P. P. Vaidyanathan, "Orthonormal and biorthonormal filter banks as convolvers, and convolutional coding gain," *IEEE Trans. on Signal Processing*, vol. SP-41, pp. 2110-2130, June 1993.

[100] P. P. Vaidyanathan, "Role of anticausal inverses in multirate filter-banks. 2. the FIR case, factorizations, and biorthogonal lapped transforms," *IEEE Trans. on Signal Processing*, vol. SP-43, pp. 1103-1115, May 1995.

[101] M. A. Vetterli, "Multidimensional subband coding: some theory and algorithms," *Signal Processing,* vol. 6, pp. 97-112, April 1984.

[102] M. A. Vetterli, "Perfect transmultiplexers," Proc. IEEE Int. Conf. Acoustic, Speech and Signal Processing, pp. 2567-2570, Tokyo, Japan, April 1986.

[103] M. A. Vetterli, "A theory of multirate filter banks," *IEEE Trans. on Acoustic, Speech and Signal Processing*, vol. ASSP-35, pp. 356-372, March, 1987.

[104] M. A. Vetterli and K. M. Uz, "Multiresolution coding techniques for digital television - a review," *Multidimensional Systems and Signal Processing*, vol. 3, pp. 161-187, May, 1992.

[105] M. A. Vetterli and J. Kovacevic, *Wavelets and subband coding*, Englewood Cliffs, Prentice Hall, 1995.

[106] V. C. Liu and P. P. Vaidyanathan, "On factorization of subclass of 2D digital FIR lossless matrices for 2D QMF bank application," *IEEE Trans. Circuits And Systems*, June 1990.

[107] E. Viscito and J. P. Allebach, "The analysis and design of multidimensional FIR perfect reconstruction filter banks for arbitrary sampling lattices," *IEEE Trans. on Circuits and Systems,* Vol. CAS-38, pp. 29-41, Jan. 1991.

[108] J. W. Woods and S. D. O'Neil, "Subband coding of images," *IEEE Trans. on Accoust. Speech and Signal Proc.,* Vol. 34, pp. 1278-1288, Oct. 1986.

[109] J. W. Woods, *Subband image coding*, Norwell, Kluwer Academic Publishers, Inc., 1991.

[110] X.-G. Xia and B. W. Suter, "A family of 2-dimensional nonseparable Malvar wavelets," *Applied and Computational Harmonic Analysis,* vol. 2, pp. 243-256, July 1995.

[111] X.-G. Xia and B. W. Suter, "Construction of Malvar wavelets on hexagons," *Applied and Computational Harmonic Analysis,* vol. 3, pp. 65-71, Jan. 1996.

[112] X.-G. Xia and B. W. Suter, "A systematic construction method for spatial-varying FIR filter banks with perfect reconstruction," Proc. International Conf. on Image Processing, Austin, Texas, Nov. 1994.

[113] P. Yip, and K. R. Rao, "Fast discrete transforms," in *Handbook of digital signal processing,* edited by D. F. Elliott, Academic Press, San Diego, CA, 1987.